



Theses and Dissertations

2011-07-13

Analytical Modeling and Optimization of a Thermoelectric Heat Conversion System Operating Between Fluid Streams

Stephen H. Taylor
Brigham Young University - Provo

Follow this and additional works at: <https://scholarsarchive.byu.edu/etd>



Part of the [Mechanical Engineering Commons](#)

BYU ScholarsArchive Citation

Taylor, Stephen H., "Analytical Modeling and Optimization of a Thermoelectric Heat Conversion System Operating Between Fluid Streams" (2011). *Theses and Dissertations*. 2813.
<https://scholarsarchive.byu.edu/etd/2813>

This Thesis is brought to you for free and open access by BYU ScholarsArchive. It has been accepted for inclusion in Theses and Dissertations by an authorized administrator of BYU ScholarsArchive. For more information, please contact scholarsarchive@byu.edu, ellen_amatangelo@byu.edu.

Analytical Modeling and Optimization of a Thermoelectric
Heat Conversion System Operating Between
Fluid Streams

Stephen H. Taylor

A thesis submitted to the faculty of
Brigham Young University
in partial fulfillment of the requirements for the degree of
Master of Science

Matthew R. Jones, Chair
Dale R. Tree
Steven E. Gorrell

Department of Mechanical Engineering

Brigham Young University

August 2011

Copyright © 2011 Stephen H. Taylor

All Rights Reserved

ABSTRACT

Analytical Modeling and Optimization of a Thermoelectric Heat Conversion System Operating Between Fluid Streams

Stephen H. Taylor
Department of Mechanical Engineering, BYU
Master of Science

Analytical, closed-form solutions governing thermoelectric behavior are derived. An analytical model utilizing a thermal circuit is presented involving heat transfer into, through, out of, and around a thermoelectric device. A nondimensionalization of the model is presented. Linear heat transfer theory is applied to the model to obtain a series of closed form equations predicting net power output for the thermoelectric device. Fluid streams flowing through shrouded heat sinks with square pin fins are considered for the thermal pathways to and from the device. Heat transfer and pressure drop are characterized in a manner conducive to an analytical model using previously published experimental results.

Experimental data is presented which validates and demonstrates the usefulness of the model in predicting power output for commercially available thermoelectric generators. A specific design for a thermoelectric power harvester is suggested consisting of a pattern of thermoelectric generators. An economic model for calculating payback time is developed. An optimization process is demonstrated that allows for the payback time of such a system to be minimized through optimization of the physical design of the system. It is shown that optimization of the thermal pathways dramatically reduces payback time. Optimized design of a system is discussed in light of theoretical cases with feasible payback times.

Keywords: energy conversion, thermoelectric, waste heat, payback time, pressure drop, heat sink, optimization.

ACKNOWLEDGMENTS

The original concept of optimizing thermoelectric power conversion through manipulating the thermal pathways came from my advisor, Dr. Matthew Jones. The process of defining how to model thermoelectric devices and the heat transfer associated with them was left to me. I wish to thank him for having greater faith in me than I sometimes had in myself, and for the fantastic growing experience of wrestling with an open-ended project. He had great patience with my constant overestimation of how quickly I could accomplish the various parts of this research.

I wish to thank the *Xergy Solutions* 2009-2010 capstone team at BYU, who conducted similar research during that time. At the conclusion of their project, I inherited the data acquisition portion of their experimental setup, which was invaluable in setting up my experiments in a timely manner. Jeremy LeFevre especially helped me by providing information, answering questions about their research, and helping me learn from their experience.

I gratefully recognize the role of Kevin Cole, equipment manager for the department, whose expertise and resourcefulness came to the rescue, not only for my own research, but for many—probably most—others' research as well. Though scores of needy students are constantly clamoring for his attention and help, Kevin displays invincible cheerfulness and genuine caring. His assistance was vital for obtaining the experimental data.

TABLE OF CONTENTS

LIST OF TABLES	ix
LIST OF FIGURES	xi
1 Introduction.....	1
1.1 Recovering Available Energy	1
1.2 Thermoelectric Materials	4
1.3 Objectives	5
2 Thermoelectric Modeling.....	7
2.1 Single Thermoelement: Exact Solution	7
2.2 Single Thermoelement: Approximate Solution	12
2.2.1 Derivation	12
2.2.2 Observations on Efficiency	17
2.3 Thermoelectric Device Modeling	20
3 General System Model.....	25
3.1 Heat Path Layout	25
3.2 Governing Equations for System	28
4 Heat Sink Modeling	35
4.1 Heat Transfer	35
4.1.1 Heat Conduction in Fins	35
4.1.2 Heat Transfer Through Heat Sink.....	37
4.1.3 Interfacial Heat Transfer	41
4.1.4 Heat Transfer Correlation	42
4.2 Pressure Drop.....	44
4.2.1 Previous Work	45

4.2.2	Definition of Friction Factor	47
4.2.3	Velocity Profile and Friction Factor	48
4.2.4	Method of Determining Friction Factor.....	50
4.2.5	Power Requirement.....	57
4.3	Thermal/Hydrodynamic Behavior of Heat Sinks	57
5	Bypass Insulation	61
5.1	Device Cost and Heat Channeling	61
5.2	Single Node Approximation	62
5.3	Modeling and Nondimensionalization.....	66
6	Experimental Validation	69
6.1	Test Station	69
6.2	Method.....	71
6.3	Results.....	72
6.3.1	<i>Thermal Electronics</i> Thermoelectric Generator.....	72
6.3.2	<i>Marlow Industries</i> Set of Thermoelectric Generators	75
6.4	Uncertainty.....	79
6.4.1	Uncertainty in Power Measurement.....	79
6.4.2	Uncertainty in the Model	79
6.4.3	Uncertainty not reflected in the Plots.....	80
6.5	Weaknesses of the Model	81
6.6	Model Usefulness	85
7	Economic Modeling	87
7.1	Time Value of Money.....	87
7.2	Present Value Model.....	90
8	Complete System Modeling.....	97

8.1	Nondimensionalization for System.....	97
8.2	Spatial Dependence of Fluid Temperatures and Power Output.....	100
8.3	Solution Method: Minimizing Payback Time	107
8.4	Cases Studies	111
8.4.1	Case 1: Expensive Energy.....	112
8.4.2	Case 2: Large Temperature Difference	125
9	Conclusion	133
9.1	Summary.....	133
9.2	Conclusions on Optimized Design	136
9.3	Further Recommended Research	138
	REFERENCES.....	141
	Appendix A. Model and Optimization Mathematica Code	143
	Appendix B. Friction Factor Tables	175

LIST OF TABLES

Table 2-1: Comparison of Exact and Approximate Heat Rate Solutions.	15
Table 4-1: Values of Re_d , λ , ϵ_x , and ϵ_z for Friction Factor Tables.....	54
Table 4-2: Select Friction Factors.....	55
Table 5-1: Finite Difference Results for Single Node Approximation.....	65
Table 6-1: Parameters for Heat Sinks used in Experiments	72
Table 6-2: Calibration Points for determining Z_D and U_D'' for the TEG1-12611-6.0 Thermoelectric Device.....	73
Table 6-3: Device Characterization for Two Identical TG12-8 Thermoelectric Devices.	76
Table 8-1: Nomenclature for Temperature Variables.	102
Table 8-2: Parameters: Constant vs Design.	107
Table 8-3: Combination Parameters: Constant vs Design.	108
Table 8-4: Dimensionless Groups: Constant vs Design.	109
Table 8-5: First Optimized Case: Heat Path and Thermoelectric Device Parameters.	112
Table 8-6: First Optimized Case: Heat Sink and Cost Parameters	113
Table 8-7: Case 1 Starting and Ending Values for Design Variables.....	114
Table 8-8: Final Optimized Variables and Cost Parameters. Case 1A.	124
Table 8-9: Second Optimized Case: Heat Path and Thermoelectric Device Parameters.	125
Table 8-10: Second Optimized Case: Heat Sink and Cost Parameters.....	126
Table 8-11: Case 2 Starting and Ending Values for Design Variables.....	127
Table 8-12: Final Optimized Variables and Cost Parameters. Case 2C.	131

LIST OF FIGURES

Figure 2-1: Thermoelement and Differential Heat Interactions.	7
Figure 2-2: Thermoelement with Load.	10
Figure 2-3: Thermoelement Temperature Profiles.	13
Figure 2-4: Thermodynamic Efficiency Curves	17
Figure 2-5: Second Law Efficiency for a Thermoelement	18
Figure 2-6: Typical Arrangement of Thermoelements in a Power Harvesting Device.	20
Figure 2-7: Photo of the TEG1-12611-6.0 Thermoelectric Generator	22
Figure 3-1: Thermoelectric System Layout.	25
Figure 3-2: Thermal Circuit Corresponding to Thermoelectric System Layout.....	27
Figure 4-1: Single Fin Analysis.	36
Figure 4-2: System Layout: Fin Array Dimensions.....	38
Figure 4-3: Top View of Fin Array.....	39
Figure 4-4: Conceptual Schematic of the Porous Medium Approach	46
Figure 4-5: Calculated Friction Factor vs Dimensionless Fin Length.....	53
Figure 4-6: Friction Factor vs Reynolds number.....	56
Figure 4-7: Heat Rate/Power Requirement vs Reynolds Number	59
Figure 4-8: Heat Rate/Power Requirement vs Dimensionless Fin Length. Parameters.	60
Figure 5-1: System Layout: Device and Bypass Dimensions.....	61
Figure 5-2: Finite Difference Domain	63
Figure 5-3: Temperature Profiles on Inner Side of Heat Sink Bases.....	64
Figure 5-4: Schematic of Potential Design for High Bypass Ratios.....	66
Figure 6-1: Schematic of Test Station Flow Circuit.....	69
Figure 6-2: Photographs of Test Station.	70

Figure 6-3: Experimental Results for the TEG1-12611-6.0 Thermoelectric Generator	74
Figure 6-4: Experimental Results for the First TG12-8 Thermoelectric Generator	77
Figure 6-5: Experimental Results for the Second TG12-8 Thermoelectric Generator	78
Figure 6-6: Analytical Predictions for Normalized Thermodynamic Efficiency	83
Figure 7-1: System Layout: Normalized System Dimensions.....	90
Figure 7-2: The Arrow of Time.	91
Figure 7-3: Predicted Payback Time vs Bypass Ratio: $\Psi_H'' = 2.2$, $\Psi_L'' = 2.0$	94
Figure 7-4: Predicted Payback Time vs Bypass Ratio: $\Psi_H'' = 11$, $\Psi_L'' = 10$	95
Figure 8-1: Fluid Channel Analysis	101
Figure 8-2: Sensitivity Plots for Heat Sink Porosities	116
Figure 8-3: Sensitivity Plots for Fin Lengths and Diameters. Case 1A.....	118
Figure 8-4: Temperature Profiles of Fluid Streams. Case 1A.	119
Figure 8-5: Sensitivity Plots for Bypass Ratio, Reynolds Number, and Z^* . Case 1A.....	120
Figure 8-6: Power Output and Payback Time vs X^* . Case 1A.....	121
Figure 8-7: Gross, Required, and Net Power vs X^* . Case 1A.	123
Figure 8-8: Temperature Profiles of Fluid Streams. Case 2C.....	129
Figure 8-9: Power Output and Payback Time vs X^* . Case 2C	130

1 INTRODUCTION

The production of useful power is essential for the technological, energy-intensive economy and lifestyle enjoyed by an ever-increasing number of the world's citizens. The vast majority of the useful power is obtained through the combustion of fossil fuels. These fossil fuels are extremely energy dense and usually inexpensive to mine, rendering most other methods of power production expensive by comparison. In recent times, however, reasons for developing and refining these alternative methods on large scales have been growing. Dependence of energy-hungry nations on oil-rich nations raises increasing socio-political concerns; debate over greenhouse gases spark public support for reducing environmental impact of energy-getting; signs of fossil fuel exhaustion may already exist (Caputo, 2009); and growing world population promises that demand for useful power will only increase. For these reasons, exploration into the feasibility of creative methods of power conversion to supplement fossil fuels is an essential endeavor.

1.1 Recovering Available Energy

This section contains a brief, qualitative overview of the relevant dynamics of energy conversion. A detailed treatment of the laws of thermodynamics is necessary for a technical discussion of waste heat in general, for which the reader is referred to Cengel and Boles (2008).

The vast majority of energy utilized from fossil fuels requires conversion of the chemical energy stored in the hydrocarbons to thermal energy (combustion), and then conversion of a

portion of that thermal energy to mechanical or electrical power. Any system that accomplishes this task—including power plants, planes, trains, and automobiles—may be called a heat engine. Although a heat engine converts thermal energy into power, the proportion that may be converted (thermodynamic efficiency) is limited by the second law of thermodynamics. Thermal energy that is not converted to power is dissipated to the environment, or rejected. Even a reversible heat engine which operates at the maximum theoretical efficiency rejects some heat to its surroundings. None of this heat is available to be converted to useful power. However, it is impossible to build a reversible heat engine, so all real heat engines reject some heat that can be converted to useful power.

Coal or other fossil-fueled power plants generally have thermodynamic efficiencies less than 40%. In the United States in 2008, total electricity consumption was estimated at 400 GW (Central Intelligence Agency) suggesting that more than 1000 GW of heat was released in the process. Significant quantities of this waste heat are theoretically recoverable—able to be transformed into power.

Direct energy conversion technologies such as thermophotovoltaics, pyroelectric devices, and thermoelectric devices represent methods of converting waste heat into power. Direct energy conversion devices are typically much less efficient than a traditional steam cycle in a power plant or internal combustion cycle in an automobile engine. However efficient operation of these traditional fluid cycles requires the very high temperatures and extremely rapid heat generation associated with combustion. In contrast, the direct energy conversion devices named above can work at much lower temperatures and comparatively low rates of heat transfer. When used as a bottoming cycle for a traditional power cycle, direct conversion devices can recover a portion of the rejected heat, and thus improve the overall efficiency at which fossil fuels are utilized.

Not only may such devices be used in tandem with established methods of energy conversion, but in other locations as well. Heat from geothermal sources, solar radiation, and heat produced and dissipated by the megawatts in factories represent potential sources for energy recovery by direct conversion devices. Any object or medium exhibiting a temperature perpetually hotter than its surroundings—naturally occurring or a consequence of man-made procedures—may in theory be used to manufacture power at some efficiency.

Large scale implementation of direct energy conversion methods to extract power from waste heat and naturally occurring temperature differences has the potential to generate a significant amount of power. Direct energy conversion on a large scale can increase the useful power extracted per unit of fossil fuel used and spread the burden of society's energy hunger to sources beyond fossil fuels. The value of augmenting our energy economy with direct energy conversion systems increases as the future of fossil fuels becomes less certain. Conversion of waste heat to useful power is scientifically and technologically feasible through multiple methods at various efficiencies. The widespread implementation of such systems is currently held back by economic considerations.

This thesis specifically considers the potential of thermoelectric energy conversion devices for low temperature applications. Thermoelectric devices are already being manufactured by a number of companies for power generating applications. Research into methods of improving the performance of such devices is an active field of research—primarily in the field of materials science. This thesis, however, considers the performance of thermoelectric devices that are now generally available for purchase. A specific design for a thermoelectric power generation system is proposed and analytically modeled. Using the model developed, economic considerations are then addressed. This thesis attempts to answer the

questions: What is the payback time for waste heat recovery system?; Under what conditions is a thermoelectric waste heat recovery system economically viable?

1.2 Thermoelectric Materials

This research is concerned with thermoelectric energy conversion devices, which are composed of thermoelectric materials. Thermoelectric materials are materials that naturally create a voltage difference in the presence of a temperature difference. For one family of thermoelectric materials, known as N-type materials, this voltage is caused when electrons or negative ions, excited by the thermal energy in the hotter side of the material, diffuse toward the cooler side of the material. The imbalance of charge creates an electric potential, or voltage. For the other family of materials, P-type materials, the temperature gradient causes holes (electron voids) or positive ions, to diffuse to the cooler side, causing the opposite voltage of an N-type material.

The temperature-induced voltage of thermoelectric materials is called the Seebeck effect, after Thomas Johann Seebeck who discovered the phenomenon in 1821 (Encyclopaedia Britannica, 2011). The reverse process may also be realized, with an imposed voltage on a thermoelectric material producing a heat pump. This process is generally referred to as the Peltier effect, demonstrated by Jean Charles Athanase Peltier in 1834. For information regarding the physics of thermoelectric materials and their engineering applications, the reader is referred to a wealth of research assembled by Rowe (2006).

From a macroscopic, continuum view, materials exhibiting the Seebeck effect may be described by their Seebeck coefficient, α , which represents the voltage produced per unit of temperature gradient in a material: $\alpha = dV/dT$. For N-type materials, α is positive, and for P-type

materials, α is negative. Knowledge of the Seebeck coefficient of a material allows for predicting thermoelectric behavior from knowledge of the temperature distribution in the material.

1.3 Objectives

The objective of this thesis is to perform a first principles analysis of a direct energy conversion device based on a thermoelectric generator. This analysis will be extended to a systems level analysis of thermoelectric generators and the thermal pathways designed to transport heat to, from, and around them. A classic heat transfer solution to convecting pin fins will be combined with a Nusselt number correlation developed by other researchers to characterize the heat paths to and from thermoelectric devices as fluid streams flowing through heat sinks. A tailored definition of friction factor will be discussed to model fan or pump work requirements. The concept of bypass insulation will be introduced as well as its potential to enhance the effectiveness of cost-effective energy conversion. All relations will be incorporated into a single, closed form, analytical model that govern a specific design template for a thermoelectric energy harvester containing multiple thermoelectric devices.

Experimental results will be presented which validate the model for a system consisting of a single thermoelectric device. The mathematical model in relation to this particular experiment will be discussed.

An economic model will be developed for predicting the payback time of the proposed energy harvesting system. The physical and analytical models will be coupled and extended to capture two-dimensional spatial effects of a large system. The extended model will be used to optimize a thermoelectric energy conversion system for specific cases, with the objective function of minimizing the payback time.

2 THERMOELECTRIC MODELING

This chapter presents a recommended system of governing equations of a single thermoelectric element, derived from first principles. The usefulness of these equations in describing heat transfer through a thermoelectric device is presented, preparatory to deriving the full system model.

2.1 Single Thermoelement: Exact Solution

Consider a thermoelectric element with one-dimensional heat transfer. The ends of the element are at T_H and T_L respectively. The voltage produced by the element is connected in a circuit to an electrical load that performs useful work. Three heat interactions exist in the element: heat conduction due to the temperature gradient, heat generation due to electrical resistance heating, and heat conversion into electrical power due to the thermoelectric effect.

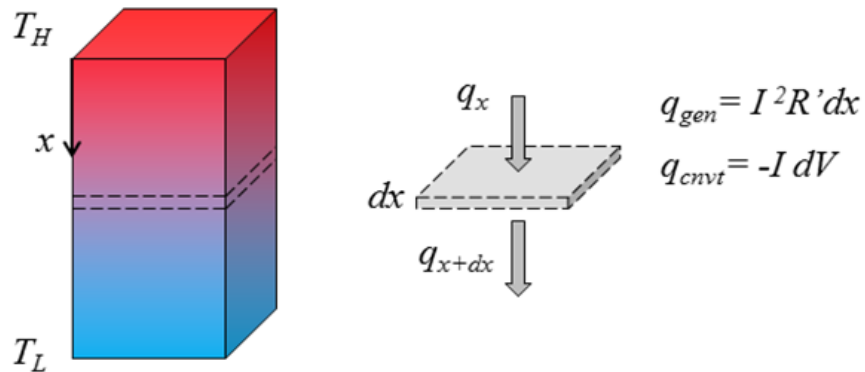


Figure 2-1: Thermoelement and Differential Heat Interactions.

The governing equation of the temperature profile may be found by constructing an energy balance on a differential piece of the thermoelement. Constant properties are assumed and heat transfer is approximated as one-dimensional. The Seebeck coefficient, α , represents the differential voltage generated across the element.

$$dV = \alpha dT \quad 2-1$$

Although Seebeck coefficient exhibits some dependency on temperature, the use of a constant, averaged value may be reasonably used (Rowe). Then Eq. 2-1 may be integrated over the entire element to yield

$$\Delta V = \alpha \Delta T \quad 2-2$$

Consider the differential section of the thermoelement in Fig. 2-1. Performing an energy rate balance yields the following differential equation:

$$q_x - \left(q_x + \frac{dq_x}{dx} dx \right) + I^2 R'_{el} dx - \left(-I\alpha \frac{dT}{dx} \right) dx = 0 \quad 2-3$$

Heat transfer is assumed to be one dimensional through the element. When Fourier's heat law of heat conduction is used in place of q_x , the following governing equation for temperature is obtained:

$$\frac{d^2 T}{dx^2} + \left(\frac{I\alpha}{k_{el} A_{el}} \right) \frac{dT}{dx} + \frac{I^2 R'_{el}}{k_{el} A_{el}} = 0 \quad 2-4$$

This equation may be solved analytically, using the temperatures at both ends as boundary conditions to obtain the temperature distribution,

$$T(x) = T_H - \left(\frac{I R'_{el}}{\alpha} \right) x + \left(\frac{T_L - T_H + \frac{I R'_{el} L}{\alpha}}{1 - e^{-\frac{I\alpha}{k_{el} A_{el}} L}} \right) \left(1 - e^{-\frac{I\alpha}{k_{el} A_{el}} x} \right) \quad 2-5$$

The nondimensionalization of this temperature profile may be done with a dimensionless current

$$i = \frac{IR'_{el}L}{\alpha(T_H - T_L)} \quad 2-6$$

The remaining nondimensionalization is performed with the definition of the thermoelectric performance parameter, $Z = \alpha^2/R'_{el}k_{el}A_{el}$. This parameter represents the ability of the thermoelement to generate a voltage compared to its other material properties. It is desirable for this parameter to be large. The significance of this parameter is discussed in Chapter 2.3, when this parameter is extended to describe an entire thermoelectric device. This parameter has units of inverse temperature, and may be nondimensionalized as $\zeta_H = ZT_H$. This and the Carnot efficiency $\eta_c = 1 - T_L/T_H$, are used to normalize Eq. 2-5 as

$$\frac{T(x)}{T_H} = 1 - i\eta_c \left(\frac{x}{L_{el}} \right) + \left(\frac{\eta_c(i-1)}{1 - e^{-\zeta_H\eta_c i}} \right) \left(1 - e^{-\zeta_H\eta_c i \left(\frac{x}{L_{el}} \right)} \right) \quad 2-7$$

Employing Fourier's law once again to solve for the heat rate into and out of the element, the nondimensional heat rates are found:

$$\frac{q_H}{U_{el}(T_H - T_L)} = i + \frac{(i - i^2)\zeta_H\eta_c}{1 - e^{-\zeta_H\eta_c i}} \quad 2-8$$

$$\frac{q_L}{U_{el}(T_H - T_L)} = i + \frac{(i - i^2)\zeta_H\eta_c e^{-\zeta_H\eta_c i}}{1 - e^{-\zeta_H\eta_c i}} \quad 2-9$$

The heat rates may be used to determine the thermodynamic (first law) efficiency of the element. Using the following relation for thermodynamic efficiency,

$$\eta_I = \frac{q_H - q_L}{q_H} \quad 2-10$$

and substituting Eqs. 2-8 and 2-9, the following equation is obtained:

$$\eta_I = \frac{(i - i^2)(1 - e^{-\zeta_H \eta_c i})}{\frac{i}{\zeta_H \eta_c} (1 - e^{-\zeta_H \eta_c i}) + i - i^2} \quad 2-11$$

Equation 2-11 gives the interesting result that the thermodynamic efficiency of a thermoelectric generator depends on the dimensionless current, i . To illustrate, consider the circuit below, with the thermoelement represented by a voltage source and an electrical resistance (Fig. 2-2).

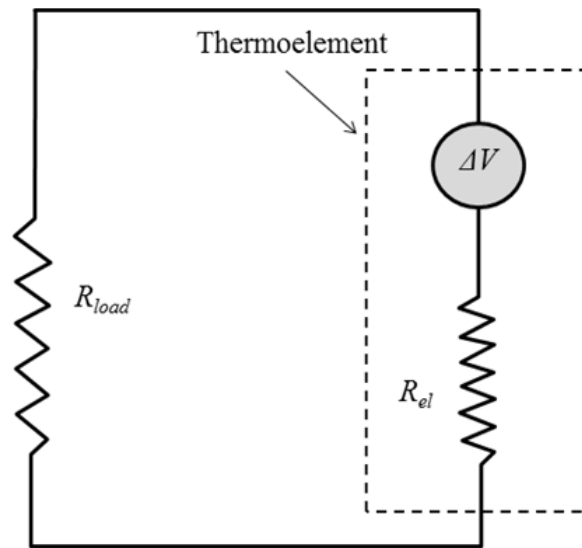


Figure 2-2: Thermoelement with Load.

A load is connected in the circuit, representing the useful power obtained from the element.

Applying Kirchoff's law results in

$$\Delta V = I(R_{el} + R_{load}) \quad 2-12$$

By solving Eq. 2-6 for current I in terms of dimensionless current i , and substituting the result into the Eq. 2-12, the voltage difference may be written

$$\Delta V = \frac{\alpha(T_H - T_L)i}{R_{el}}(R_{el} + R_{load}) \quad 2-13$$

Using Eq. 2-2 to replace voltage shows that dimensionless current, i , may be written as

$$i = \frac{R_{el}}{R_{el} + R_{load}} \quad 2-14$$

This equation shows the usefulness of the parameter i . The load imposed on a thermoelectric system is a critical design choice, affecting the efficiency and power output of the system. The chosen load is manifest in the thermodynamic efficiency through the variable i . Efficiency may be maximized by using Eq. 2-11 to calculate the derivative of the thermal efficiency with respect to dimensionless current, $d\eta/di$. Setting this to zero yields the maximum efficiency when $i_{eff} = 1/2$.

Alternatively, the power produced by the thermoelement is given by the product of the heat rate into the device and the thermal efficiency, $\eta I q_H$, or the product of Eqs. 2-8 and 2-11. Nondimensionalizing the power produced with U_{el} and T_H results in

$$\frac{\dot{W}_{out}}{U_{el}T_H} = \zeta_H \eta_c^2 (i - i^2) \quad 2-15$$

This parabolic behavior of power output is maximized at $i_{pow} = 1/2$.

The preceding analysis has shown that the governing equation derived for the thermoelement, Eq. 2-4, predicts that maximum efficiency and maximum power both occur at $i = 1/2$. Observing Eq. 2-14, this corresponds to an electrical load resistance equal to the electrical resistance of the thermoelement. Henceforth, this will be referred to as the matched load condition.

2.2 Single Thermoelement: Approximate Solution

2.2.1 Derivation

The exact solution to the temperature profile and work output of a thermoelement is convenient when the temperatures T_H and T_L of the thermoelement are known. However, in most real situations, these temperatures would be impractical to measure directly. In order to develop a full system model (see Chapter 3), thermoelement behavior must be coupled with equations modeling heat transfer from a heat source and to an ambient reservoir. Coupling the heat rates associated with the exact solution developed in the last chapter (Eqs. 2-8 and 2-9) with heat transfer analysis yields a coupled system of implicit algebraic equations. In order to form a model that yields closed-form solutions when coupled with heat transfer equations, the exact solution developed in the last section is now modified. The method of deriving this approximate solution is now presented.

The approximate solution is introduced as follows. First, the thermoelectric effect, q_{cvt} , is neglected in the governing energy balance of Fig. 2-1. This reduces the governing equation to

$$\frac{d^2T}{dx^2} + \frac{I^2 R'_{el}}{k_{el} A_{el}} = 0 \quad 2-16$$

Again, the temperatures at each end are used as boundary conditions. The solution to this equation is a parabolic profile,

$$T(x) = -\left(\frac{I^2 R'_{el}}{2k_{el} A_{el}}\right)x^2 + \left(\frac{T_L - T_H}{L_{el}} + \frac{I^2 R'_{el} L_{el}}{2k_{el} A_{el}}\right)x + T_H \quad 2-17$$

When this temperature profile is nondimensionalized in the same manner as Eq. 2-7, the result is

$$\frac{T(x)}{T_H} = 1 + \eta_c \left(\frac{1}{2} \zeta_H \eta_c i^2 - 1\right) \left(\frac{x}{L_{el}}\right) - \frac{1}{2} \zeta_H \eta_c^2 i^2 \left(\frac{x}{L_{el}}\right)^2 \quad 2-18$$

Note that there are no exponential terms in this profile. This characteristic will prove useful when the profile is used to calculate heat rates, which in turn must be coupled with heat transfer relationships. The temperature profiles predicted by Eq. 2-7 and Eq. 2-18 are compared in Fig. 2-3 for a typical thermoelement.

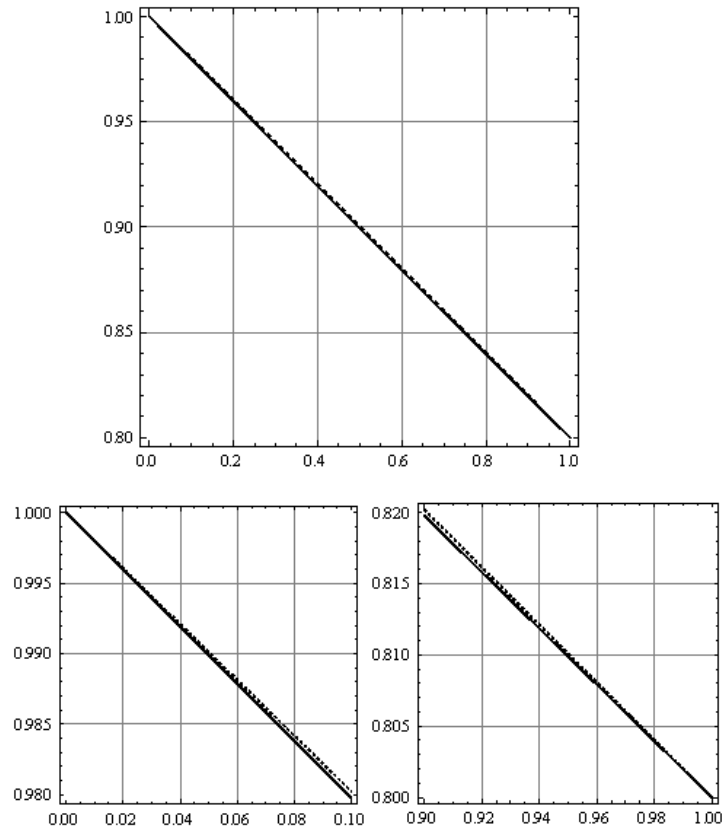


Figure 2-3: Thermoelement Temperature Profiles. $T(x)/T_H$ vs x/L for a typical case. The dashed line neglects power conversion in the element (Eq. 2-18), and the solid line incorporates it (Eq. 2-7).

Although the difference between the temperature profiles in Fig. 2-3 is barely discernable, it can be seen that the gradients are slightly steeper for the case incorporating power generation. The heat rates calculated when neglecting power generation will predict slightly less heat drawn into the element and slightly more heat rejected from the element than in the real case

with power generation. This is because the real element must draw in extra heat to replace the thermal energy lost to power conversion. Likewise, the heat that is rejected from the element is lessened because some of the heat input was converted to power as it passed through the element. In both cases, the linear effect of the heat transfer dominates, but the temperature gradient of the exact solution is slightly steeper at the hot end and slightly shallower at the cold end.

Heat rates for the dimensional temperature profile when power generation is neglected (Eq. 2-17) are calculated as

$$q_H = U_{el}(T_H - T_L) - \frac{1}{2}IR_{el} \quad \mathbf{2-19}$$

$$q_L = U_{el}(T_H - T_L) + \frac{1}{2}IR_{el} \quad \mathbf{2-20}$$

Now the thermoelectric effect will be reintroduced. Recall Eq. 2-2, which makes the approximation of constant Seebeck coefficient, α , but is independent of the nature of the temperature profile through the element. Thus, the voltage across the element is

$$V = \alpha(T_H - T_L) \quad \mathbf{2-21}$$

Thus, the power created by the Seebeck voltage is

$$P = I\alpha(T_H - T_L) \quad \mathbf{2-22}$$

The quantification of the power produced by the thermoelement together with the observations relating to Fig. 2-3 lead to the following approximation: the heat rate predicted by Eq. 2-19 is augmented by the Seebeck effect by roughly half of the Seebeck power, and the heat rate predicted by Eq. 2-20 is decreased by roughly the same amount. Modifying Eqs. 2-19 and 2-20 accordingly yields the true heat rates for the approximate solution:

$$q_H = U_{el}(T_H - T_L) - \frac{1}{2}I^2R_{el} + \frac{1}{2}I\alpha(T_H - T_L) \quad 2-23$$

$$q_L = U_{el}(T_H - T_L) + \frac{1}{2}I^2R_{el} - \frac{1}{2}I\alpha(T_H - T_L) \quad 2-24$$

Equations 2-23 and 2-24 are comparable to Eqs. 2-8 and 2-9. Due in large part to the dominance of the linear characteristic of the heat transfer, the difference between the approximate heat rates and the exact heat rates is negligible. The following table illustrates the discrepancy between the heat rates predicted by Eqs. 2-8 and 2-9 compared to Eqs. 2-23 and 2-24 with typical values for the parameters. The difference is far smaller than the general uncertainty calculated in the experimental validation (Chapter 6) performed in this research, which was on the order of several percent.

Table 2-1: Comparison of Exact and Approximate Heat Rate Solutions.

<i>Example Cases</i>			<i>Heat Into Element: q_H</i>			<i>Heat Rejected From Element: q_L</i>		
<i>U (K/W)</i>	<i>$T_H - T_L$ (K)</i>	<i>$Z \times 10^3$ (K⁻¹)</i>	Exact Eq. 2-8 (W)	Approximate Eq. 2-23 (W)	% Difference	Exact Eq. 2-9 (W)	Approximate Eq. 2-24 (W)	% Difference
2	200	0.8	408.10666	408.00000	-0.0261%	392.10666	392.00000	-0.0272%
2	50	0.8	100.50167	100.50000	-0.0017%	99.50167	99.50000	-0.0017%
1	100	0.5	100.62760	100.62500	-0.0026%	99.37760	99.37500	-0.0026%
1	30	0.5	30.05632	30.05625	-0.0002%	29.94382	29.94375	-0.0002%

The approximate solutions for heat rates may be used to predict the thermodynamic efficiency of the element in the same manner done for the exact solution. Substituting Eqs. 2-23 and 2-24 into the definition of thermodynamic efficiency and using the same nondimensionalization gives

$$\eta_I = \frac{i - i^2}{\frac{1}{Z(T_H - T_L)} + \frac{1}{2}(i - i^2)} \quad 2-25$$

Equation 2-25 may be multiplied by the heat rate of the hot end (Eq. 2-23) to predict the power output for the element, and can be shown algebraically to be equivalent to the equation for power output for the exact solution (Eq. 2-15). This establishes that the approximate solution, in agreement with the exact solution, predicts maximum power output at the matched load condition. Equation 2-25 has an analytical optimum at $i = 1/2$. Thus, like the exact solution, the approximate solution predicts that maximum power and maximum efficiency coincide at matched load conditions.

Although both solutions developed in this chapter predict that the matched load condition, $i = 1/2$, maximizes both power output and efficiency, these two do not necessarily coincide when the assumptions underlying the derivation are changed. Gordon (1991) presented a similar derivation for a thermoelement under different assumptions, and obtained

$$q_H = U_{el}(T_H - T_L) - \frac{1}{2}I^2R_{el} + I\alpha T_H \quad 2-26$$

$$q_L = U_{el}(T_H - T_L) + \frac{1}{2}I^2R_{el} + I\alpha T_L \quad 2-27$$

These are observed to be similar to Eqs. 2-23 and 2-24. These equations may be used to derive an efficiency equation using the same method outlined in this section to obtain the efficiency equation:

$$\eta_I = \frac{\left(1 - \frac{T_L}{T_H}\right)(i - i^2)}{i - i^2 \frac{\left(1 - \frac{T_L}{T_H}\right)}{2} + \frac{2 - \left(1 - \frac{T_L}{T_H}\right)}{2 \left(\frac{Z(T_H + T_L)}{2}\right)} \quad 2-28$$

This equation, like the ones developed here, predicts maximum power output at matched load ($i = 1/2$), but predicts that the optimum efficiency occurs at slightly greater than matched load. Despite their similarity to Eqs. 2-23 and 2-24, Eqs. 2-26 and 2-27 do not allow for a closed-form solution of the type that will be developed in Chapter 3 when coupled with heat transfer equations.

2.2.2 Observations on Efficiency

Some behavior regarding efficiency is noted. Comparison of Eq. 2-25 with 2-28 is shown in Fig. 2-4 for a specific case.

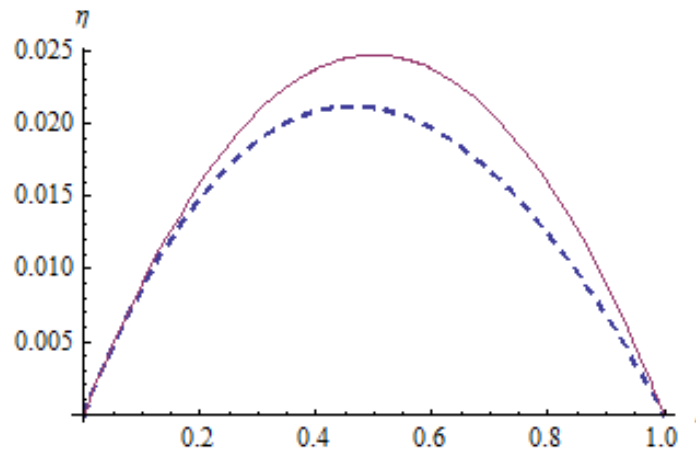


Figure 2-4: Thermodynamic Efficiency Curves. Comparison of relations derived by Gordon (dashed) and Taylor (solid). Values used: $T_H = 400\text{K}$, $T_L = 300\text{K}$, $Z = .001$.

The function derived here, is observed to be more optimistic than that derived by Gordon. Implications of this relating to the experimental data obtained in this research are mentioned in Chapter 5.

A topic of interest that is recommended for further research is the modeling of thermoelectric energy conversion using a second law of thermodynamics approach. The second law efficiency, η_{II} , is related to the thermodynamic efficiency through the relation

$$\eta_I = \eta_{II} \left(1 - \frac{T_L}{T_H}\right) \quad 2-29$$

Using this relation, η_{II} , may be derived from Eq. 2-25 as

$$\eta_{II} = \frac{i - i^2}{\zeta_H^{-1} + \frac{1}{2} \left(1 - \frac{T_L}{T_H}\right) (i - i^2)} \quad 2-30$$

When matched load is imposed, $i = 0.5$, and Eq. 2-28 is plotted, it is seen that the dependence on T_L/T_H is very weak.

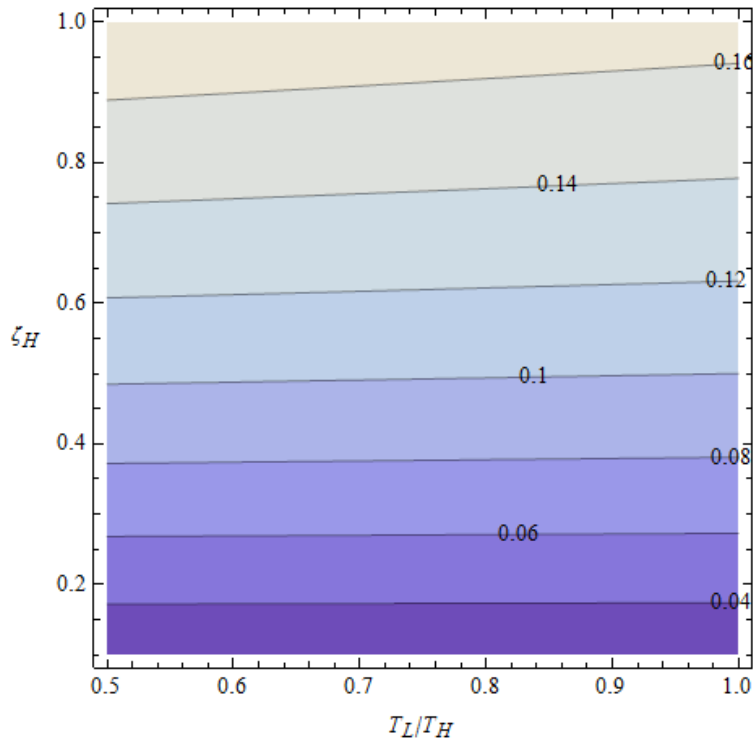


Figure 2-5: Second Law Efficiency for a Thermoelement. Contours of η_{II} (Equation 2-28).

When a plot similar to Fig. 2-5 is made for Eq. 2-26, the conclusion is the same. The relative independence of second law efficiency from T_L/T_H suggests that approximating η_{II} with Eq. 2-30 by simply holding T_L/T_H constant, rendering $\eta_{II} = \eta_{II}(\zeta_H)$ may provide a viable method of modeling the device. However, the approach would need to be different than that taken in this research, as it will be seen that the efficiency function is not used directly in Chapter 3 when a model is developed for the entire thermoelectric system. Rather, both heat rates from which the first law efficiency was derived, Eqs. 2-23 and 2-24, are used (and needed) to fully constrain the system.

As a topic of interest, it is noted that other methods of obtaining a solution of the type presented in Chapter 3 are theoretically possible. The limiting factor in obtaining this closed-form solution is the requirement that heat transfer equations describing heat into and out of the thermoelements be coupled with the characterization of the thermoelements themselves. Instead of using both heat rates, an efficiency function (such as Eq. 2-25, 2-28, or 2-30) together with one of the heat rates is sufficient to provide closure to the system. However, the author found this approach algebraically untenable when attempted with Eq. 2-25. Another possibility is to couple one of the heat rate equations with Eq. 2-30, when Eq. 2-30 is modified with T_L/T_H constant or as a simplified curve fit of the form $\eta_{II} = \eta_{II}(\zeta_H)$. This possibility was not explored in detail.

Another potential approximation might include modeling the temperature gradient as exactly linear through the element. This approximation was also explored by the author in conjunction with Eq. 2-28. It was found that an analytical solution under these conditions required a general solution to a cubic polynomial, which is attainable, but requires complex analysis. It is unlikely that closed-form solutions of the type developed in Chapter 3 could be

formed for all possible combinations of approximations, but it is also unlikely that this thesis utilizes the only such combination.

2.3 Thermoelectric Device Modeling

Thermoelectric devices are composed of many thermoelements. These elements are arranged such that all experience the same temperature gradient by being thermally parallel, but are connected end to end in electrical series (Fig, 2-6). The serial connection produces a single circuit incorporating all the elements, summing their voltages. N-type elements and P-type elements alternate in the circuit, so that voltages sum throughout the circuit. Power may be harvested by connecting an electrical load to contacts at the first and last element.

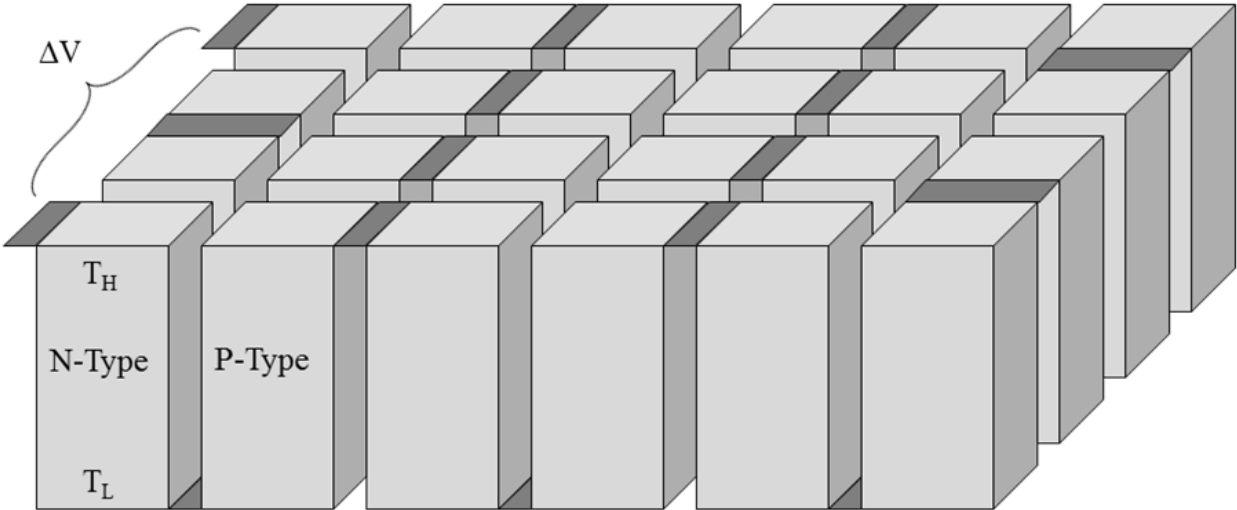


Figure 2-6: Typical Arrangement of Thermoelements in a Power Harvesting Device.

The analysis presented for a single element may be extended to an array of elements. The thermal conductance, the electrical resistance, and the effective Seebeck coefficient of the array

are the sum of those of the individual thermoelements. The Z parameter mentioned in conjunction with Eq. 2-7 may now be extended to represent the entire device as

$$Z_D = \frac{\alpha_D^2}{R_D U_D} \quad \text{2-31}$$

where the subscript, D , serves to remind that the figure of merit now serves for an entire device. This parameter, based on Seebeck coefficient, electrical resistance, and thermal conductance, has units of inverse temperature. This parameter represents a ratio of desired behavior (useful voltage) to undesirable requirements (internal resistance and ease of heat passage). The Z_D value represents the consolidation of these three characteristics, difficult to measure individually, into a single parameter that may be found through straightforward experimentation.

The Z_D value represents the thermoelectric device itself, independent of the operating temperatures (assuming constant properties) and as such is aptly described as a figure of merit (Gordon). However, because it is not dimensionless, the term “figure of merit” is used by many authors to indicate $Z_D T_{ref}$, where T_{ref} is some reference temperature related to the anticipated operating conditions of the device. Reference temperatures reported include T_L (Marlow Industries), and $(T_H + T_L)/2$ (Gordon, 1991). In this thesis, Z_D will be normalized against the temperature of a hot fluid stream, T_S , representing the source of thermal energy to be directed into the thermoelectric device. This temperature is chosen because it is constant for a given application. The temperature of the available fluid stream is not affected by the design of the system, whereas T_H and T_L are. This makes T_S more convenient for normalizing Z_D as well as many other variables that will be presented throughout the research.

Commercially available thermoelectric devices may contain hundreds of thermoelements. One thermoelectric device, manufactured by Thermal Electronics Corp., is pictured in Fig. 2-7. This device is one of the larger models available: 56 mm square and about 4 mm thick.

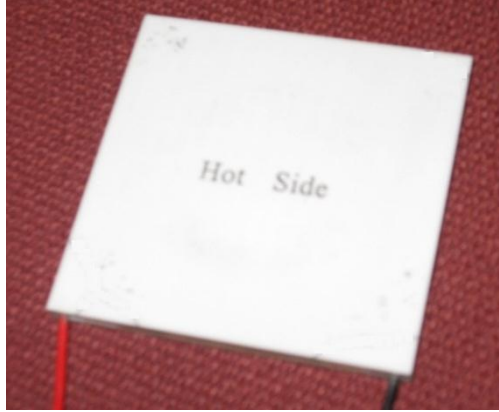


Figure 2-7: Photo of the TEG1-12611-6.0 Thermoelectric Generator. This device is manufactured by Thermal Electronics Corporation.

The heat rates calculated for a single thermoelement (Eqs. 2-23 and 2-24) may be used to calculate the heat rate of an array of thermoelements. Each term in these equations may be summed over all thermoelements to give the entire heat rate. The overall thermal conductance (being thermally parallel) is $U_D = \sum U_{el}$. The electrical resistance (being electrically in series) is $R_D = \sum R_{el}$. Considering that the N-type thermoelements and the P-type elements experience opposite temperature gradients with respect to their electrical connections, the voltage created by the Seebeck effect is

$$V_D = \sum_i \alpha_{Ni}(T_H - T_L) - \sum_j \alpha_{Pj}(T_H - T_L) \quad 2-32$$

Where α_N is the Seebeck coefficient for the N-type materials, and α_P is the Seebeck coefficient for the P-type materials. The existence of P materials would appear to compromise the voltage produced by the device. However, recall that the Seebeck coefficient of P-type materials is negative. Thus, the voltage created by the device may be represented

$$V_D = (T_H - T_L) \left(\sum_i \alpha_{Ni} + \sum_j |\alpha_{Pi}| \right) \quad 2-33$$

It is now convenient to define the term in parenthesis as a Seebeck parameter, α_D , that represents the voltage created by the entire array of elements. The heat rates developed for single thermoelement may be extended to describe an entire device composed of an array of elements:

$$q_{HD} = U_D(T_H - T_L) - \frac{1}{2}I^2R_D + \frac{1}{2}I\alpha_D(T_H - T_L) \quad 2-34$$

$$q_{LD} = U_D(T_H - T_L) + \frac{1}{2}I^2R_D - \frac{1}{2}I\alpha_D(T_H - T_L) \quad 2-35$$

These equations for heat rates are the critical contribution from the thermoelement analysis that will be used in deriving the general system solution in Chapter 3. Throughout the remainder of the thesis, the thermoelectric generators will be modeled as operating at matched load conditions.

3 GENERAL SYSTEM MODEL

3.1 Heat Path Layout

Consider a thermoelectric device sandwiched between two fin array heat sinks. One heat sink is exposed to a hot fluid stream at source temperature T_S , while the other heat sink is exposed to ambient temperature T_A .

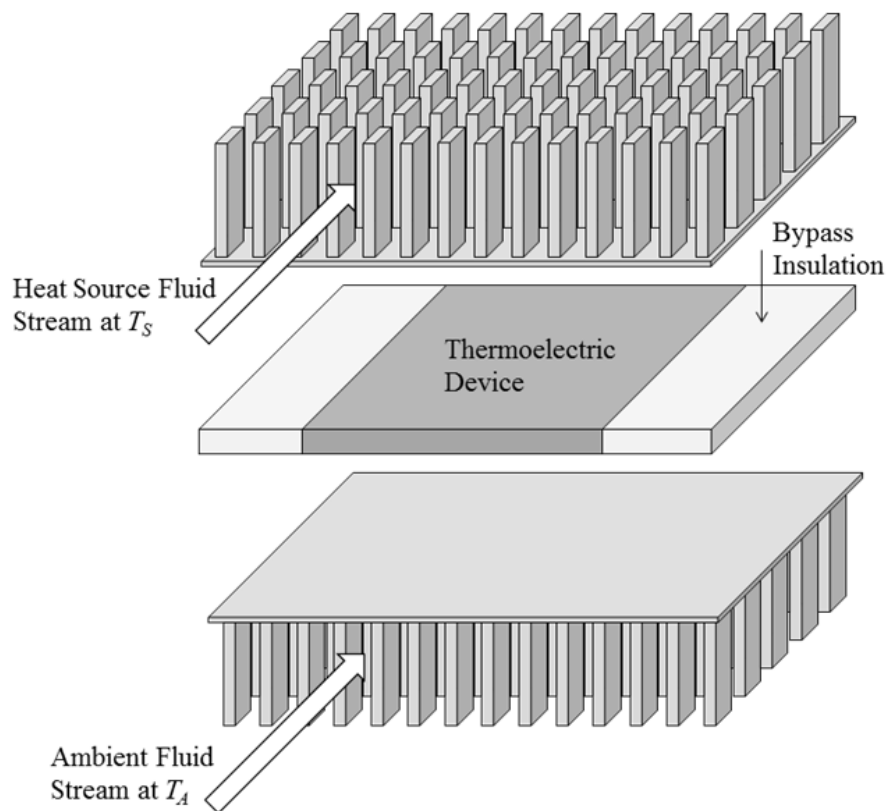


Figure 3-1: Thermoelectric System Layout.

Insulation surrounding the thermoelectric device allows for the heat sinks to be larger than the device itself and channels heat from the sinks through the device (Fig. 3-1). Although not shown in the figure, the system is shrouded along the sides and from above and below at exactly at the fin height.

Six temperatures in this model are of explicit importance. Two of these, the source temperature of the hot fluid stream, T_S , and the temperature of the stream of air taken from the ambient, T_A , are known. The other four must be solved for; they include:

- The temperature at the underside of the hot heat sink, T_{IH}
- The temperature at the underside of the cool heat sink, T_{IL}
- The temperature at the hot end of the thermoelements inside the device, T_H
- The temperature at the cool end of the thermoelements inside the device, T_L .

The subscript, I , in the first two temperatures was chosen to represent the word “Interface”, reflecting the fact that at this place the heat sinks interface with the thermoelectric device.

Figure 3-2 illustrates a thermal circuit describing the thermoelectric system. In this circuit, the temperatures T_S and T_{IH} are related through heat transfer from the hot fluid stream through the heat sink. Heat transfer is modeled with a linear heat transport coefficient, U_H . The same relationship is provided for T_A , T_{IL} , and U_L . Approximating T_{IH} and T_{IL} as single temperature nodes is equivalent to the assumption that the temperature of the heat sink base is everywhere the same. The validity of this particular assumption depends on the size of the bypass insulation. This particular assumption is discussed in detail in Chapter 5.

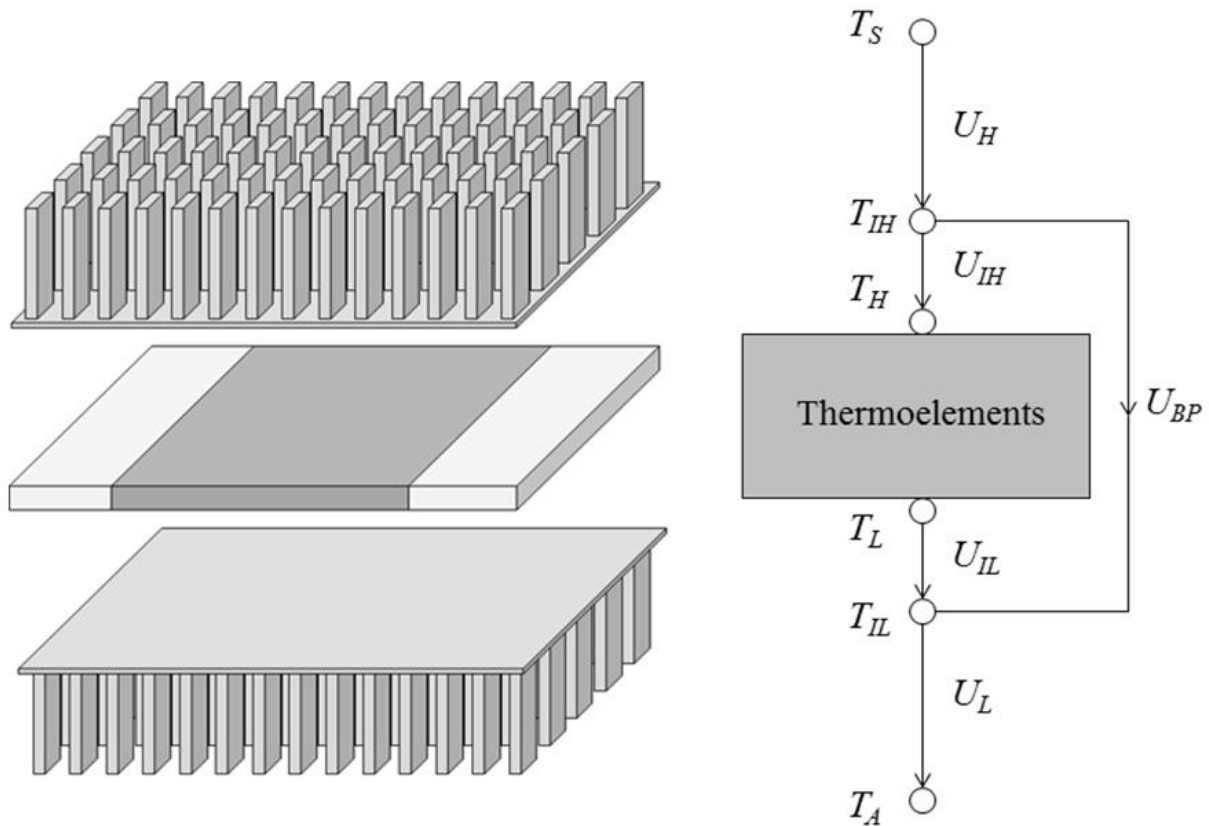


Figure 3-2: Thermal Circuit Corresponding to Thermoelectric System Layout.

The thermal conductance U_{IH} lumps the thermal resistance associated with the contact of the heat sink and the thermoelectric devices together with the thermal conductance of the ceramic cover of the device that protects the thermoelectric elements within. The conductance term U_{IH} separates T_H from T_{IH} , and U_{IL} accounts for the same path between T_L from T_{IL} . With these definitions, the variables T_H and T_L describe the actual high and low temperatures of the thermoelements within the device, as in Chapter 2. The thermal conductance of the bypass insulation, U_{bp} , is ideally much smaller than any of the other four, forcing heat to flow through the thermoelectric device. The thermoelectric device itself is characterized by a thermal conductance, U_D , usually on the order of 1 W/K depending on the size of the device. A common

thermal conductance per area, U_D ”, for a thermoelectric device would be $\sim 500 \text{ W/m}^2\text{K}$ (Marlow Industries), (Thermal Electronics Corp.).

3.2 Governing Equations for System

Modeling the thermoelectric system together with its heat paths begins with observing the thermal circuit in Fig. 3-2. The heat transport coefficients are modeled as uniform, and the heat rate through any part of the circuit may be represented

$$q_i = U_i \Delta T_i \quad 3-1$$

Using this relationship to represent heat rates, node balances may be performed on T_{IH} and T_{IL} to give the following equations:

$$U_H(T_S - T_{IH}) = U_{bp}(T_{IH} - T_{IL}) + U_{IH}(T_{IH} - T_H) \quad 3-2$$

$$U_L(T_{IL} - T_A) = U_{BP}(T_{IH} - T_{IL}) + U_{IL}(T_L - T_{IL}) \quad 3-3$$

Heat flow into and out of the thermoelement array as represented in the circuit may be equated with heat flow into and out of the thermoelements as expressed in Eqs. 2-30 and 2-31.

$$U_{IH}(T_{IH} - T_H) = U_D(T_H - T_L) - \frac{1}{2}I^2R_D + \frac{1}{2}I\alpha_D(T_H - T_L) \quad 3-4$$

$$U_{IL}(T_L - T_{IL}) = U_D(T_H - T_L) + \frac{1}{2}I^2R_D - \frac{1}{2}I\alpha_D(T_H - T_L) \quad 3-5$$

An energy balance on the device results in the equation for power output,

$$\dot{W}_{out} = U_{IH}(T_{IH} - T_H) - U_{IL}(T_L - T_{IL}) \quad 3-6$$

Finally, imposing the matched load condition imposes the following constraint on the electrical current through the device (see Eq. 2-6),

$$\frac{1}{2} = \frac{IR_D}{\alpha_D(T_H - T_L)} \quad 3-7$$

Equations 3-2 through 3-7 comprise the analytical model used to predict the behavior of a thermoelectric energy conversion system. In these six equations, the unknowns are T_H , T_{IH} , T_L , T_{IL} , I , and \dot{W}_{out} . Nondimensionalization and manipulation of these equations is presented here in sufficient detail to be replicated.

First, use Eq. 3-7 to eliminate electrical current, I , from Eqs. 3-4 and 3-5. Define the known temperature ratio, \mathbf{T} , as:

$$\mathbf{T} = \frac{T_A}{T_S} \quad 3-8$$

and the following unknown temperature ratios:

$$\tau = \frac{T_L}{T_H} \quad 3-9$$

$$\tau_I = \frac{T_{IL}}{T_{IH}} \quad 3-10$$

$$\gamma = \frac{T_H}{T_S} \quad 3-11$$

$$\gamma_H = \frac{T_H}{T_{IH}} \quad 3-12$$

Then Eqs. 3-2 through 3-5 may be nondimensionalized with $\zeta = Z_D T_S$ and using the thermal conductance of the device, U_D , to create thermal conductance ratios, Ψ , according to the pattern: $\Psi_i = U_i/U_D$. With these definitions and manipulations, the following system of equations is obtained.

$$\Psi_H \left(1 - \frac{\gamma}{\gamma_H}\right) = \Psi_{IH} \left(\frac{\gamma}{\gamma_H} - \gamma\right) + \Psi_{bp} \left(\frac{\gamma}{\gamma_H} - \frac{\tau_I \gamma}{\gamma_H}\right) \quad 3-13$$

$$\Psi_L \left(\frac{\tau_I \gamma}{\gamma_H} - \mathbf{T}\right) = \Psi_{IL} \left(\tau \gamma - \frac{\tau_I \gamma}{\gamma_H}\right) + \Psi_{bp} \left(\frac{\gamma}{\gamma_H} - \frac{\tau_I \gamma}{\gamma_H}\right) \quad 3-14$$

$$\Psi_{IH} \left(\frac{\gamma}{\gamma_H} - \gamma\right) = (\gamma - \tau \gamma) + \frac{\zeta}{8} (\gamma - \tau \gamma)^2 \quad 3-15$$

$$\Psi_{IL} \left(\tau\gamma - \frac{\tau_I \gamma}{\gamma_H} \right) = (\gamma - \tau\gamma) - \frac{\zeta}{8} (\gamma - \tau\gamma)^2 \quad 3-16$$

These four equations contain several nonlinearities. The following substitutions remove many of these nonlinearities to facilitate the solution:

$$X_o = \gamma - \tau\gamma \quad 3-17$$

$$Y_o = \frac{\gamma}{\gamma_H} - \gamma \quad 3-18$$

$$Z_o = \frac{\tau_I \gamma}{\gamma_H} \quad 3-19$$

$$W_o = \tau\gamma - \frac{\tau_I \gamma}{\gamma_H} \quad 3-20$$

Making these substitutions, Eq. 3-14 may be rearranged:

$$Z_o = \mathbf{T} + \frac{\Psi_{IL}}{\Psi_L} W_o + \frac{\Psi_{bp}}{\Psi_L} (X_o + Y_o + W_o) \quad 3-21$$

Using the same substitutions together with Eq. 3-21, Eq. 3-13 may be rearranged for Y_o :

$$Y_o = \frac{\Psi_H(1 - \mathbf{T}) - X_o \left(\Psi_H + \frac{\Psi_H \Psi_{bp}}{\Psi_L} + \Psi_{bp} \right) - W_o \left(\Psi_H + \frac{\Psi_H \Psi_{IL}}{\Psi_L} + \frac{\Psi_H \Psi_{bp}}{\Psi_L} + \Psi_{bp} \right)}{\Psi_{IH} + \Psi_H + \Psi_{bp} + \frac{\Psi_H \Psi_{bp}}{\Psi_L}} \quad 3-22$$

In this same manner, Eqs. 3-15 and 3-16 may both be solved for X_o using the quadratic solution.

In doing so, it can be seen that in both cases, only the upper root will give physical solutions due to the fact that X_o must be positive.

$$X_o = \frac{4}{\zeta} \left(1 - \sqrt{1 - \frac{\zeta}{2} \Psi_{IH} W_o} \right) \quad 3-23$$

$$X_o = \frac{4}{\zeta} \left(-1 + \sqrt{1 + \frac{\zeta}{2} \Psi_{IH} Y_o} \right) \quad 3-24$$

Removing X_o from these two equations and solving for W_o results in

$$W_o = \left(\frac{2}{\zeta \Psi_{IL}} \right) \left(1 - \left(2 - \sqrt{1 + \frac{1}{2} \zeta \Psi_{IH} Y_o} \right)^2 \right) \quad 3-25$$

Substitution of 3-23 and 3-25 into 3-22 gives an implicit solution for Y_o .

$$Y_o = \left(\frac{1}{\Psi_{IH} + \Psi_H + \Psi_{bp} + \frac{\Psi_H \Psi_{bp}}{\Psi_L}} \right) \left(\Psi_H (1 - \mathbf{T}) - \left(\frac{4}{\zeta} \left(-1 + \sqrt{1 + \frac{1}{2} \zeta \Psi_{IH} Y_o} \right) \right) \left(\Psi_H + \frac{\Psi_H \Psi_{bp}}{\Psi_L} + \Psi_{bp} \right) \right. \\ \left. - \left(\frac{2}{\zeta \Psi_{IH}} \right) \left(1 - \left(2 - \sqrt{1 + \frac{1}{2} \zeta \Psi_{IH} Y_o} \right)^2 \right) \left(\Psi_H + \frac{\Psi_H \Psi_{IL}}{\Psi_L} + \frac{\Psi_H \Psi_{bp}}{\Psi_L} + \Psi_{bp} \right) \right) \quad 3-26$$

With this equation, the system has been cast into a single equation and single unknown. However, the equation is implicit. By defining a new variable Y_1 containing Y_o , (and significant algebra!) this equation will yield a closed form solution.

$$Y_1 = \left(\frac{4D_o + C_o - \sqrt{(4D_o + C_o)^2 - 4(D_o - 1)(1 + B_o + C_o + 3D_o)}}{2(D_o - 1)} \right)^2 \quad 3-27$$

where

$$Y_o = \frac{Y_1 - 1}{\frac{1}{2} \zeta \Psi_{IH}} \quad 3-28$$

and

$$D_o = 1 + \frac{\Psi_H \Psi_{IL} - \Psi_{IH} \Psi_L}{\Psi_{bp}(\Psi_L + \Psi_H) + \Psi_L(\Psi_H + \Psi_{IH})} \quad 3-29$$

$$C_o = 2\Psi_{IH} \left(1 + \frac{\Psi_L \Psi_{IH}}{\Psi_{bp}(\Psi_L + \Psi_H) + \Psi_H \Psi_L} \right)^{-1} \quad 3-30$$

$$B_o = \frac{\zeta}{2} \left(\frac{\Psi_L \Psi_H \Psi_{IH} (1 - \mathbf{T})}{\Psi_L(\Psi_{IH} + \Psi_H) + \Psi_{bp}(\Psi_L + \Psi_H)} \right) \quad 3-31$$

Note that Eq. 3-27 is undefined when $D_o = 1$. In the special case where $D_o = 1$, the solution for Y_I is

$$Y_1 = \left(1 + \frac{B_o}{C_o + 4}\right)^2 \quad 3-32$$

When thermal conductance on each side of the device is equal ($\Psi_H = \Psi_L$ and $\Psi_{IH} = \Psi_{IL}$) then $D_o = 1$, and Eq. 3-32 must be used instead of Eq. 3-27. This approximation is appropriate if heat sinks, fluid properties, and flow velocity are anticipated to be the same on each side of the system.

Equation 3-27 (or Eq. 3-32) represents the first step of the solution in which an unknown parameter is solved for by combinations of known inputs. The knowledge of Y_I is then back-substituted to find the intermediate equations X_o , Y_o , W_o , and Z_o . Rearranging Eqs. 3-17 through 3-20 allows the temperature ratios to be calculated:

$$\tau = \frac{Z_o + W_o}{X_o + Z_o + W_o} \quad 3-33$$

$$\tau_I = \frac{Z_o}{X_o + Y_o + Z_o + W_o} \quad 3-34$$

$$\gamma = X_o + Z_o + W_o \quad 3-35$$

$$\gamma_H = \frac{X_o + Z_o + W_o}{X_o + Y_o + Z_o + W_o} \quad 3-36$$

From here, the temperatures and the power output may be solved from knowledge of T_S . In nondimensional space, Eq. 3-6 is used to expressed power output as

$$\frac{\dot{W}_{out}}{U_D T_S} = \dot{W}_{out}^* = \Psi_{IH} \gamma (\gamma_H^{-1} - 1) - \Psi_{IL} \gamma (\tau - \tau_I \gamma_H^{-1}) \quad 3-37$$

Although this is a convenient, closed-form solution, it is somewhat unwieldy for efficient use by hand. For programming purposes, however, the model is much more versatile as closed-form

functional relationships than an equation or set of implicit equations requiring numerical techniques to solve.

In this analysis, the thermal conductance ratios Ψ_H , Ψ_{IH} , Ψ_L , Ψ_{IL} , and Ψ_{bp} are treated as known. However, calculating the thermal transport coefficients and obtaining these ratios is an involved process. The next chapter is devoted to the detailed analysis of the heat sinks, which provides for the calculation of Ψ_H , Ψ_{IH} , Ψ_L , and Ψ_{IL} .

4 HEAT SINK MODELING

4.1 Heat Transfer

In order for thermoelectric energy conversion to be most effective, the temperature at the hot side of the thermoelements, T_H , in the device must be as close as possible to the temperature of the source stream, T_S . Likewise, the temperature T_L must be as close as possible to T_A . This is achieved by minimizing thermal resistance between the streams and the thermoelements. In order to achieve this, the use of straight, rectangular fin arrays is considered. Fins of regular, rectangular cross-section are inexpensive to manufacture and provide high heat transfer. The approach outlined here builds on previous work regarding fins of rectangular cross-section published by Kim, Kim, and Ortega (2004).

4.1.1 Heat Conduction in Fins

The individual fins of a heat sink are modeled as having one-dimensional heat conduction. Heat conduction through the fin is assumed to obey Fourier's Law:

$$q'' = -k \frac{dT}{dy} \quad 4-1$$

A differential energy balance illustrated in Fig. 4-1 yields Eq. 4-2 which may be solved using the boundary condition of T_B at the fin base. Fins are modeled as being exactly as long as the shroud height containing the fluid stream. Thus, the fin tips will be in contact with the shroud, which

will inhibit heat transfer. For this reason, an adiabatic fin tip is used as the most appropriate tractable boundary condition in analytically solving for the temperature distribution of the fin.

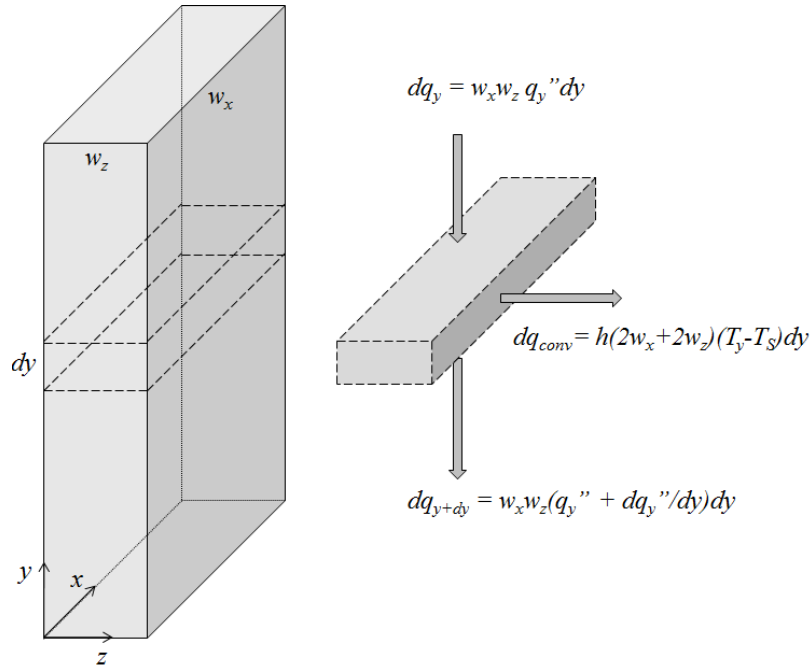


Figure 4-1: Single Fin Analysis.

Summing the heat interactions on the differential element results in the governing equation for the fin. The equation together with its boundary conditions is

$$\frac{d^2 T}{dy^2} - \frac{4h}{k_{sink} d_p} (T - T_S) = 0 \quad y = 0, T = T_B; \quad y = L, \frac{dT}{dy} = 0 \quad 4-2$$

The solution to this equation yields the temperature profile

$$T(y) = T_S + (T_B - T_S) \frac{\cosh\left(2(L - y) \sqrt{\frac{h}{k_{sink} d_p}}\right)}{\cosh\left(2L \sqrt{\frac{h}{k_{sink} d_p}}\right)} \quad 4-3$$

Substituting Eq. 4-3 into Eq. 4-1 at the base of the fin ($y = 0$) yields the rate at which heat travels to the base of the fin,

$$q_{fin} = 2 \sqrt{\frac{h k_{sink}}{d_p}} w_x w_z \tanh \left(2L \sqrt{\frac{h}{k_{sink} d_p}} \right) (T_B - T_S) \quad 4-4$$

For a fluid stream cooler than the heat sink, T_A is used in place of T_S , and the preceding analysis yields the rate of heat out of the base of the fin. The fin analysis presented here is duplicated in most heat transfer texts. For further information on this and other classical solutions for fins, Incropera et al. (2007) is recommended.

4.1.2 Heat Transfer Through Heat Sink

The previous analysis will be extended to the array of fins in the system; in doing so, it is necessary to describe the total cross-sectional area of the entire system. Fig. 4-2 shows a potential system with 20 thermoelectric generators. Rows of thermoelectric generators are separated by rows of insulation. Observe that the cross-sectional area of the system is equal to the cross-sectional area of the devices plus the area of all the bypass insulation. All of this area is covered by each fin array. When representing the total area spanned by the system, it is convenient to use the fin array. The total area of the system is expressed as the sum of the areas apportioned to each fin multiplied by the number fins spanning the entire system. The area spanned by this system is calculated by calculating the area allotted to each fin, and multiplying by the number of fins.

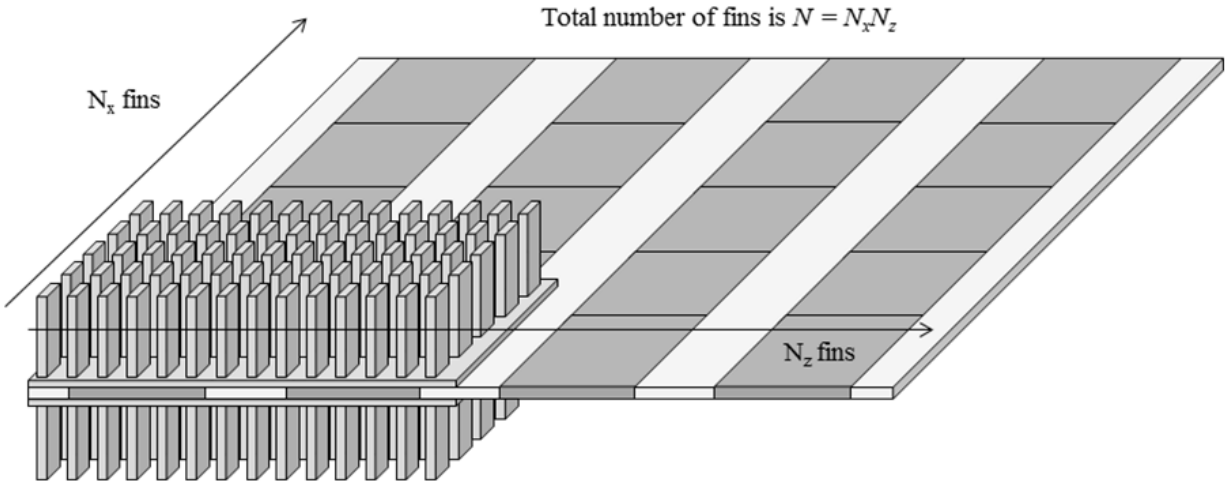


Figure 4-2: System Layout: Fin Array Dimensions.

Figure 4-3 provides a zoomed view of the individual fins of the array. The area allotted to each w_x by w_z fin is t_x by t_z . The system contains N_x fins in the flow direction and N_z fins in the normal direction for a total of $N_x N_z = N$ fins. The total area that the system spans is

$$A_{sys} = N t_x t_z \quad 4-5$$

Heat transfer is modeled with an average uniform convection coefficient, h . Although the true convection coefficient is a function of the detailed characteristics of the field, it is standard practice to correlate heat transfer to an *average* Nusselt number. The average Nusselt number allows for calculation of an average convection coefficient, h , which is correlated to predict heat transfer under the assumption of uniformity.

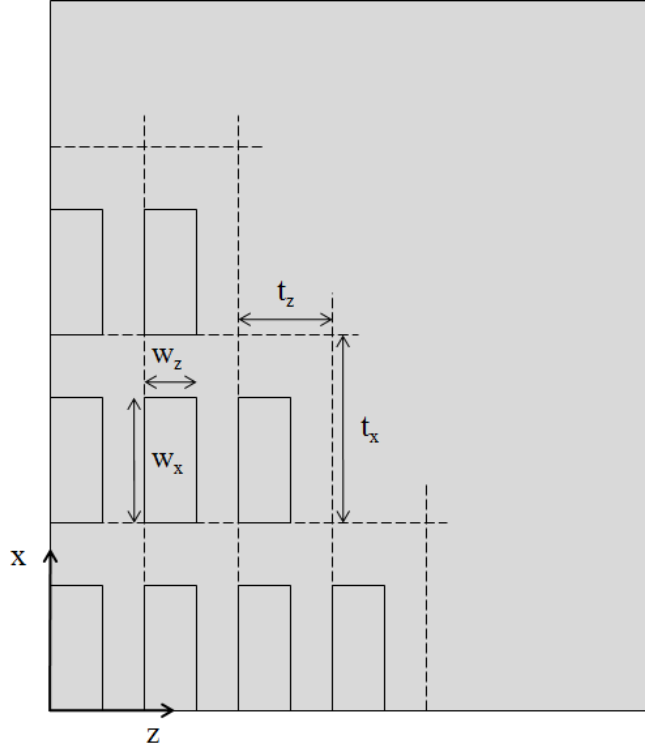


Figure 4-3: Top View of Fin Array. Each w_x by w_z fin requires a t_x by t_z area. The area spanned by the entire system is $Nt_x t_z$.

The sum total of heat transferred from the hot fluid stream to the heat sink is

$$q_{sink} = N \left(2 \sqrt{\frac{h k_{sink}}{d_p}} w_x w_z \tanh \left(2L \sqrt{\frac{h}{k_{sink} d_p}} \right) \right) (T_B - T_S) + N(t_x t_z - w_x w_z) h (T_B - T_S) \quad 4-6$$

It follows that the thermal conductance associated with the fins of the sink is

$$U_{Hfins} = N \left(2 \sqrt{\frac{h k_{sink}}{d_p}} w_x w_z \tanh \left(2L \sqrt{\frac{h}{k_{sink} d_p}} \right) \right) + N(t_x t_z - w_x w_z) h \quad 4-7$$

The thermal conductance through the base of the heat sink is

$$U_{Hbase} = \frac{k_{sink} N t_x t_z}{L_b} \quad 4-8$$

where L_b is the thickness of the base of the heat sink, and the fins and base are assumed to be characterized by the same thermal conductivity, k_{sink} . These thermal conductances are arranged in series, which means that for an equivalent thermal conductance they must be combined in the following manner to form the overall thermal conductance U_H .

$$U_H = \frac{U_{Hfins}U_{Hbase}}{U_{Hfins}+U_{Hbase}} \quad 4-9$$

This process is the same for calculating U_L , where parameters and geometry pertaining to the heat sink exposed to the ambient stream are used.

In Chapter 8, the equations for U_H and U_L will be used to form the dimensionless thermal conductance ratios Ψ_H and Ψ_L . When this is done, the thermal conductance per area will be useful. These are denoted with the double prime, " , having units of W/Km^2 instead of W/K . They are defined by dividing by area thus,

$$U_{Hfins}'' = \frac{U_{Hfins}}{Nt_x t_z} \quad 4-10$$

$$U_{Hbase}'' = \frac{U_{Hbase}}{Nt_x t_z} \quad 4-11$$

The combined thermal conductance per area is found by Eqs. 4-10 and 4-11 in the same manner as before, or equivalently, by dividing the combined thermal conductance by the total area.

$$U_H'' = \frac{U_{Hfins}''U_{Hbase}''}{U_{Hfins}'' + U_{Hbase}''} = \frac{U_H}{Nt_x t_z} \quad 4-12$$

Equations 4-6 through 4-12 may be adapted to yield U_L'' , when parameters pertaining to the sink exposed to the ambient stream are used. In Chapter 8, the equations for U_H'' and U_L'' will be used to form the dimensionless thermal conductance ratios Ψ_H and Ψ_L .

4.1.3 Interfacial Heat Transfer

The thermal conductance separating the temperature T_{IH} from T_H (T_{IL} from T_L on the ambient side) is treated similarly. These thermal conductances are termed “interfacial” conductances and are given a subscript I . This interfacial conductance is composed of the reciprocal of the thermal contact resistance between the heat sink and the thermoelectric device together with the thermal conductance of the protective ceramic cover shielding the thermoelements. The thermal conductances per area are:

$$U''_{IHcontact} = \frac{1}{R''_{contact}} \quad 4-13$$

$$U''_{IHcover} = \frac{k_{cover}}{L_{cover}} \quad 4-14$$

Combining these equations yields a single parameter describing the overall interfacial thermal conductance per area.

$$U''_{IH} = \frac{U''_{IHcontact}U''_{IHcover}}{U''_{IHcontact} + U''_{IHcover}} \quad 4-15$$

which may be simplified to

$$U''_{IH} = \frac{k_{cover}}{L_{cover} + k_{cover}R''_{contact}} \quad 4-16$$

The interfacial conductance, U''_{IL} , is found in like manner with parameters pertaining to the heat sink in the ambient stream. These conductances have units of W/m^2K . However, unlike U_H and U_L , The ‘per area’ aspect of this conductance does not refer to the entire area spanning the system, but only those parts of the cross-sectional area associated with the thermoelectric devices contained in the system.

In Chapter 8, the equations for U''_{IH} and U''_{IL} will be used to form the dimensionless thermal conductance ratios Ψ_{IH} and Ψ_{IL} .

4.1.4 Heat Transfer Correlation

In order to use the equations so far discussed to find U_H or U_L , the average convection coefficient, h , must be known. For this purpose, a Nusselt Number correlation approach is taken. When calculating convective heat transfer for a large number of cases, or for a case where only a first approximation is needed, this approach is usually preferable over numerical simulations if a correlation is readily available. Recent experimental work in developing a Nusselt number correlation for heat sinks of regularly repeating, rectangular, in-line fins was performed by Kim, Kim, and Ortega (2004). Using air as the working fluid, they tested 16 square fin heat sinks with varying geometries. The heat sinks were tested in a shroud that circumscribed the fins of the sinks in the same manner proposed for the design of a thermoelectric power conversion system. The reader is referred to their paper for details regarding that work. The average Nusselt number, Nu , was correlated to Reynolds number, Re_d with the following form:

$$Nu = \frac{h d_p}{\epsilon k_f} = C_1 Re_d^m \quad 4-17$$

This correlation is based upon total heat sink porosity ϵ . The directional porosities describe fin spacing. The x-directional porosity describes fin spacing normal to the x direction, and likewise for the z-directional porosity.

$$\epsilon_x = 1 - \frac{w_z}{t_z} \quad 4-18$$

$$\epsilon_z = 1 - \frac{w_x}{t_x} \quad 4-19$$

The total porosity of the heat sink is

$$\epsilon = 1 - \frac{w_x w_z}{t_x t_z} = \epsilon_x + \epsilon_z - \epsilon_x \epsilon_z \quad 4-20$$

The Reynolds number, based on hydraulic fin diameter, is defined as

$$Re_d = \frac{\rho u_m d_p}{\mu \epsilon_x} \quad 4-21$$

The hydraulic fin diameter is defined as

$$d_p = \frac{2w_x w_z}{w_x + w_z} \quad 4-22$$

For this type of flow, Masuoka and Takatsu (1997) showed that the transition number from laminar to turbulent flow is approximately $Re_d \sim 1000$. This was in general agreement with the results found by Kim, Kim, and Ortega, who separated their Nusselt number correlation into a laminar and turbulent regime based on a transition Reynolds number of 1000, citing that work. However, if the laminar and turbulent portions of this correlation (Eq. 4-23) are equated to solve for the point of transition, the Reynolds number 1512 is obtained, suggesting that transition to turbulent flow may take place closer to this Reynolds number. In order to provide smooth analytical results, 1512 is regarded as the transition Reynolds number for thermal analysis in this work. With this modification, the correlation is:

$$Nu_{air} = \begin{cases} 0.36283 Re_d^{54219} & Re_d < 1512 \\ 0.04433 Re_d^{82934} & Re_d \geq 1512 \end{cases} \quad 4-23$$

Because this correlation was developed only for one fluid (atmospheric air), dependence on Prandtl number could not be represented. However, a first approximation of this dependence may be reasonably introduced by allowing the Nusselt number to vary proportionately with Pr^n . For similar heat transfer correlations, n takes on a constant value between 0.3 and 0.37. These bounds encompass the values of n suggested by Hilpert (1933), Zukauskas (1972), and Churchill and Bernstein (1977) for various types of external flow. For many correlations, n is set at a value of 1/3. This value may be used and the coefficients modified such that the correct coefficients are

yielded when the Prandtl number of air at room temperature ($Pr = 0.71$) is inserted. Modifying the correlation in this way extends its usefulness by providing a reasonable prediction for other fluids, such as water. However, this extension of the heat transfer correlation was not suggested by Kim, Kim, and Ortega, and was not experimentally validated in this research. The modified Nusselt number correlation is

$$Nu = \begin{cases} 0.40671Pr^{1/3}Re_d^{.54219} & Re_d < 1512 \\ .04969Pr^{1/3}Re_d^{.82934} & Re_d \geq 1512 \end{cases} \quad \mathbf{4-24}$$

Equation 4-23 or 4-24 may be used to calculate heat transfer coefficients for the heat sink equations discussed at the beginning of this chapter. When the governing equations of the energy conversion system are fully nondimensionalized in Chapter 8, this correlation itself will be substituted into the heat transfer equations instead of the variable h .

4.2 Pressure Drop

Blowing or pumping a fluid over the heat sink fins requires power. For the conversion system to be feasible, the power required to move the fluid through the sink must be significantly less than the power that may be harvested from the system. A model is now developed to predict pressure loss through a shrouded channel of fins, ultimately so that the design of the system can be chosen to encourage heat transfer and discourage pressure loss. The work presented here also builds on work published by Kim, Kim, and Ortega.

4.2.1 Previous Work

Recent experimental work on pressure drop through arrays of rectangular fins has been performed by Kim, Kim, and Ortega (2004). The approach taken treats the volume containing the pin fins as a porous medium, in other words, a volume that provides a volumetrically homogeneous continuum type resistance to fluid flow. This approach had previously been developed Koh and Colony (1986), and You and Chang (1997). The porous medium approach provides the ability to construct a representative, spatially-averaged velocity profile from a governing equation adapted to flow through a porous medium. The two dimensional, volume-averaged momentum equation chosen to model the flow differs slightly between authors, but in each case may be written in the form

$$0 = -\frac{\partial P}{\partial x} + \mu \frac{\partial^2 u}{\partial y^2} - (A_1 \mu)u - (A_2 \rho)u^2 \quad 4-25$$

where A_1 and A_2 are composed of experimentally determined constants dependent on geometry. Kim, Kim, and Ortega utilized the form

$$0 = -\frac{\partial P}{\partial x} + \mu \frac{\partial^2 u}{\partial y^2} - \left(\frac{\epsilon}{K}\mu\right)u - \left(\frac{C_E \epsilon^2 \rho}{\sqrt{K}}\right)u^2 \quad 4-26$$

where K is the permeability (m^2) and C_E is the Ergun constant (dimensionless) which are determined experimentally for a given heat sink. The method of determining these constants is discussed by You and Chang (1997). Kim, Kim, and Ortega determined these constants for 16 different rectangular fin heat sinks of varying directional porosities. The concept behind representation of a flow volume containing fins as a porous medium is illustrated in Fig. 4-4. Flow is assumed to be fully developed. Flow characteristics in the z direction are neglected.

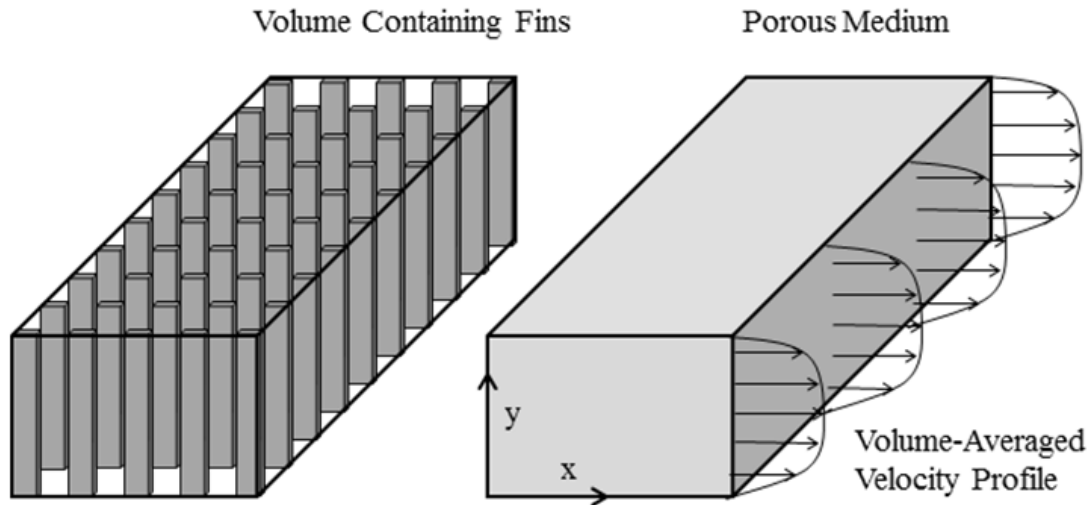


Figure 4-4: Conceptual Schematic of the Porous Medium Approach. A smooth, representative velocity profile is calculated from Eq. 4-26.

In their experimental work, Kim, Kim, and Ortega confirmed that pressure drop from row to row is almost perfectly linear. However, they also showed that pressure drop created by the first row of fins is an exception, being greater than that produced by each subsequent row. Also, after the last row of fins, the flow dynamics create a pressure rise. Analytical methods of accounting for this beginning pressure drop at the entrance and a pressure rise at the exit of the fin array were employed. The total measured pressure drops were confirmed to be within 9% of the predicted values for all cases and within 4% for most cases. The pressure drop and rise upon entering and exiting the fins are significant when there are few fin rows normal to the flow direction (nine rows of fins for the experiments of Kim, Kim, and Ortega). For large numbers of fin rows these effects become very small compared to the linear pressure drop through the main body of the sink. Although Kim, Kim, and Ortega only tested sinks with nine rows of fins, their results strongly indicate that for fin arrays of several dozen rows, these end effects will be negligible. The beginning and end effects are not taken into account in the pressure drop analysis in this work.

4.2.2 Definition of Friction Factor

The work done by Kim, Kim, and Ortega is now built upon to develop a generalized model for pressure drop through a wide range of potential heat sinks with varying fluid speeds and geometries. A friction factor approach is used. This approach was used by Zukauskas (1972) with external flow through an array of pipes (also applicable to an array of round fins). Zukauskas defined the friction factor for an array of round pipes as

$$f_{round} = \frac{\Delta P}{\chi N_{row} \frac{\rho}{2} (u_{max})^2} \quad 4-27$$

where $u_{max} = u_m/\epsilon_x$ and N_{row} and χ are, respectively, the number of cylinder rows aligned normal to the flow direction and a correction factor based on cylinder spacing. This friction factor was correlated to a Reynolds number based on cylinder diameter and spacing.

A similar technique is now developed for the array of rectangular fins. Considering that the porous medium approach has removed direct dependence from flow characteristics on the number of fin rows, a friction factor definition more closely resembling the traditional Darcy friction factor is appropriate. The Darcy friction factor for internal flow is defined as

$$f_{Darcy} = \frac{\Delta P}{\frac{L}{D} \left(\frac{\rho u_m^2}{2} \right)} \quad 4-28$$

where ΔP describes internal pressure loss through a pipe. For the purposes of calculating pressure drop through a heat sink, pressure change is assumed to be linear, and the velocity $u_{max} = u_m/\epsilon_x$ replaces u_m as it does in the Zukauskas friction factor for round fins. Because the pressure drop through the sink is best correlated to the nature of the fins rather than the channel containing them, the characteristic diameter of the channel D is replaced with d_p , the characteristic diameter of the fins. Making these changes, a friction factor describing pressure drop through a shrouded heat sink is defined:

$$f = \frac{dP}{dx} \left(\frac{d_p \epsilon_x^2}{\frac{1}{2} \rho u_m^2} \right) \quad 4-29$$

If this friction factor is known, then the pressure drop may be predicted from fin geometry and flow velocity through the fin array.

4.2.3 Velocity Profile and Friction Factor

A method of finding the friction factor, f , through solving the porous-medium momentum equation is now presented. First, Eq. 4-26 is solved for dP/dx and substituted into the momentum equation (Eq. 4-26). The momentum equation is then nondimensionalized with previously defined parameters as

$$\frac{d^2 u^*}{dy^{*2}} = f \left(\frac{\lambda^2 Re_d}{2 \epsilon_x} \right) + \left(\epsilon \lambda^2 \frac{d_p^2}{K} \right) u^* + \left(C_E \lambda^2 Re_d \epsilon_x \epsilon^2 \sqrt{\frac{d_p^2}{K}} \right) u^{*2} \quad 4-30$$

where λ represents the ratio of fin height L to fin diameter, d_p , (see Eq. 4-49). Dimensionless velocities $u = u_m u^*$ and $y = Ly^*$ are introduced. The boundary conditions come from the no-slip condition at the walls:

$$BC: \quad y^* = 0, u^* = 0; \quad y^* = 1, u^* = 0 \quad 4-31$$

In theory, the Ergun Constant C_E and the dimensionless parameter d_p^2/K are dependent solely on the directional porosities ϵ_x and ϵ_z . These values must be determined experimentally for each heat sink. The values used in this research are calculated from C_E , K , and d_p data published by Kim, Kim, and Ortega.

If the friction factor, f , is known, Eq. 4-30 may be solved numerically to obtain the velocity profile. Because of the nonlinear term, u^{*2} , numerical solution techniques must be employed in solving the equation. When the friction factor is not known, the momentum

equation must be coupled with the conservation of mass in order to solve for the velocity profile. This approach is taken to calculate the friction factor f . Simulating a real life system, assume that the mean velocity, u_m , of fluid through the sink may be reasonably measured, and thus the Reynolds number based on fin diameter, Re_d , is known. The integral average of the velocity profile must satisfy

$$u_m = \frac{1}{L} \int_0^L u \, dy \quad 4-32$$

If $u = u_m u^*$ and $y = Ly^*$ are substituted into Eq. 4-32, including changing the limits of integration, the equation simplifies to

$$1 = \int_0^1 u^* \, dy^* \quad 4-33$$

Thus, the correct dimensionless velocity profile, when integrated, must be equal to unity. By invoking symmetry about $y = L/2$, another set of appropriate boundary conditions may be written as

$$BC: \quad y^* = 0, \quad u^* = 0; \quad y^* = \frac{1}{2}, \quad \frac{du^*}{dy^*} = 0 \quad 4-34$$

It follows that the mass conservation constraint may be written alternatively as

$$\frac{1}{2} = \int_0^{1/2} u^* \, dy^* \quad 4-35$$

The conservation of mass constraint may be coupled with Eq. 4-30 to determine the velocity profile and determine the correct friction factor.

4.2.4 Method of Determining Friction Factor

The method of determining friction factor in this research is now presented. Using the values of C_E and dp^2/K determined experimentally by Kim, Kim, and Ortega (2004), the momentum and conservation of mass equations were used to produce an array of predictions for friction factors under various conditions. The following solution process was utilized:

1. Estimate a value for the friction factor f .
2. Numerically solve the velocity profile between $y^* = 0$ and $y^* = 0.5$.
3. Numerically integrate the velocity profile
4. Compare the integrated value to the correct value of $1/2$.
5. Use the difference between the profile integration and the correct value to update a new estimate for the friction factor
6. Repeat until the friction factor used in the momentum equation satisfies conservation of mass.

This process was carried out for all 16 heat sinks tested by Kim, Kim, and Ortega. Porosities of these heat sinks ranged from 0.2 to 0.8 in 0.2 increments in both x and z directions. With the exception of Re_d and λ , all non-constants in the nondimensionlized momentum equation, are dependent only on the fin porosities ϵ_x and ϵ_z . Therefore, the porous medium approach predicts that the friction factor for a heat sink as defined above depends on exactly four dimensionless variables: ϵ_x , ϵ_z , Re_d , and λ .

Solving the momentum equation (Eq. 4-30) for values in realistic ranges is straightforward, but computationally difficult. The equation is numerically volatile for high

Reynolds numbers and especially for λ values above 2. After experiencing difficulty with general built-in differential equation solvers, the author developed an original code to solve the momentum equation utilizing a 4th order Runge-Kutta method with built-in checks to ensure that the algorithm converged properly. The domain and boundary conditions of Eq. 4-34 were used, and the step size halved until the final answer for the friction factor differed by less than the third significant digit. For high λ values, this required a step size of $2.5 \cdot 10^{-5}$, or 40,000 steps to generate a velocity profile. When the appropriate step size was established for a family of cases, each case was solved by the method outlined above. First, a friction factor was estimated and the profile solved (steps 1,2). Then the profile was numerically integrated (step 3), and error observed (step 4). Linear interpolation of the error observed in the previous two iterations was used to update the estimate of the friction factor (step 5). Usually 20-30 iterations of this process were needed to converge (error less than 10^{-6}) upon the friction factor value for a single case.

As one goal of the research done for this thesis, friction factors were found for a sufficient number of cases to generate a tabular function of four variables for friction factor. A range of Reynolds numbers were chosen, accompanied by a range of values for λ . With friction factors for all these combinations for each of the 16 heat sinks, a data set is presented which allows for an estimate of friction factor to be calculated without the need to solve the porous medium momentum equation.

Because of the computationally intensive nature of solving for the friction factor, an approximation was used that allowed for some friction factors to be calculated from others. This approximation begins with the observation that the form of the momentum equation is robust enough to provide a prediction in the limiting case when the channel (fin height) is so large that the no slip condition at the walls becomes insignificant. For $\lambda \rightarrow \infty$, the influence of the no slip

condition vanishes, and the profile may be approximated as a slug flow (channel flow with a uniform velocity profile). The fluid in a slug flow experiences no gradient at the wall, thus

$$\frac{du^*}{dy^*} = 0, \quad 0 \leq y^* \leq 1 \quad 4-36$$

The consequence of this condition, considering the conservation of mass requirement, is that the flow field satisfies

$$\frac{d^2u^*}{dy^{*2}} = 0, \quad u^* = 1, \quad \text{for } 0 \leq y^* \leq 1 \quad 4-37$$

Because these values are constant, they may be substituted directly into the momentum equation (Eq. 4-30), after which λ^2 cancels out of every term, and the friction factor for this limiting case is solved for directly as

$$f_\infty = \frac{2\epsilon_x}{Re_d} \left(\epsilon \frac{d_p^2}{K} + C_E Re_d \epsilon_x \epsilon^2 \sqrt{\frac{d_p^2}{K}} \right) \quad 4-38$$

This represents the limiting value of the friction factor for increasing λ . On a plot of f vs λ , (Fig. 4-5) it is manifest as a horizontal asymptote.

The usefulness of this observation becomes clear when considering a particular case. Figure 4-5 plots friction factors taken from the family of friction factors belonging to $\epsilon_x = 0.4$, $\epsilon_z = 0.4$, and $Re_d = 500$. Each point represents a friction factor solved through the numerical process described at the beginning of this section. Beyond $\lambda = 5$, the numerical difficulties associated with the momentum equation begin to render this process unreasonably time consuming, as the number of steps required to maintain stability grows enormous. Although more advanced numerical methods would improve this computational expense, the approach taken in this research is to eliminate the need for directly calculating the friction factors in the high λ regime altogether.

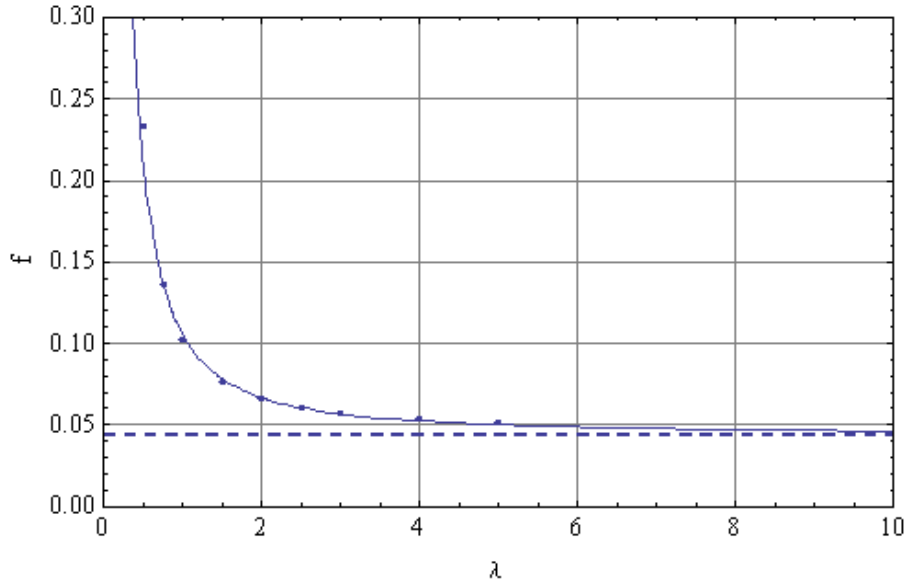


Figure 4-5: Calculated Friction Factor vs Dimensionless Fin Length. Parameters: $\epsilon_x = 0.4$, $\epsilon_z = 0.4$, $Re_d = 500$. Curve fit and limiting value, f_∞ (dashed), shown.

The calculated points lead, as expected, toward the limiting value f_∞ . Not only this, but they are observed to fit very well to a power regression of the type

$$f = A\lambda^B + C \tag{4-39}$$

The fit is observed to match well enough that such a curve generated with these data points is a highly accurate prediction of the friction factor values for the high λ cases.

Considering the expected accuracy of this method compared to the computational expense, this process was stripped down to a minimalist version. For generating the friction factor tables, only two friction factors, $f(\lambda=0.75)$ and $f(\lambda=2.5)$, were calculated for each combination of Re_d , ϵ_x , and ϵ_z that can be formed from Table 4-1. The curve shown in Fig. 4-5 was calculated with only these two points. In this way, the calculation of 5888 friction factors was accomplished while only carrying out the numerical method described above for 736 cases. Beginning with the regression form above (Eq. 4-39) and a set of two points $(0.75, f_1)$, $(2.5, f_2)$

together with the known asymptote, f_∞ , it is a simple matter to show that the coefficients of the curve fit are

$$A = \frac{f_2 - f_\infty}{2.5^{\left(\frac{\ln\left(\frac{f_1 - f_\infty}{f_2 - f_\infty}\right)}{\ln\left(\frac{0.75}{2.5}\right)}\right)}} \quad 4-40$$

$$B = \frac{\ln\left(\frac{f_1 - f_\infty}{f_2 - f_\infty}\right)}{\ln\left(\frac{0.75}{2.5}\right)} \quad 4-41$$

$$C = f_\infty = \frac{2\epsilon_x}{Re_d} \left(\epsilon \frac{d_p^2}{K} + C_E Re_d \epsilon_x \epsilon^2 \sqrt{\frac{d_p^2}{K}} \right) \quad 4-42$$

Friction factors were calculated for each of the 16 heat sinks tested by Kim, Kim, and Ortega.

Table 4-1: Values of Re_d , λ , ϵ_x , and ϵ_z for Friction Factor Tables.

Re_d	λ	ϵ_x	ϵ_z
10	0.5	0.2	0.2
15	0.75	0.4	0.4
20	1	0.6	0.6
25	1.5	0.8	0.8
30	2		
40	2.5		
50	3		
75	4		
100	5		
150	6		
200	8		
250	10		
300	15		
400	20		
500	100		
750			
1000			
1500			
2000			
2500			
3000			
4000			
5000			

Table 4-1 shows the cases for which friction factors were calculated. A friction factor was calculated for every combination of Re_d , λ , ϵ_x , and ϵ_z shown. An abbreviated friction factor table is shown in Table 4-2 for the heat sink with porosities $\epsilon_x = 0.4$ and $\epsilon_z = 0.4$. Only select Reynolds numbers are shown. For the complete set of tables, see Appendix B.

Table 4-2: Select Friction Factors. Parameters: $\epsilon_x = 0.4$, $\epsilon_z = 0.4$.
Note: the format of this table is transposed compared to the format of the tables in Appendix B.

λ	Re_d				
	10	50	100	500	1000
0.5	9.08536	1.82892	0.92436	0.20899	0.12289
0.75	5.02822	1.03544	0.53626	0.13630	0.08591
1	3.45496	0.72302	0.38099	0.10511	0.06947
1.5	2.21872	0.47399	0.25536	0.07815	0.05477
2	1.73934	0.37594	0.20510	0.06658	0.04824
2.5	1.50032	0.32651	0.17946	0.06038	0.04464
3	1.36265	0.29779	0.16443	0.05659	0.04240
4	1.21658	0.26701	0.14816	0.05230	0.03981
5	1.14375	0.25150	0.13986	0.05000	0.03838
6	1.10180	0.24249	0.13499	0.04859	0.03749
8	1.05729	0.23283	0.12973	0.04700	0.03646
10	1.03510	0.22796	0.12704	0.04615	0.03589
15	1.01124	0.22266	0.12408	0.04515	0.03520
20	1.00199	0.22057	0.12289	0.04472	0.03490
100	0.98840	0.21742	0.12105	0.04396	0.03432

The use of these tables would be somewhat unwieldy for manual use. However, any software package with a built-in capability to treat tabular functions allows the tables to be used with ease and convenience. The advantage for this approach lies in versatility and speed of computation. Using linear interpolation, the software package, *Mathematica*, was used to plot

friction factors against Reynolds number in Fig. 4-6. The high values at low Reynolds numbers and leveling out at high Reynolds numbers are in general agreement with friction factor data for flow over circular tubes presented by Zukauskas for arrays of cylinders (1977).

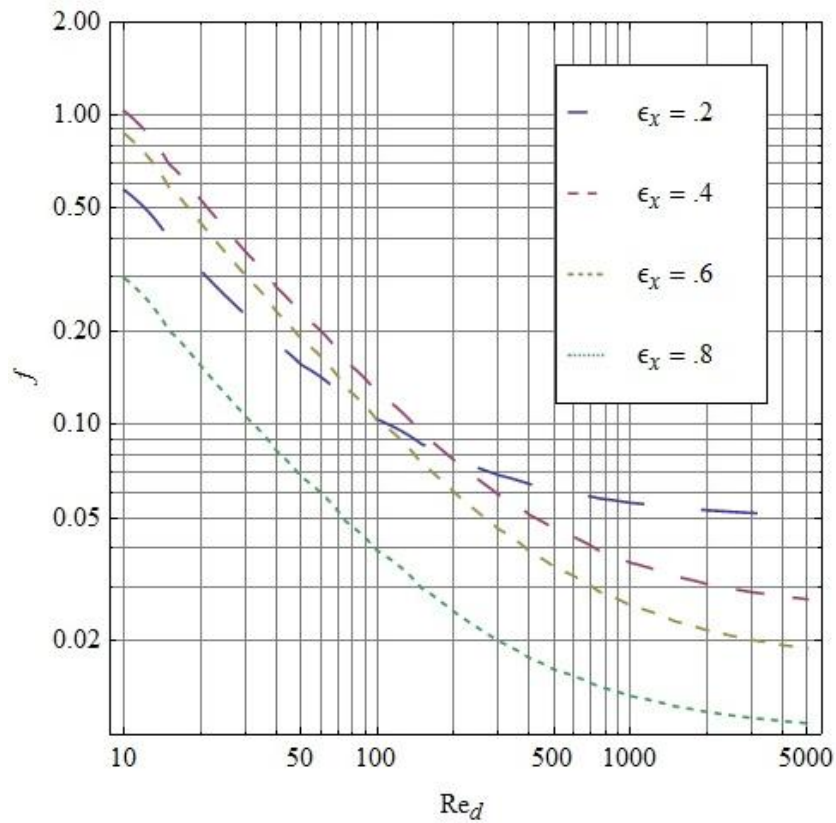


Figure 4-6: Friction Factor vs Reynolds number. Parameters: $\epsilon_z = 0.2$, $\lambda = 10$.

This method of finding friction factors from ready-made tables is integrated into the optimization analysis. With the ability to easily calculate friction factor, pressure drop and power needed to move fluid may be incorporated into the process of finding the optimum design point.

4.2.5 Power Requirement

The idealized power requirement for any incompressible, internal flow is equal to the volumetric flow rate multiplied by the pressure loss. Consider the volumetric flow rate through a shrouded fin array with fin length L :

$$\dot{V} = LH_1 u_m \quad 4-43$$

where H_1 is the width of the heat sink normal to the flow direction. The pressure loss through a length along the flow direction H_2 , is represented by rearranging the definition of the friction factor (Eq. 4-29) to express pressure drop

$$\frac{dP}{dx} = \frac{\Delta P}{H_2} = f \left(\frac{\rho u_m^2}{2 d_p \epsilon_x^2} \right) \quad 4-44$$

The ideal work requirement may then be written

$$\dot{W}_{req} = f \left(\frac{\rho u_m^2}{2 d_p \epsilon_x^2} \right) H_2 (LH_1 u_m) \quad 4-45$$

When the notation from Fig. 4-2 is applied, then $H_1 = t_z N_z$ and $H_2 = t_x N_x$, and this equation may be arranged as

$$\dot{W}_{req} = N t_x t_z \lambda f \left(\frac{\rho u_m^3}{2 \epsilon_x^2} \right) \quad 4-46$$

This equation allows power requirement to be calculated and compared with the total heat transfer achieved by the heat sink.

4.3 Thermal/Hydrodynamic Behavior of Heat Sinks

The velocity of the fluid through the heat sink is the primary factor that determines the magnitude of the convection coefficient. Faster flows will result in greater heat transfer, but also in higher fan or pump work. Optimizing the flow velocity is paramount to designing a properly

optimized heat exchange system. With both heat transfer and pressure drop predicted as function of design variables, some heat sink behavior may be observed.

One useful criterion by which the sink may be evaluated is the ratio of heat moved through the sink to power required to move fluid through the heat sink. This ratio is found by dividing Eq. 4-6 by 4-46. At the same time, Eq. 4-17 is used to replace the convection coefficient, h , with the Nusselt number correlation. The resulting ratio is

$$\frac{q}{\dot{W}_{req}} = \frac{1}{N t_x t_z \lambda f \frac{\rho u_m^3}{2 \epsilon_x^2}} \left((T_B - T_S) N (t_x t_z - w_x w_z) \frac{\epsilon k_f}{d_p} C_1 Re_d^m \right. \\ \left. + 2 w_x w_z \sqrt{\frac{\epsilon k_f}{d_p} C_1 Re_d^m \frac{k_{sink}}{d_p}} \tanh \left(2L \sqrt{\frac{\epsilon k_f}{d_p} C_1 Re_d^m \frac{1}{k_{sink} d_p}} \right) \right) \quad 4-47$$

Equation 4-47 may be cast in nondimensional form as

$$\frac{q}{\dot{W}_{req}} = \frac{2\Lambda^2}{\epsilon_x \lambda Re_d^3 f} \left(\epsilon^2 C_1 Re_d^m + 2(1 - \epsilon) \sqrt{\epsilon \kappa C_1 Re_d^m} \tanh \left(2\lambda \sqrt{\frac{\epsilon C_1 Re_d^m}{\kappa}} \right) \right) \quad 4-48$$

where several dimensionless groups are introduced: the dimensionless fin length (mentioned in Chapter 4.2.3),

$$\lambda = L/d_p \quad 4-49$$

the ratio of thermal conductivities,

$$\kappa = \frac{k_{sink}}{k_f} \quad 4-50$$

and Λ is introduced as a dimensionless fin diameter.

$$\Lambda = d_p \sqrt{\frac{\rho^2 k_f (T_B - T_\infty)}{\mu^3}} \quad 4-51$$

In Fig. 4-7, the heat to work ratio is observed vs Reynolds number for a fixed geometry. As flow velocity increases, each unit of power supplied drives a smaller quantity of heat through the sink. It will be seen in Chapter 8 that this effect tends to keep the optimal operating point of the proposed thermoelectric conversion system in the laminar regime ($Re_d < 1000$).

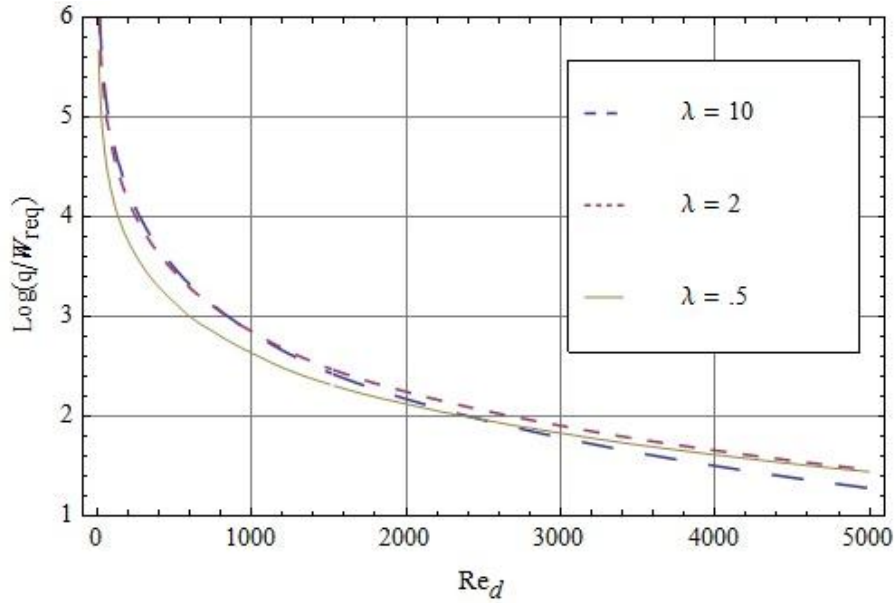


Figure 4-7: Heat Rate/Power Requirement vs Reynolds Number. Parameters: $\epsilon_x = \epsilon_z = 0.4$, $A = 20,000$, $\kappa = 6667$.

Optimization of the heat sink geometry as a problem unto itself is not performed in this research. Instead, the various nondimensional parameters of the heat sinks will be included as part of the overall optimization of the entire system in Chapter 8.

However, at this time, one more pertinent observation will be made. Consider the dimensionless fin height, $\lambda=L/d_p$. Heat transfer increases with fin height, but after the fins have reached an optimal length, the additional heat transfer gained is not worth the added flow work to move fluid through the taller channel. This effect is shown for a laminar flow case in Fig. 4-8.

The plots show a distinct optimum fin height between about 3 and 7 fin diameters. It will be seen in Chapter 8 that the optimum fin length for the hot fluid stream when the entire system is optimized generally agrees with the optimum fin length defined by maximized q/\dot{W}_{req} .

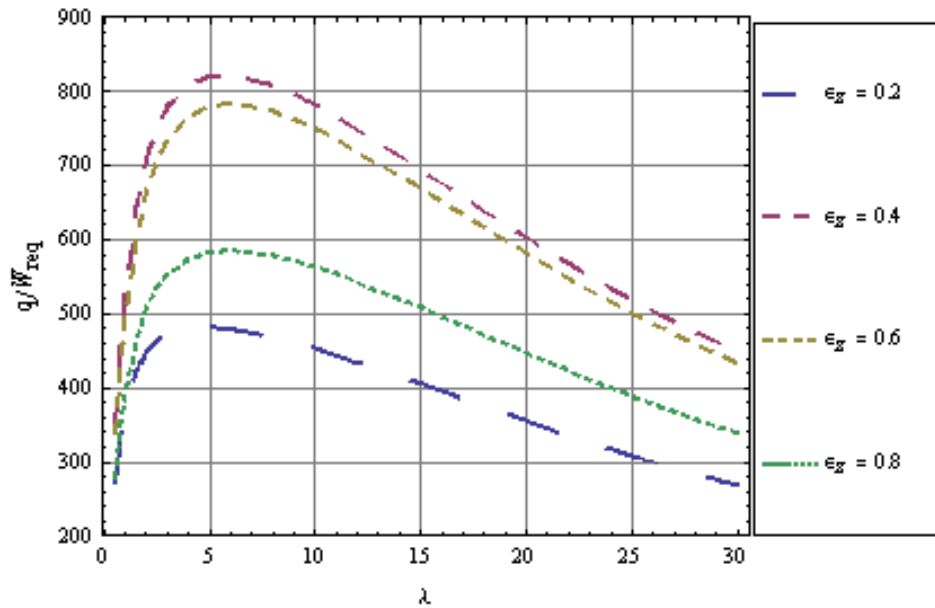


Figure 4-8: Heat Rate/Power Requirement vs Dimensionless Fin Length. Parameters: $Re_d = 500$, $A = 20,000$, $\epsilon_x = 0.4$.

Although the heat to work ratio (Eq. 4-48) is not used when the overall system modeling is conducted in Chapter 8, the observations in heat sink behavior observed by examining this ratio provide valuable understanding. The heat sink behaviors observed here manifest themselves as recognizable trends in the overall system optimization.

5 BYPASS INSULATION

In this chapter, the bypass insulation of the thermoelectric power generation system is discussed. The purpose of this insulation is to provide an economic improvement to the system by increasing the efficiency of each device.

5.1 Device Cost and Heat Channeling

The thermoelectric conversion system is envisioned with rows of bypass insulation separating rows of devices as shown in Fig. 5-1. The total area of the system is $A_{sys} = XZ$.

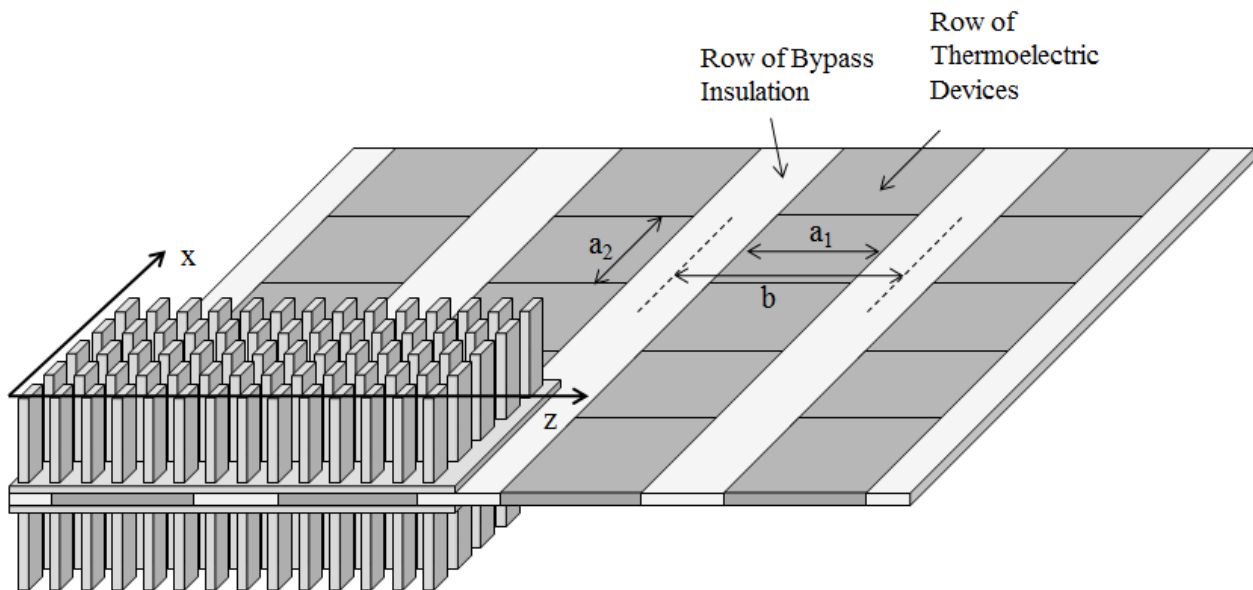


Figure 5-1: System Layout: Device and Bypass Dimensions. Rows of insulation separate rows of thermoelectric devices. Each device has area of $A_{oneD} = a_1a_2$.

The purpose behind laying rows of insulation between thermoelectric devices is cost-based. Bypass insulation channels heat into the devices, making each one more effective at generating power. This is achieved physically by providing large thermal resistance between the fin arrays. The thermal resistance of the bypass insulation maintains a larger temperature difference between the heat sinks than if the area of the system were completely spanned by thermoelectric devices. Because each device is more efficient with bypass insulation, a system with few devices and optimized bypass insulation can produce almost as much power as a much more expensive system with many devices. The system utilizing bypass insulation will have a significantly lower startup cost per watt of electricity produced.

5.2 Single Node Approximation

The circuit diagram illustrating the analytical model in Fig. 3-2 presupposes that the temperature of the system in all locations represented by that node is uniform. More specifically, this approximation assumes that temperature nodes T_{IH} and T_{IL} are spatially non-varying. Recall that these temperatures represent the temperatures of the undersurfaces of the two large fin arrays. These surfaces are in contact with the thermoelectric devices in some areas and in contact with the bypass insulation in other areas. In the real system, the temperature of the heat sink base would tend to vary over these locations. The temperature difference between the heat sink bases will be larger over locations of insulation and smaller over the center of the devices. High thermal conductivity in the base of the heat sink tends to reduce this variation by allowing heat to flow in the plane normal to the assumed direction of heat transfer as necessary to equalize the temperature throughout the base. The bypass ratio, r , is introduced as the ratio of total area

spanned by the system to area spanned by thermoelectric devices. This ratio is equivalent to b/a_1 (see Fig. 5-1). When this ratio is equal to 1, no bypass thermal pathway exists.

Some simple numerical simulations were carried out as an exploratory investigation to gauge the accuracy of neglecting these temperature variations. A finite-difference approach with square temperature cells was used to predict heat conduction characteristics through a row of devices and its accompanying insulation. Figure 5-2 shows the analyzed system with boundary conditions, which is a view in the y - z plane. The heat sink bases (with conductivity of aluminum) are represented on each side of a thermoelectric device with insulation. The fins that would extend from the heat sink bases are not represented explicitly, but incorporated through the use of fixed thermal conductances, U'' , to the stream temperatures. Volume-averaged properties are used, including a volume-averaged effective thermal conductivity representative of real thermoelectric devices. As bypass ratio increases, the discrepancy in temperature difference over the insulation and the device increases, and the accuracy of the governing equations is compromised.

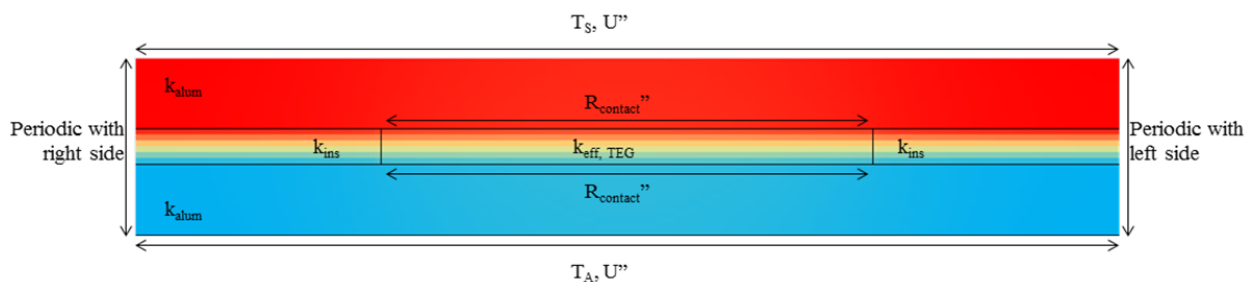


Figure 5-2: Finite Difference Domain. Parameters: $k_{sink} = k_{alum} = 180$, $k_{eff\ TEG} = 2.0$, $k_{bp} = k_{ins} = .05\ \text{W/m}^2\text{K}$, $R_{contact} = 3 \times 10^{-5}\ \text{km}^2/\text{W}$, $r = 2$.

The system above was analyzed as a grid of 30 by 160 square nodes. *Microsoft Excel* was used to perform calculations on a spreadsheet where each cell represented a temperature node, containing the equation describing its dependency on the surrounding nodes. The iterative

solving capabilities of the software were called upon to solve the entire system of equations to a convergence criterion of less than 0.0001 °C change for any cell between iterations.

Of particular interest in this simulation is the temperature of the base of the heat sink along the z direction where it interfaces with the thermoelectric device and the insulation. Again, the thermal circuit used to model the overall system assumes that this temperature is spatially constant. Figure 5-3 illustrates the case when a U'' value of 1000 W/m²K is used for both boundaries exposed to the fluid streams. The spatial average of $T_{IH} - T_{IL}$ over the device is observed to be slightly less than the spatial average of $T_{IH} - T_{IL}$ over the entire system. This causes the model to slightly over-predict the temperature difference in the thermoelectric device.

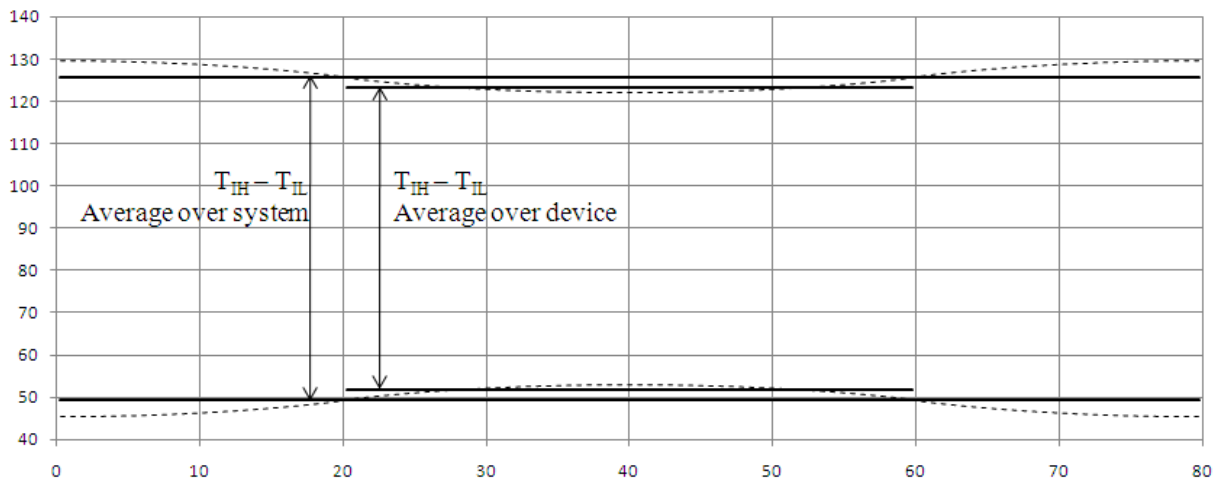


Figure 5-3: Temperature Profiles on Inner Side of Heat Sink Bases. The average temperature difference is slightly less over the device than over the entire system. $U'' = 1000 \text{ W/m}^2\text{K}$, $r = 2$.

This type of model was analyzed for a bypass ratio of 2.0 for several values of U'' . Higher thermal conductances resulted in a more accurate approximation. The percentage of the average temperature difference $(T_{IH} - T_{IL})_{Dev}$ over the device as a percentage of the average temperature difference $(T_{IH} - T_{IL})_{Sys}$ over the entire system is illustrated in Table 5-1. Reasonable

values for U'' where the fluid consists of air range from roughly 100 to 1000. For fluid streams using water, reasonable values range from roughly 1000 to 10,000. The very high value of 1,000,000 illustrates the limiting case where the top side of the fin sink base is essentially kept at the same temperature as the fluid. In all cases, the temperature difference experience by the thermoelectric device is several percent less than the average temperature difference between the heat sinks.

Table 5-1: Finite Difference Results for Single Node Approximation. Temperature differences between heat sink bases are averaged across the thermoelectric device and across the entire system span.

U''	$\Delta T_{IHD} = (T_{IH} - T_{IL})_{System}$	$\Delta T_{IHS} = (T_{IH} - T_{IL})_{Device}$	$\% \Delta T_{IHD} / \Delta T_{IHS}$
10	3.33	3.07	92.0%
100	17.7	16.3	92.3%
1000	76.6	71.3	93.1%
10,000	115.5	110.8	96.0%
100,000	121.8	119.4	98.0%
1,000,000	122.5	120.5	98.4%

In this work, the model is used up to a bypass ratio of 2. For modeling of larger bypass ratios, two dimensional effects of heat conduction in the fin base should be considered. Further research on how to simplify these effects for incorporation into an analytical model is outside the scope of this thesis. Such analysis would include higher accuracy numerical modeling with specialized software, such as *Fluent*, to assess the influence of the thickness of the heat sink base and the size of the thermoelectric device on heat transfer through the bypass. Through nondimensionalized correlations, perhaps these effects could be incorporated analytically into the closed-form model. For reasons illustrated in chapter seven, analytical characterization of arbitrarily large bypass ratios is highly recommended for further research.

One way to maintain the accuracy of the temperature node approximation and achieve higher bypass ratios would be to design the system with insulation surrounding every device as shown in Fig. 5-4.

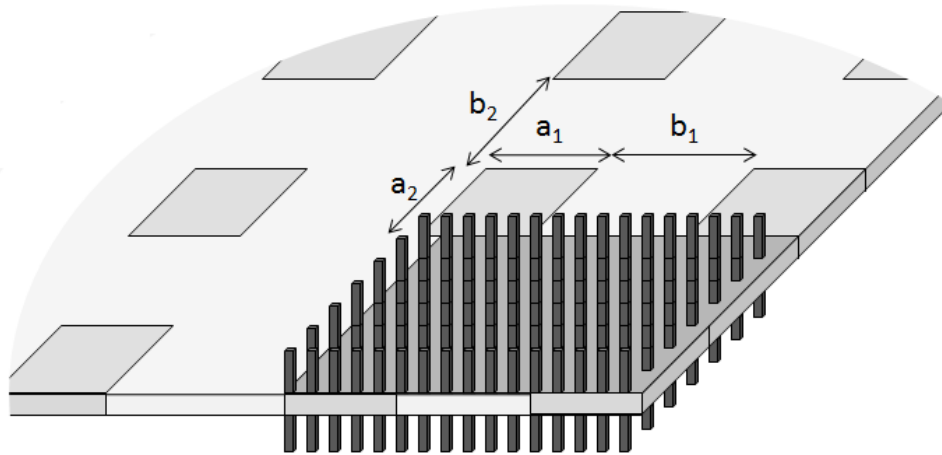


Figure 5-4: Schematic of Potential Design for High Bypass Ratios.

With this type of design, the bypass ratio would be equal to b_1b_2/a_1a_2 , and ratios up to 3 or 4 might be modeled with reasonable accuracy using the single node approximation. However, for the development of the model used in this research, only the design of Fig. 5-1 is considered, and the bypass ratio is limited to a maximum of 2.

5.3 Modeling and Nondimensionalization

Consider the system illustrated in Fig. 5-1, where the thermoelectric devices each have area A_{oneD} . Again, in this arrangement, the ratio of total area spanned by the system to area with bypass insulation is equivalent to b/a_1 . In addition, the thermal conductance per area of the device is introduced as

$$U_{bp}'' = \frac{k_{bp}}{L_D} \quad 5-1$$

where L_D is the thickness of the device (and consequently of the bypass insulation).

This and the other thermal conductances, U_i , discussed up to this point may be expressed as the products of thermal conductance per area, U_i'' , and the total area applicable to that particular conductance. Inspection of Fig. 5-1 allows these to be expressed:

$$U_D = U_D'' N_D A_{oneD} \quad 5-2$$

$$U_{bp} = U_{bp}'' (A_{sys} - N_D A_{oneD}) \quad 5-3$$

$$U_{IH} = U_{IH}'' N_D A_{oneD} \quad 5-4$$

$$U_{IL} = U_{IL}'' N_D A_{oneD} \quad 5-5$$

$$U_H = U_H'' A_{sys} \quad 5-6$$

$$U_L = U_L'' A_{sys} \quad 5-7$$

where N_D represents the number of thermoelectric devices. This number may be expressed as a function of areas:

$$N_D = \frac{A_{sys}}{A_{oneD} r} \quad 5-8$$

Through dividing Eqs. 5-3 through 5-7 by the total thermal conductance of the devices, (Eq. 5-2), the thermal conductance ratios are obtained. Considering that $A_{oneD} = a_1 a_2$ and $r = b/a_1$ (Fig. 5-1), the thermal conductance ratios may be written

$$\Psi_{bp} = \Psi_{bp}'' (r - 1) \quad 5-9$$

$$\Psi_{IH} = \Psi_{IH}'' \quad 5-10$$

$$\Psi_{IL} = \Psi_{IL}'' \quad 5-11$$

$$\Psi_H = \Psi_H'' r \quad 5-12$$

$$\Psi_L = \Psi_L'' r \quad 5-13$$

The thermal conductance ratios may be substituted into the governing equations of the entire system derived in Chapter 3 in order to express the governing equations in terms of their dependence on bypass ratio, r . Increasing this bypass ratio will decrease the number of devices for a given area, but increase the temperature difference between each device. These competing effects allow for optimization of the measure of bypass insulation that balances total power output against total system cost. In Chapter 6, an economic model of the system is developed, and the cost effectiveness of the bypass concept is illustrated.

6 EXPERIMENTAL VALIDATION

The model was validated with experimental data collected from a test station constructed to hold a single thermoelectric device in the configuration proposed for the system.

6.1 Test Station

The test station constructed for this research consists of a carefully structured flow circuit. Air at ambient temperature flows through the fin array of a heat sink, where the channel width is exactly the fin height, shrouding the flow.

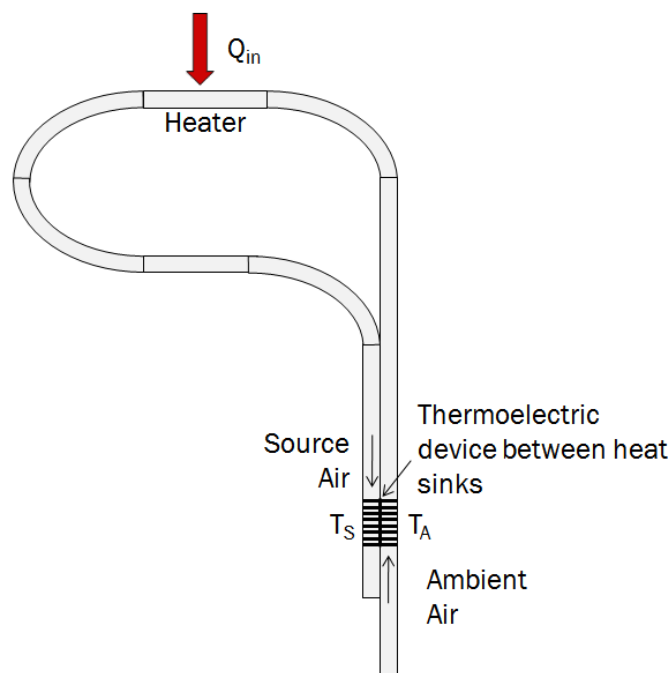


Figure 6-1: Schematic of Test Station Flow Circuit.

The air passes through a section of the circuit containing a heater, rising to a high temperature before flowing around to the fins of another heat sink and then escaping. The two heat sinks sandwich a thermoelectric device. Heat flowing from the hot airstream transfers through the heat sink, through the thermoelectric device, and through the other heat sink, with some energy converted into electrical power.

Power is measured through directing the electrical current produced by the device through a matched-load resistor and calculating power output as $\Delta V^2/R$. The resistor dissipates the power produced by the thermoelectric device.

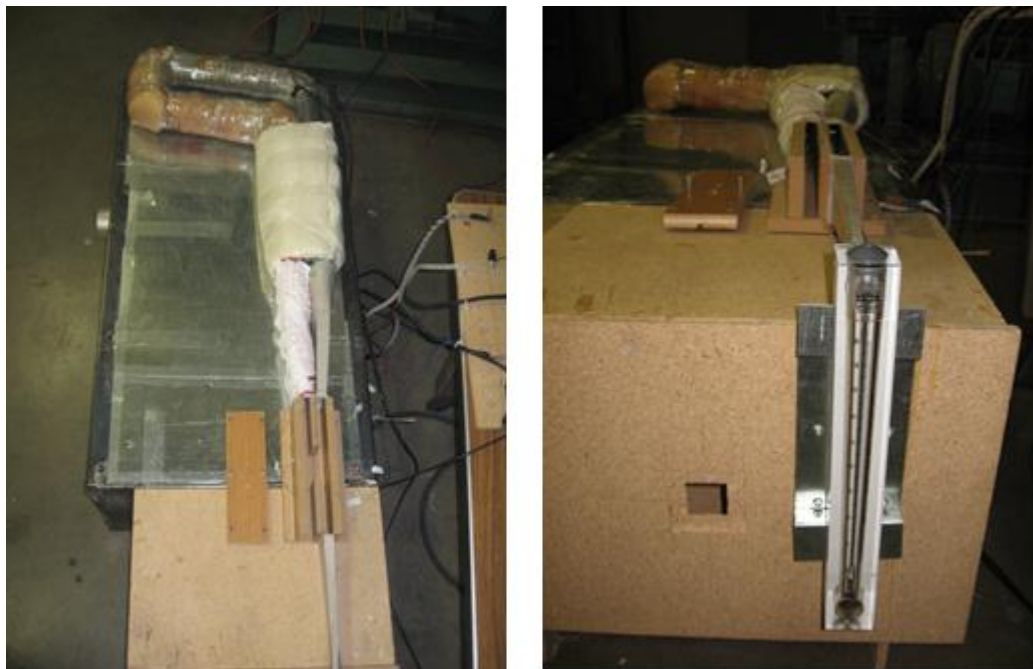


Figure 6-2: Photographs of Test Station. Left: View from above of the flow circuit. Right: Front view. Air passes up through the rotameter, which measures volumetric flow, and then enters a specially constructed box. The box contains two separate flow paths and holds a thermoelectric device and a heat sink exposed to each stream.

Known parameters included all geometry pertaining to the thermoelectric device, heat sinks, and channels; Reynolds numbers obtained through knowledge of the volumetric flow rate and temperatures, which are measured with thermocouples inserted into the flow path before and after each heat sink.

6.2 Method

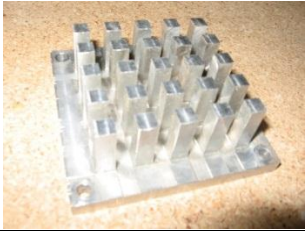

Two sets of heat sinks were used in the experiments. The first heat sink (referred to as sink *A*) was manufactured by the 2009-2010 *Exergy Solutions* senior design team at BYU. The large fins of this heat sink make it ideal for testing Reynolds numbers in the turbulent regime ($Re_d > 1000$). The second heat sink (sink *B*) was purchased from Alpha Novatech Inc. The very small fins of this heat sink make it ideal for testing Reynolds numbers in the laminar regime. Heat sink *B* represents the type of high-performance heat sink recommended for the proposed system. Characteristics of these heat sinks are given in Table 6-1.

Manipulation of the heater input and flow rate was used to test the system at various airstream temperature differences ($T_S - T_A$) and ambient stream Reynolds numbers $Re_{d,A}$. Reynolds numbers of the hot stream, $Re_{d,S}$, were slightly higher than $Re_{d,A}$ for each case due to property changes resulting from the temperature increase.

Two properties, Z_D and U_D'' , of the thermoelectric device are required for using the model, but were not initially known. In order to estimate these parameters, four settings were tested using heat sinks of type *A*, and the results used to calculate the parameters Z_D , and U_D'' using a least squared error approach using percent error between the measured power output and the power output predicted by the model. These parameters were then used to predict power output at a number of other experimental conditions involving a range of temperature differences for

both sets of heat sinks. The power measurements and predictions are compared in the sections that follow.

Table 6-1: Parameters for Heat Sinks used in Experiments

		
	<i>Left: Sink A</i>	
	<i>Right: Sink B</i>	
<i>Parameters</i>		
w_x (mm)	6.3	9.8
w_z (mm)	6.3	.53
d_p (mm)	6.3	1.0
t_x (mm)	12.8	11.4
t_z (mm)	12.8	2.0
N	25	250
L (mm)	19.1	20.0
L_B (mm)	6.5	5.0
Active Area: $Nt_x t_z$ (mm ²)	4096	5700
<i>Dimensionless Parameters</i>		
ε_x	.508	.735
ε_z	.508	.140
λ	3.03	20.0
$r: Nt_x t_z / A_{TEG}$ (TEG-12611-6.0)	1.31	1.82
$r: Nt_x t_z / A_{TEG}$ (TG12-8)	2.57	3.56


6.3 Results

6.3.1 Thermal Electronics Thermoelectric Generator

The tests described above were performed for a TEG1-12611-6.0 thermoelectric device from Thermal Electronics Corporation. The four data points shown in Table 6-2 were used for

calculating the values of Z_D and U_D'' for the thermoelectric device. Because two parameters must be characterized (Z_D and U_D''), at least two data points must be obtained to fit values for them. It is shown in this research that four empirical data points is sufficient to characterize Z_D and U_D'' with reasonable results.

Table 6-2: Calibration Points for determining Z_D and U_D'' for the TEG1-12611-6.0 Thermoelectric Device. Photo courtesy of Thermal Electronics Corp (Specifications).

			
$Re_{d,A}$	$T_S - T_A$ (C)	Empirical Power Measurement	Best Fit Power Calculation
1960	63.4	76.0	73.5
2020	25.2	11.8	11.7
3210	24.0	17.2	17.7
3170	61.9	115.0	118.9
Fitted values: $Z = 6.25 \times 10^{-4}$ $U_D'' = 354 \text{ W/m}^2\text{K}$			

Six more points were tested, all in the turbulent regime (heat sink A), and the Z_D and U_D'' values used in the analytical model to predict power output. The power output was correctly predicted to within 5% for Reynolds numbers ranging between 1500 and 4000 (Fig. 6-3, turbulent regime).

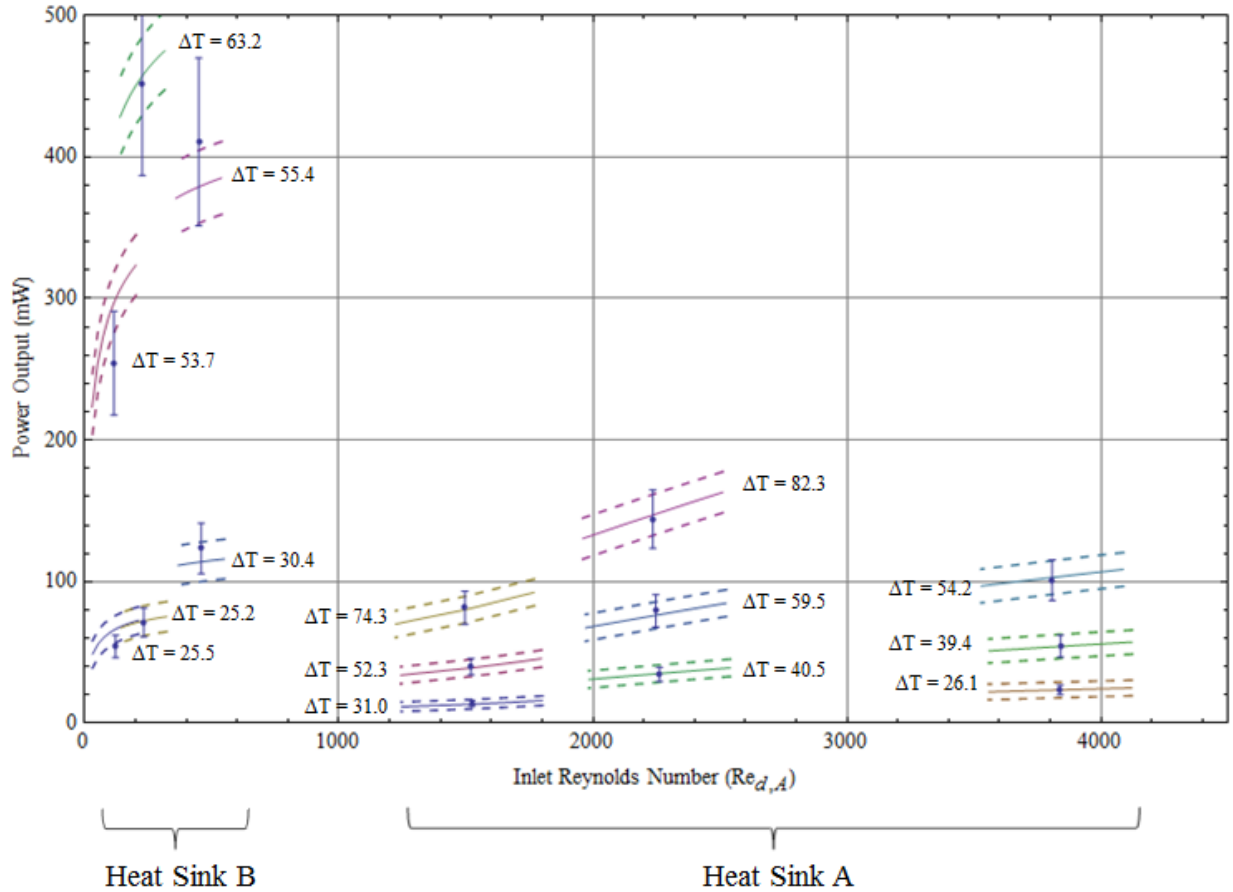


Figure 6-3: Experimental Results for the TEG1-12611-6.0 Thermoelectric Generator. Curves represent predicted values with accompanying uncertainty. Points represent measured values with their uncertainty. Transition to turbulent flow occurs at $Re_{d,A} \sim 1000$.

With values for Z_D and U_D'' , power output for this particular thermoelectric device may be modeled in different situations. The value of the analytical model lies in the ability to predict the behavior of the thermoelectric device in a wide range of Reynolds numbers, heat sink geometries, temperature differences, and bypass ratios. The same thermoelectric device was tested using heat sinks of type *B* on each side in order to provide a very different set of thermal pathways with which to measure predictions. Although air velocity for this test is comparable to the previous case, Reynolds numbers are much lower, placing them well into the laminar flow regime. Also, the fin quantity, geometry, and porosities are vastly different on this heat sink, as is

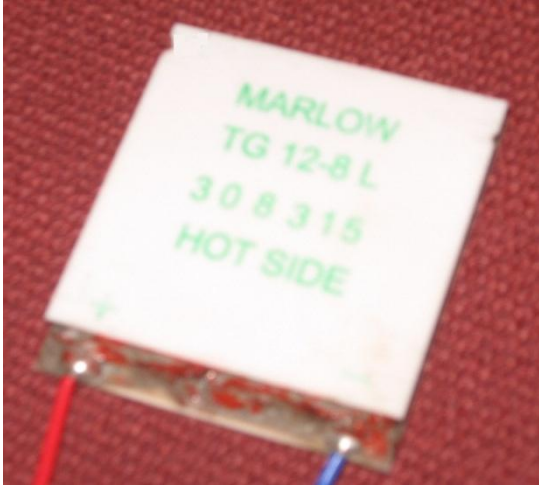
the bypass ratio. Despite these changes, the analytical model performs well. The largest power outputs, several times higher than the power outputs at which Z_D and U_D'' were characterized, are predicted within 8% (Fig. 6-3, laminar regime), the worst predictions are roughly 20% different. The results of these experiments support the model as a first-order approximation.

Throughout this testing, the thermoelectric device itself is calculated to experience a temperature difference of around 15°C in the most extreme cases. Manufacturer specifications for the TEG1-12611-6.0 indicate that with a temperature difference of 200°C (hot side at 250°C and the cool side at 50°C) it will produce 14.1 watts of power with 320 watts of heat passing through the device (Thermal Electronics Corp.). Fitting this information to the efficiency function derived in chapter two (eq. 2-25), suggests that Z_D and U_D'' under these conditions take on values of $8.62 \times 10^{-4} \text{ K}^{-1}$ and $521 \text{ W/m}^2\text{K}$ respectively. When the values suggested by this design point are used, the power output in the regime tested is over-predicted by up to 30 percent. The differences between the values calculated from the tests and the values suggested by this design point are attributed to differences in thermoelectric properties at the relatively low temperatures of these experiments and potentially several effects, discussed later in this chapter.

6.3.2 Marlow Industries Set of Thermoelectric Generators

The tests described in the previous section were carried out for a set of two TG12-8 thermoelectric devices manufactured by Marlow Industries Inc. Four points at turbulent Reynolds numbers were used to estimate Z_D and U_D'' for each device (Table 6-3). The difference in the values is well within the fluctuation expected due to uncertainty and imperfect repeatability in the nature of the experiment.

Table 6-3: Device Characterization for Two Identical TG12-8 Thermoelectric Devices.

		
Device	$Z_D (K^{-1})$	$U_D'' (W/m^2K)$
First	10.49×10^{-4}	336
Second	10.46×10^{-4}	355

Six test conditions were tested for each set of heat sinks. The comparisons of measured power to predicted power output are shown in Figs. 6-4 and 6-5. Due to the indirect nature of controlling the flow rate and the temperature difference in the air streams, the conditions at each test point are not replicated exactly. However, the behavior of each device is seen to be essentially the same.

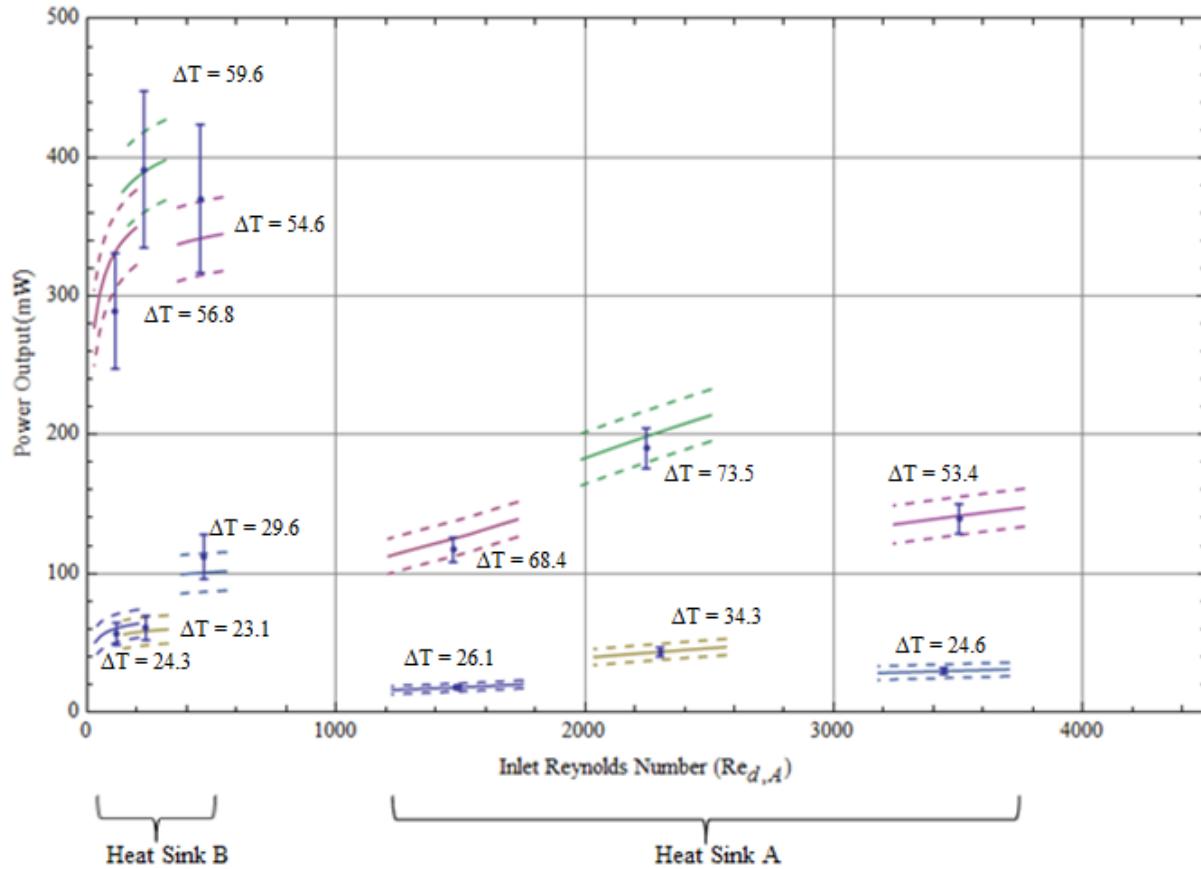


Figure 6-4: Experimental Results for the First TG12-8 Thermoelectric Generator. Curves represent predicted values with accompanying uncertainty. Points represent measured values with their uncertainty.

Two properties, Z_D and U_D'' , of the thermoelectric device are required for using the model, but were not initially known. In order to estimate these parameters, four settings were tested using heat sinks of type A, and the results used to calculate the parameters Z_D , and U_D'' using a least squared error approach using percent error between the measured power output and the power output predicted by the model. These parameters were then used to predict power output at a number of other experimental conditions involving a range of temperature differences for both sets of heat sinks. The power measurements and predictions are compared in the sections that follow.

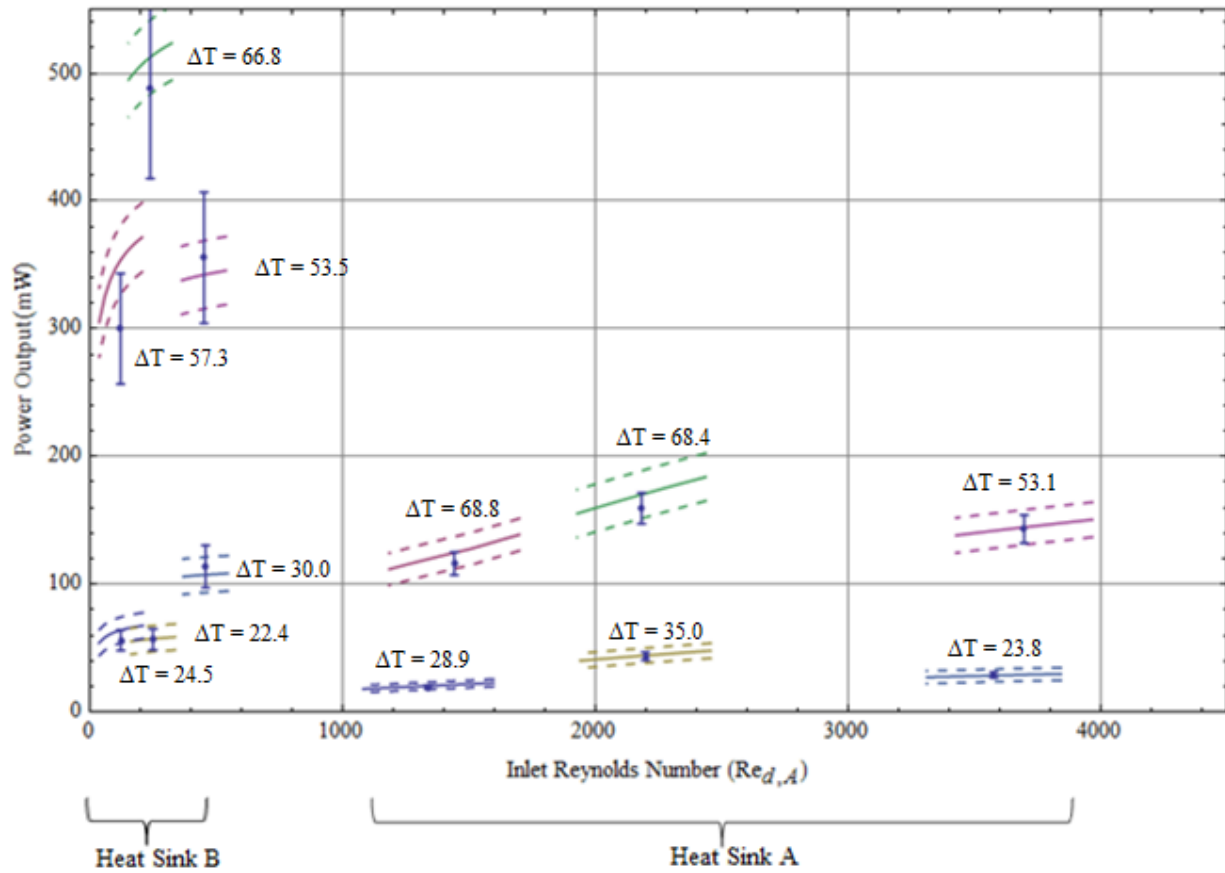


Figure 6-5: Experimental Results for the Second TG12-8 Thermoelectric Generator. Curves represent predicted values with accompanying uncertainty. Points represent measured values with their uncertainty.

Manufacturer specifications for the Marlow TG12-8 thermoelectric generator indicate that with the hot side at 110°C and the cool side at 50°C, it will produce 1.19 watts of electricity and exhibit a thermal resistance of 1.20 K/W (Marlow Industries Inc.). When fitted to the analysis associated with the efficiency relation (Eq. 2-25), these values suggest that Z_D and U_D'' under these conditions take on values of $15.9 \times 10^{-4} \text{ K}^{-1}$ and $521 \text{ W/m}^2\text{K}$ respectively. The differences between the values calculated from the tests and the values suggested by this design

point are attributed to differences in thermoelectric properties at the relatively low temperatures of these experiments and potentially several effects, discussed later in this chapter.

6.4 Uncertainty

6.4.1 Uncertainty in Power Measurement

The power calculation involves only two values, voltage and resistance. The uncertainty resulting from the measurement of these two is dominated by the uncertainty in resistance. Electrical loads of 1.4 Ohms and 2.62 Ohms were connected to the TEG1-12611-6.0 and TG12-8 thermoelectric devices respectively through the use of a custom resistor and measured length of resistance wire. Equipment with the resolution required to verify the accuracy of these small resistances was not available. A conservative value for this uncertainty of 0.2 Ohms was used in both cases. As power measurements reached hundreds of milliwatts, the uncertainty in power grew significantly, resulting in the large error bars in the data points. For a system with many thermoelectric devices, the load to match would be the sum of all the device impedences. With a larger impedance to match, an uncertainty of a similar magnitude would have a much smaller effect on total power uncertainty.

6.4.2 Uncertainty in the Model

The error bands in the predicted power output are the result of uncertainty in the measurements that were fed into the analytical model. Although uncertainty was included for every physical value, the uncertainty in temperature measurements was found to completely overshadow all other sources of uncertainty. Temperatures were measured with one thermocouple junction in the flow path before the fin array and another after the fin array for

each flow stream. Exploratory tests revealed that the location of the thermocouple in the channel cross-section had a significant effect on the reading. Cursory effort was made to position the thermocouples in a position that best represented the average temperature in the flow, but temperature profile effects as such could not be incorporated into the analysis.

In addition, T_S and T_A represent averages of readings before and after the fins in each case. Temperature changes of several degrees were observed as these airstreams lost or gained thermal energy, respectively. A better, but more complex method of accounting for temperature changes in the streamwise direction is treated in Chapter 8.

Because of these approximations and the general uncertainty expected in temperature measurements, T_S and T_A were assigned uncertainties of 1.5 degrees Kelvin. The resulting uncertainty in the temperature ratio $T = T_A/T_S$ causes essentially all the uncertainty in the power prediction curves shown in the plots. The power output is, unsurprisingly, extremely sensitive to this ratio. When the ratio of T_A to T_S increases, not only does less heat flow into the device due to a smaller temperature difference, but like heat engines in general, the device becomes less efficient at converting it.

6.4.3 Uncertainty not reflected in the Plots

Unmatched load. The task of creating matched load conditions is not as difficult as the preliminary task of first determining the electrical impedance of the device. Exploratory attempts to characterize this parameter showed that the equipment used in this research was unable to maintain uniform conditions stable enough to deduce the matched load condition from manipulating the load. The values chosen upon were based on manufacturer data, despite the fact that this data was obtained at higher temperatures than were experienced by the devices in this particular test. The matched load condition is inherent in the model; there is no functional

relationship (except in the derivation) from which uncertainty in the device resistance can be projected into power uncertainty. Error introduced from this uncertainty likely affects the empirical estimates for Z_D and U_D ”.

Constant properties. Inherent in the model is the assumption that all properties are independent of temperature. Although the range of temperatures experienced by the device in this test is not large, significant errors would be expected when using the values for Z_D and U_D ” found in this experiment in the higher temperature regimes. Rowe (2006) suggests that the use of constant, averaged properties generally allows for calculations within 10%.

6.5 Weaknesses of the Model

Although the model works well when it is first used to characterize Z_D and U_D ”, the values found in the experiments are significantly different than those that are calculated from manufacturer data. Below are some suggestions that might render the perceived values of these parameters different from their true values. For each of these sources of weakness, any error produced by them would inevitably be absorbed into the calculation of Z_D and U_D ”, which, unlike all other parameters, were not measured directly, but fitted to match empirical data.

Inaccuracy in the Nusselt Number correlation. The correlation fitted by Kim, Kim, and Ortega to a set of experiments performed with heat sinks attempts to calculate Nusselt number for pin fin heat sinks based only on hydraulic fin diameter and porosity. Absent from this correlation is a dependence on aspect ratio w_x/w_z . The aspect ratio of sink *A* is 1.0, while the aspect ratio of sink *B* is 18.5. The effect of aspect ratio may or may not be significant, but any inaccuracy in the convection analysis will affect the calculations for the thermal conductances U_H and U_L . This dramatic difference in aspect ratio may be the cause of the observed trend that

power output is underpredicted at the lowest Reynolds numbers, and overpredicted at the highest Reynolds numbers for heat sink B (laminar regime).

Effectiveness of Bypass Insulation. As discussed in Chapter 5, the model approximates the heat sink base as isothermal in the z direction. A simple finite-difference simulation suggested that this approximation was reasonable for bypass ratios (r) up to 2 with the design considered. In the experiment, bypass insulation surrounded the thermoelectric devices on all four sides. In Chapter 5, it was speculated that bypass ratios of about 3 might be reasonably modeled this way, but beyond this, the decrease in accuracy would likely become dramatic. It is important to remember that this approximation is always an optimistic one, as spatial effects will always tend to make the temperature difference through the device slightly less than the spatial average between heat sink bases. The equipment available for experimentation at the time of this research necessitated high bypass ratios, especially for the smaller TG12-8 devices (See Table 6-1). The approximation made by the model will thus overestimate the temperature difference across the device—which in this case was probably compensated for in part by underestimating its effectiveness at energy conversion.

Efficiency Function. The analysis that results in the efficiency function derived in this research (Eq. 2-25) was the backbone of the analytical model. In the case of the TG12-8 device, Marlow Industries indicates that the optimum load for highest efficiency is approximately 1.3 (TG12-8 Data Sheet). Insofar as this is true, the efficiency function derived in Chapter 3—which predicts that maximum power and maximum efficiency coincide at matched load—misrepresents the device. A similar plot is shown in Fig. 6-7 using the efficiency equation derived in Chapter 2 (Eq. 2-25) as well as the efficiency equation derived by Gordon (1991) (Eq. 2-28) modified with Eq. 2-14 to represent dependency on load ratio.

The efficiency curve derived by Gordon predicts a maximum efficiency at a ratio of 1.16 for the parameters used to create the plot in Fig. 6-7, while the curve derived in Chapter 2 predicts maximum efficiency at matched load. Because it predicts maximum efficiency at a load ratio of greater than 1.0, this efficiency curve more closely resembles the manufacturer’s data in at least this respect.

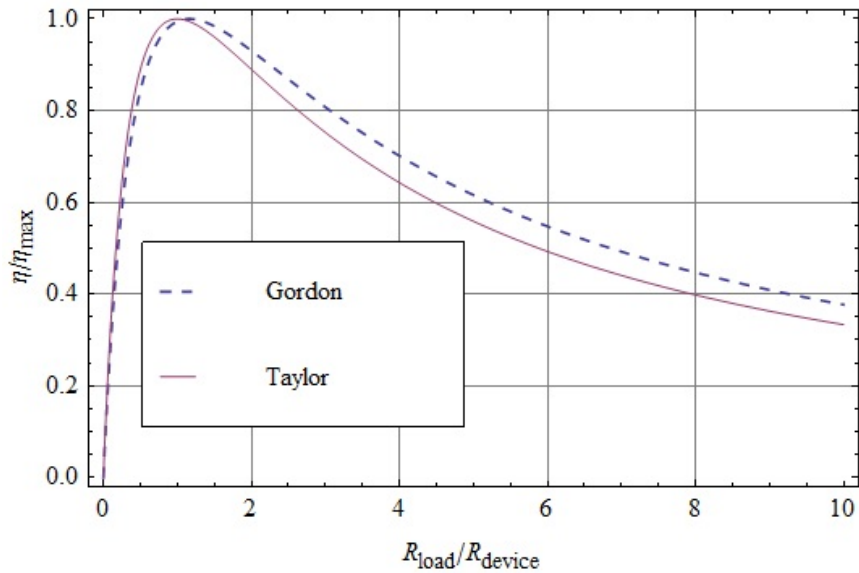


Figure 6-6: Analytical Predictions for Normalized Thermodynamic Efficiency. Parameters used: $T_H = 400\text{K}$, $T_L = 300\text{K}$, $Z_D = .001\text{K}^{-1}$.

In addition, recall Fig. 2-4, where these two efficiency functions are plotted—non-normalized—against dimensionless current, i . The function derived in this research predicted efficiency generally higher than that predicted by Gordon. If Gordon’s efficiency derivation is more accurate in this regard also, then the model used here likely has the additional inaccuracy of over-predicting the device efficiency at matched load. In this case, the inaccuracy is doubtless compensated for in part by underestimating its effectiveness at energy conversion through a low empirical estimate of Z_D .

Bias at Low Power Outputs. In the course of the experimental work, some test points were taken in which the power output was extremely low (less than 10 mW). These were test points involving small temperature differences combined with very low Reynolds number using heat sink A. After analysis, these points were observed as ill-fit for the model, suggesting that it is simply less accurate at very low power outputs. Thus, the method of solving for Z_D and U_D'' , in which two low power outputs are equally weighted by percentage with two high power outputs, may be subject to some of the inaccuracy that was observed at very low power outputs. This inaccuracy would not only affect the parameters calculated for the thermoelectric device, but likely compromise the accuracy of the model at higher power outputs.

Correlation between Z and U_D'' . Through the course of fitting values for Z_D and U_D'' to the model, an optimization routine was used, minimizing the squared percent error of the four data points taken for that purpose. While, in theory, this process is valid for characterizing the device, it was found that the relationship between Z_D and U_D'' in the model is insensitive to trade-offs between the two parameters when fitting them to a particular data set. For example, consider the TEG1-12611-6.0 thermoelectric device. Although the values given previously ($Z_D = 6.25 \times 10^{-4} \text{ K}^{-1}$, $U_D'' = 354 \text{ W/m}^2\text{K}$), provide a good prediction (within ~20%) of power output for heat sink B (laminar flow), using the wildly different values of $Z_D = 4.94 \times 10^{-4} \text{ K}^{-1}$ and $U_D'' = 998 \text{ W/m}^2\text{K}$ matches all six laminar points within 2.5%. Clearly, the device characteristics could not be changing this drastically, but the mathematical relationship between Z_D and U_D'' in the model is such that an undervalued estimate of one may be compensated for by an overvalued estimate of the other. As can be seen by the values mentioned, the sensitivity of the model to the value of U_D'' is particularly low, indicating that a reasonable prediction of a similar thermoelectric device could likely be made with only a knowledge of Z_D .

6.6 Model Usefulness

Despite the weaknesses of the model and the uncertainties in these particular experiments, it has been shown that by characterizing a thermoelectric device under a small number of conditions, behavior under very different thermal pathways may be predicted with reasonable accuracy. The fact that this model is an analytical solution makes it vastly easier to optimize when compared to a numerical simulation. This model is proposed as a starting point for analyzing whether a given waste heat stream may be economically used in a thermoelectric harvesting system of the design proposed in this thesis. This first-order approximation can answer the question of feasibility, suggest optimized designs, and provide useful starting designs for more computationally intensive analysis.

7 ECONOMIC MODELING

This chapter develops an economic model for estimating the value of installing a thermoelectric energy harvesting system of the type described. The physical model developed thus far is joined to the economic model, and the concept behind the incorporation of bypass insulation validated.

7.1 Time Value of Money

In order to optimize the bypass ratio, it is necessary to express the ability of a system to pay for itself over a reasonable time. A meaningful economic analysis incorporates the time value of money.

Of primary importance in this analysis is the prevailing interest rate. The prevailing interest rate, i_{prev} , represents the rate of return that can be expected on money prudently invested in the economy. The prevailing interest rate causes money in the present to be worth more than the same amount in the future because of the potential for money to grow with time. When comparing dollar amounts in the present to dollar amounts in the future, it is standard procedure to use the prevailing interest rate to represent all quantities as dollar amounts in the present. This is achieved through

$$V_{future} = V_{present}(1 + i_{prev})^n \quad 7-1$$

where n is the number of years into the future. When yearly compounding is used, any quantity of money in the future may be represented in terms of the present value through Eq. 7-1.

Also of significant importance in economic analysis is the rate of inflation, i_{infl} . The rate of inflation represents the diminishing value of money as money itself becomes more abundant in the economy relative to goods and services. Because inflation decreases the value of money over time, it competes with the prevailing interest rate in determining the present value of a dollar amount in the future. The actual buying power of a dollar amount in the future, measured in present dollars, is attenuated through inflation thus:

$$B_{power} = \frac{V_{future}}{(1 + i_{infl})^n} \quad 7-2$$

When considering both the prevailing interest rate and inflation, it is possible to establish an equivalent interest rate that incorporates the effects of both on buying power. Substituting Eq. 7-1 into 7-2 renders the true buying power of a present value after both effects have been accounted for.

$$B_{power} = V_{present} \frac{(1 + i_{prev})^n}{(1 + i_{infl})^n} \quad 7-3$$

Now, arbitrarily require that Eq. 7-3 could be rewritten more simply as

$$B_{power} = V_{present} (1 + i_{equiv})^n \quad 7-4$$

where i_{equiv} is some equivalent interest rate. Set both equations for buying power equal to each other to obtain the equivalent interest rate (Eq. 7-5). This derivation is adapted from Jaluria (1998), to which the reader is referred for a condensed survey of time-valued economic modeling relating to thermal systems.

$$i_{equiv} = \frac{1 + i_{prev}}{1 + i_{infl}} - 1 \quad 7-5$$

In the economic analysis to follow, this interest rate is used to model continuous time value change of money. When compounding is not yearly, but continuous, the equivalent interest rate may be used to describe the buying power of money in the future according to

$$B_{power} = V_{future} e^{-n i_{equiv}} \quad 7-6$$

One more monetary rate is of interest in this analysis. The rate of change of the price of energy in the United States is considered. The *present* price of energy (dollars per kilowatt hour) is represented $\chi_{\$o}$. The price of energy in the future is expected to rise roughly with inflation, rendering the price of energy as function of time according to the inflation rate. In order to provide flexibility in the analysis, a constant is introduced to model the possibility that the price of energy increases faster than inflation. As environmental concerns impose more demands on facilities that provide electric power from fossil fuels and those same concerns provide impetus toward renewable sources, the price of energy may indeed rise faster than inflation in coming years. An arbitrary constant, ω , is multiplied to the inflation rate when determining the cost of energy. If this constant is one, the cost of energy is modeled as increasing exactly with inflation, if it is greater than one, then it increases in cost faster than inflation. Continuous compounding yields,

$$\chi_{\$}(n) = \chi_{\$o} e^{n \omega i_{infl}} \quad 7-7$$

These rates will be used in creating an economic model that allows for the value of the power produced by the thermoelectric system through time to be converted into a present value for comparison with the initial cost of the system.

7.2 Present Value Model

Consider the system illustrated in Fig. 7-1. The size of the system in the x and z directions are represented by the capital letters X and Z . These are normalized against the dimensions of the thermoelectric device, a_1 and a_2 , to obtain unitless width Z^* and depth X^* .

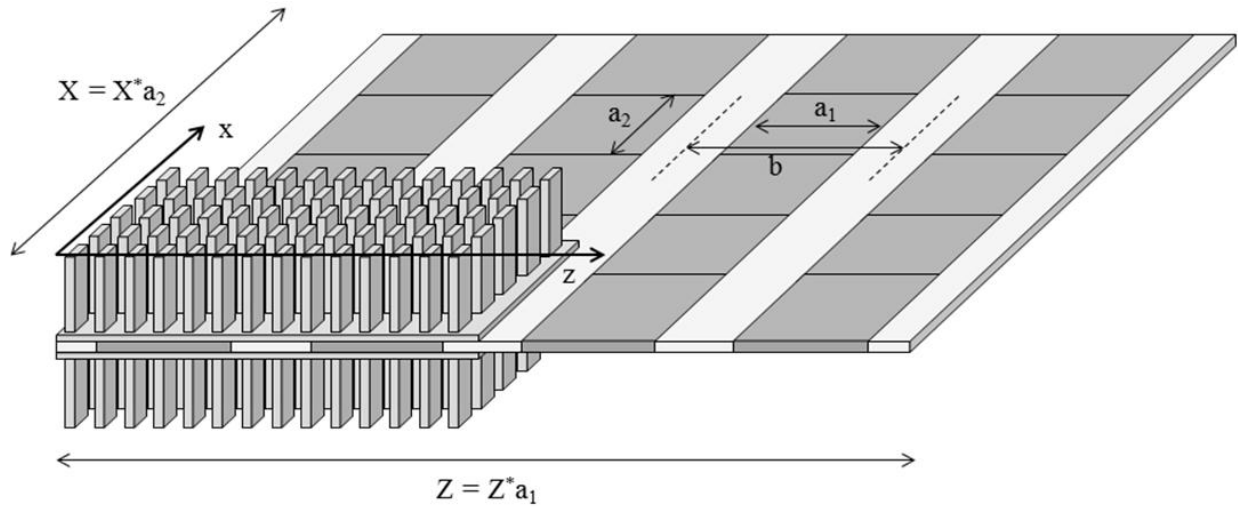


Figure 7-1: System Layout: Normalized System Dimensions. The system is characterized with dimensionless width Z^* and depth X^* .

The total number of devices in the system is calculated as

$$N_D = \frac{X^* Z^*}{r} \quad 7-8$$

As a first approximation, the only cost associated with the energy conversion system is the initial cost to implement it. A simple model of this cost is used in the analysis. The cost of a single device is termed C_{oneD} , and the cost of the whole system is given by

$$C_{sys} = C_L + C_M + N_D C_{oneD} \quad 7-9$$

The variable C_L represents the cost of labor involved with installation of the system, and any other fixed cost whose value may be modeled as independent of the design of the system. The

variable C_M represents the materials cost of the two large heat sinks, which have price per square meter p_{HS} (\$/m²) and the insulation, which has price per square meter p_{ins} (\$/m²). Incorporating Eq. 7-8 for the number of thermoelectric devices, these costs may be normalized against the cost of one thermoelectric device:

$$p_{HS}^* = \frac{a_1 a_2 p_{HS}}{C_{oneD}} \quad 7-10$$

$$p_{ins}^* = \frac{a_1 a_2 p_{ins}}{C_{oneD}} \quad 7-11$$

Equations 7-8, 7-10, and 7-11 are used in Eq. 7-9 to express the present value cost of the system in terms of the fixed cost, C_L , the cost of a single device, C_{oneD} , and dimensionless system geometry.

$$C_{sys} = C_L + C_{oneD} \left(\frac{X^* Z^*}{r} \right) (2p_{HS}^* r + p_{ins}^* (r - 1) + 1) \quad 7-12$$

Now consider the value of the energy produced by the system, which is subject to the effective interest rate i_{equiv} . This value is modeled as a continuous income stream. Consider a system that produces a smooth income stream through n years.

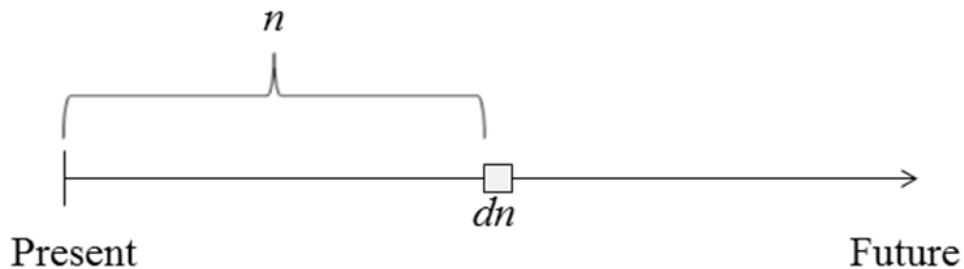


Figure 7-2: The Arrow of Time. The location in time is measured in years, n , with a differential unit of time, dn .

At a representative point in time, a differential unit of revenue created in the time dn is given by

$$dRev = 8.76 \theta \chi_{\$}(n) e^{-n i_{equiv}} \dot{W}_{out} dn \quad 7-13$$

Where the units of $\chi_{\$}$ are \$/kW*hour, n is years, and \dot{W}_{net} is watts. The conversion constant 8.76 has units of kW*hour/year*watt. The constant θ is introduced as a time-averaged percentage of how often the system runs. If it is never shut down, this constant is equal to one. A value of $\theta = 0.71$ is roughly equivalent to 20 hours of operation a day, 6 days a week. Substitute Eq. 7-7 into 7-13 and then integrate from the present through n years to obtain the present-valued revenue of the system:

$$Rev(n) = \frac{8.76 \theta \chi_{\$o} \dot{W}_{out}}{\omega(i_{infl} - i_{equiv})} \left(e^{n(\omega i_{infl} - i_{equiv})} - 1 \right) \quad 7-14$$

This equation now allows for the total revenue to be calculated up through any time, n , as measured in present value. When this revenue reaches the startup cost value, C_{start} , the system has reached its payback time. The payback time may be solved for directly by equating Eqs. 7-12 and 7-14, and solving for the number of years, n_{pb} . This process yields

$$n_{pb} = \left(\frac{1}{\omega i_{infl} - i_{equiv}} \right) \ln \left(\frac{(\omega i_{infl} - i_{equiv})(C_L r + C_{oneD} X^* Z^* (2p_{HS}^* r + p_{ins}^* (r - 1) + 1))}{8.76 \theta \chi_{\$} \dot{W}_{out} U_D'' T_S A_{oneD} X^* Z^*} + 1 \right) \quad 7-15$$

Where \dot{W}_{out}^* is the nondimensional power output (Eq. 3-37) of the system introduced in chapter three. In addition to payback time, other pertinent equations include actual gross power output for the entire system, \dot{W}_{out} , and the actual gross power output for one device, \dot{W}_{oneD} .

$$\dot{W}_{out} = \dot{W}_{out}^* U_D'' T_S \frac{X^* Z^*}{r} A_{oneD} \quad 7-16$$

$$\dot{W}_{oneD} = \dot{W}_{out}^* U_D'' T_S A_{oneD} \quad 7-17$$

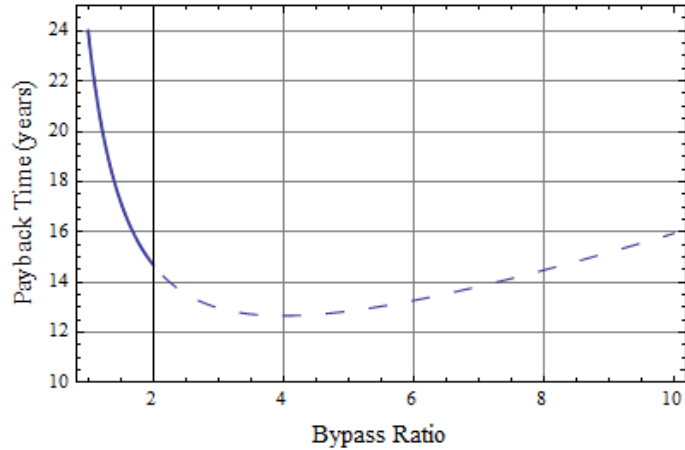
With this model, the economic benefit of designing the system with bypass insulation can be observed through the following procedure:

1. Identify known parameters for a given system except for bypass ratio r .
2. Choose a bypass ratio $r = b/a_I$.
3. Solve the system model equations from chapter three for the vital parameters τ , τ_b , γ , γ_H , and \dot{W}_{out}^* . (Chapter 8.3, step 5a may be referred to as a guide to these equations.)
4. Solve Eq. 7-15 for the payback time in years, n_{pb} .
5. Repeat steps 2 through 4 modifying the value for r until the value is found which minimized the dimensionless payback time.

This process was used to calculate the bypass ratio that minimizes payback time for two cases, which illustrate the effect of the thermal conductance ratios Ψ_L'' and Ψ_H'' on optimum bypass ratio.

First, values for thermal conductance ratios per area were chosen of $\Psi_L''=2.0$ and $\Psi_H''=2.2$. These values are representative of achievable thermal transport using airstreams. The results are summarized in Fig. 7-3. The model predicts that the optimum bypass ratio that minimizes the payback time is about four. Unfortunately, the model becomes inaccurate beyond bypass ratios of about two, as discussed in Chapter 5. However, the results indicate that a bypass ratio of at least two is desirable for reducing the payback time of the system by about 10 years. Notice the power output per device for the different bypass ratios.

The dashed line indicates the single node approximation beyond bypass ratios of two. Because this is an overly optimistic approximation, it is expected that the true payback time after $r = 2$ would begin to increase more rapidly than shown. Thus, the true optimum ratio is probably less than four.



With Bypass Ratio of 3.99679

Total System Cost \$4882.2
 Total Watt Output 344.722
 Number of Devices 125
 Watts per Device 2.75778
 Payback Time 12.7 Years

Without Bypass

Total System Cost \$14250.
 Total Watt Output 581.622
 Number of Devices 500.
 Watts per Device 1.16324
 Payback Time 24. Years

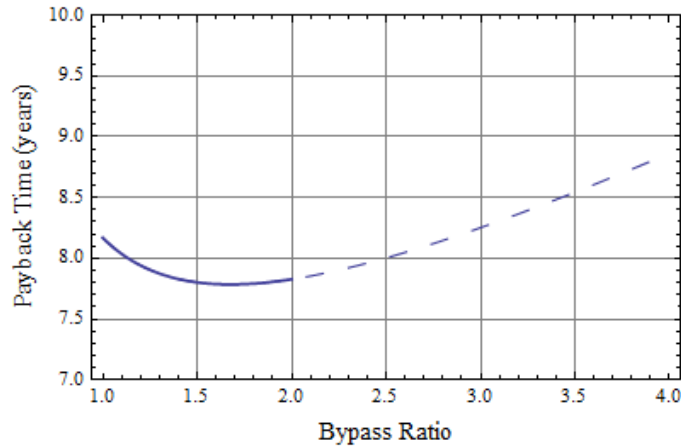
With Bypass Ratio of 2.0

Total System Cost \$8003.12
 Total Watt Output 495.096
 Number of Devices 250
 Watts per Device 1.98038
 Payback Time 14.7 Years

Figure 7-3: Predicted Payback Time vs Bypass Ratio: $\Psi_H'' = 2.2$, $\Psi_L'' = 2.0$. Parameters used: $T_S = 100^\circ\text{C}$, $T_A = 25^\circ\text{C}$, $\zeta = .7$, $U_D'' = 500 \text{ W/m}^2\text{K}$, $A_{oneD} = 36 \text{ cm}^2$, $C_L = \$500$, $p_H^* = .05$, $p_{ins}^* = 5 \cdot 10^{-4}$, $\chi_S = \$.20$, $i_{infl} = .03$, $i_{prev} = .08$, $\omega = 1.05$, $\theta = .71$, $Z^*X^* = 500$, $\Psi_{IL}'' = 30$, $\Psi_{IH}'' = 30$, $\Psi_{bp}'' = .01$.

The second example, Fig. 7-4, demonstrates the effect of bypass insulation when values for Ψ_L'' and Ψ_H'' are increased to 11 and 10 respectively to represent thermal transport

achievable with water streams. In this case, the reduction in payback time due to using bypass insulation is much more modest (0.4 years). The optimum bypass ratio is about 1.7.



With Bypass Ratio of 1.67597

Total System Cost \$9210.89
 Total Watt Output 1015.54
 Number of Devices 298
 Watts per Device 3.40784
 Payback Time 7.8 Years

Without Bypass

Total System Cost \$14250.
 Total Watt Output 1502.15
 Number of Devices 500.
 Watts per Device 3.0043
 Payback Time 8.2 Years

Figure 7-4: Predicted Payback Time vs Bypass Ratio: $\Psi_H'' = 11$, $\Psi_L'' = 10$. All other parameters have the same values as in Figure 7-3.

The examples indicate that as the effectiveness of thermal transport increases, payback time is greatly reduced (24 years vs 8.2 years respectively without bypass). They also indicate that, with more effective thermal transport, the ability of bypass insulation to further reduce payback time is diminished (improvements of 9.3 years vs 0.4 years respectively through adding bypass).

The lower optimum bypass ratio of the second case also suggests that the optimum r value decreases as thermal transport becomes more effective.

Note that in these examples, the power requirement to move the fluid through the fin array is not included in the model. This power requirement will draw from the net harvestable power and affect the payback time. In the next chapter, the effects of bypass ratio and all other aspects of the model previously developed will be combined. With the ability to model the conversion system both physically and economically, a complete system modeling may now be developed.

8 COMPLETE SYSTEM MODELING

In previous chapters, models of various aspects of the thermoelectric power generation system have been created. For the design of an entire system, all of these models will be combined into a single, analytical simulation.

8.1 Nondimensionalization for System

Not all of the nondimensionalizations presented in previous chapters are ideal when all aspects of the model are combined. Some modifications to the nondimensionalization heretofore developed are presented here.

First, consider the fan or pump power required to move the fluid through the fin array. The heat to flow power ratio q/\dot{W}_{req} discussed in Chapter 4 (Eq. 4-48) is valuable for assessing the behavior of a heat sink, but is not a ratio of direct interest in modeling the entire thermoelectric system. Instead, this power requirement is nondimensionalized in terms of the total thermal conductance of the devices in the system, U_D (W/K), and the hot stream temperature, T_S (K). This is the method of nondimensionalization for power introduced in Eq. 3-37 of chapter three. Divide Eq. 4-46 by $U_D T_S$ and rearrange to obtain

$$\dot{W}_{req}^* = \frac{1}{2} \phi f r \epsilon_x \lambda \left(\frac{Re_d}{d_p^*} \right)^3 \quad 8-1$$

The dimensionless fin diameter, d_p^* , now fills the role previously filled by \mathcal{A} in Chapter 4 (see Eq. 4-51). While \mathcal{A} is a convenient nondimensionalization for observing heat sink behavior, it

involves the temperature at the fin base, T_B , which is not of importance nor accounted for explicitly in the general model. The dimensionless fin diameter, d_p^* is defined as

$$d_p^* = d_p \frac{U_D''}{k_{sink}} \quad \mathbf{8-2}$$

The parameter φ represents a dimensionless group of parameters, none of which are design variables:

$$\varphi = \frac{\mu^3 U_D''^2}{T_S \rho^2 k_f^3} \quad \mathbf{8-3}$$

The power requirement must be calculated from Eq. 8-1 for both the hot fluid stream at T_S and the ambient fluid stream at T_A . In doing this, the parameter φ is evaluated for each stream, but always contains T_S (never T_A) in the denominator. The other fluid properties composing φ are evaluated at the temperature of the respective stream.

In order to use the system model in nondimensional space, the thermal conductance per area ratios must be expressed in terms of nondimensional inputs. These ratios are formed by dividing each thermal conductance per area U_i'' by the device conductance, U_D'' (see Chapter 5.3):

$$\Psi_i'' = \frac{U_i''}{U_D''} \quad \mathbf{8-4}$$

where i represents all the types of thermal conductances (H, IH, L, IL, bp). Preliminary to using Eq. 8-4, two more dimensionless groups are introduced: a convenient, dimensionless group of constants, Π_{uka} :

$$\Pi_{uka} = \frac{k_{sink}}{a_1 U_D''} \quad \mathbf{8-5}$$

and the dimensionless heat sink base, L_b^* :

$$L_b^* = \frac{L_b}{a_1} \quad 8-6$$

As seen in Eq. 8-6, the thickness of the base of each heat sink, L_b , is normalized against the width of the thermoelectric device, a_1 . As this parameter becomes very small, lateral heat transfer in the sink base will be inhibited, and the single temperature node approximation for thermal bypass will eventually be compromised. Values for L_b^* in the experiments (Chapter 6) ranged from 0.09 to 0.16.

Now the thermal conductance ratio Ψ_H'' is found from the heat sink analysis of chapter four. Insert Eqs. 4-7 and 4-8 into Eqs. 4-10 and 4-11, then substitute these into Eq. 4-12 to obtain thermal conductance U_H'' . When this is divided by U_D'' , the thermal conductance per area ratio Ψ_H'' is formed. Then, the ratio may be cast in terms of dimensionless parameters previously defined (Eqs. 8-6, 8-5, 8-2, 4-50, 4-49, and 4-17 through 4-22) to become

$$\frac{U_H''}{U_D''} = \Psi_H'' = \frac{\frac{\Pi_{uka}}{L_b^*} \left(2\sqrt{\frac{\epsilon C_1 Re_d^m}{\kappa}} (1 - \epsilon_x) (1 - \epsilon_z) \tanh \left(2\lambda \sqrt{\frac{\epsilon C_1 Re_d^m}{\kappa}} \right) + \frac{\epsilon^2 C_1 Re_d^m}{\kappa} \right)}{d_p^* \frac{\Pi_{uka}}{L_b^*} + \left(2\sqrt{\frac{\epsilon C_1 Re_d^m}{\kappa}} (1 - \epsilon_x) (1 - \epsilon_z) \tanh \left(2\lambda \sqrt{\frac{\epsilon C_1 Re_d^m}{\kappa}} \right) + \frac{\epsilon^2 C_1 Re_d^m}{\kappa} \right)} \quad 8-7$$

The interfacial thermal conductance per area ratio Ψ_{IH}'' is likewise found by dividing Eq. 4-16 by U_D'' to obtain

$$\Psi_{IH}'' = \frac{k_{cover}}{U_D'' (R_{contact} k_{cover} + L_{cover})} \quad 8-8$$

Equations 8-7 and 8-8 may be applied to the low temperature side thermal pathways exactly as in the high temperature side to obtain Ψ_L'' and Ψ_{IL}'' , using parameter values pertaining to the ambient fluid stream and heat sink.

One more dimensionless parameter is introduced, M_5 , which represents the mass flow of the hot fluid stream,

$$M_S = \frac{\dot{m}_S}{a_1 \mu_S} \quad 8-9$$

When considering a thermoelectric conversion system for a particular application, the available mass flow of the hot fluid stream, \dot{m}_S is likely to be a known and constraining parameter. If this was not held constant, the model thus far developed would predict ever increasing power outputs for larger and larger systems, unable to design around a finite quantity of source heat. The constant M_S allows for this flow rate to be specified in a nondimensional manner, and is related to the Reynolds number through

$$Re_{dS} = \frac{M_S}{Z^* \epsilon_{xS} \lambda_S} \quad 8-10$$

With these dimensionless parameters, the model may be applied to the entire thermoelectric conversion system.

8.2 Spatial Dependence of Fluid Temperatures and Power Output

Up until this point, the fluid temperatures have been treated as constants. However, when considering the entire system, it is important to note that the temperature of the source stream T_S will not be constant along the flow direction because the fluid is losing thermal energy into the heat sink. As observed in the experiment, the source temperature T_S will decrease as the fluid progresses through the fin array. It will eventually become too cool to produce an economically viable quantity of power. Modeling the decrease in available thermal energy of the hot stream allows for the length of the entire system in the flow direction to be appropriately determined. In the same manner, the ambient airstream will increase above its initial temperature T_A through the system.

Figure 8-1 depicts the system, with an emphasis on the hot stream. A differential control volume allows for relations to be constructed describing the temperature with flow direction.

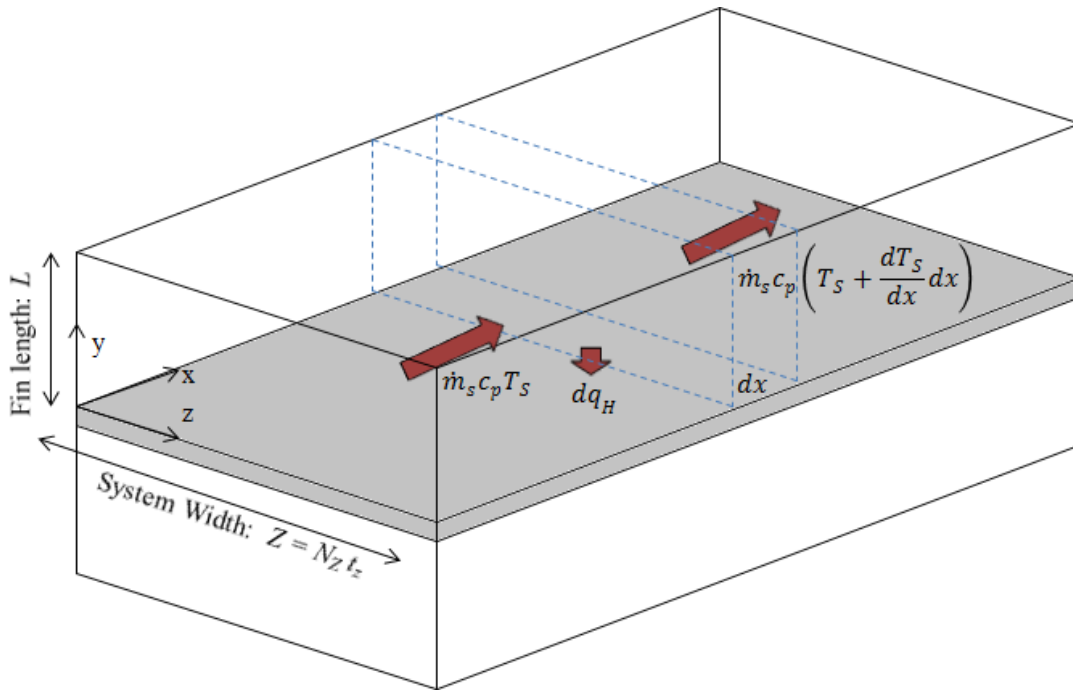


Figure 8-1: Fluid Channel Analysis. The schematic illustrates relations governing the temperature profile, $T_S(x)$. The thermoelectric devices and bypass insulation are incorporated into the gray area. Fins (not shown) fill each channel above and below.

Conservation of energy is applied for the control volume. Observing Fig. 3-2, the heat rate flowing from the hot fluid stream into the fin array at any point is $q_H = U_H(T_S - T_{IH})$. For the differential control volume, this is

$$dq_H = dU_H(T_S - T_{IH}) \quad 8-11$$

Equation 4-12 is similarly invoked (recognizing that $N_x t_x = X$) to obtain

$$dU_H = U_H'' N_z t_z dx \quad 8-12$$

After these two differential relations are substituted into the energy balance of Fig. 8-1, the following equation is obtained:

$$\frac{dT_S}{dx} = \left(\frac{U_H''}{c_{pS} \rho_S u_{mS} L_S} \right) \left(\frac{\gamma}{\gamma_H} - 1 \right) T_S \quad 8-13$$

Performing the analogous analysis on the other fluid stream, the following equation is obtained:

$$\frac{dT_A}{dx} = \left(\frac{U_L''}{c_{pA} \rho_A u_{mA} L_A} \right) \left(\frac{\tau_I \gamma}{\gamma_H T} - 1 \right) T_A \quad 8-14$$

Normalizing this equation requires the relation $x = a_2 x^*$ and also the new dimensionless group,

σ —a convenient group of constant parameters,

$$\sigma = \frac{U_D'' a_2}{c_p \mu} \quad 8-15$$

In addition, some new notation for describing the fluid temperatures is presented in Table 8-1, which accommodates an expanded representation of temperatures.

Table 8-1: Nomenclature for Temperature Variables.

<i>Variable</i>	<i>Defined As</i>	<i>Initial Value At $x^* = 0$</i>
<i>Dimensional</i>		
T_A	Temperature of cold stream (Ambient)	T_{AO}
T_S	Temperature of hot stream (Source)	T_{SO}
<i>Dimensionless</i>		
T	$\frac{T_A}{T_S}$	$T_o = \frac{T_{AO}}{T_{SO}}$
T_{RA}	$\frac{T_A}{T_{AO}}$	1
T_{RS}	$\frac{T_S}{T_{SO}}$	1
ζ	$Z_D T_S$	$\zeta_o = Z_D T_{SO}$

As with the temperature ratio $\mathbf{T} = T_A/T_S$ introduced in Chapter 3, the bold letter \mathbf{T} indicates a dimensionless ratio.

Using this notation, Eqs. 8-13 and 8-14 may be cast in dimensionless form

$$\frac{d\mathbf{T}_{RA}}{dx^*} = \frac{\sigma_A \Psi_L''}{\epsilon_{xA} \lambda_A Re_{dA}} \left(\frac{\tau_l \gamma}{\gamma_H \mathbf{T}} - 1 \right) \mathbf{T}_{RA} \quad 8-16$$

$$\frac{d\mathbf{T}_{RS}}{dx^*} = \frac{\sigma_S \Psi_H''}{\epsilon_{xS} \lambda_S Re_{dS}} \left(\frac{\gamma}{\gamma_H} - 1 \right) \mathbf{T}_{RS} \quad 8-17$$

Although these may appear at first to be simple linear differential equations, recall that the four temperature ratios τ , τ_l , γ , γ_H , are solved in the model through a knowledge of $\mathbf{T} = T_A/T_S$. These terms create implicit dependencies that require a numerical approach to solving the profiles for \mathbf{T}_{SO} and \mathbf{T}_{AO} . However, despite their nonlinearity, these equations were found to be numerically well-behaved, lending themselves to a first order (Euler) numerical method. When solving these equations numerically, the relationship

$$\mathbf{T} = \mathbf{T}_O \frac{\mathbf{T}_{RA}}{\mathbf{T}_{RS}} \quad 8-18$$

is used at each step to calculate \mathbf{T} . In addition, the analysis used to solve for the four temperature ratios τ , τ_l , γ , and γ_H (Eqs. 3-27 through 3-36) calls upon $\zeta = Z_D T_S$. Because T_S is now dependent on x^* , the change of ζ is accommodated by extended notation as well (Table 8-1) to yield

$$\zeta = (Z_D T_{SO}) \left(\frac{T_S}{T_{SO}} \right) = \zeta_O \mathbf{T}_{RS} \quad 8-19$$

This dependency must be used to calculate ζ at each step when Eqs. 8-16 and 8-17 are solved numerically. In the course of solving these equations, temperature profiles will be calculated not only for \mathbf{T} , \mathbf{T}_{RA} , and \mathbf{T}_{RS} , but also for τ , τ_l , γ , γ_H ; these four profiles will also be needed to model the system.

After profiles for the temperature ratios are solved, the dimensionless power output, \dot{W}_{out}^* must be addressed. Power output itself is a function of flow direction, and an integral approach needs to be used. The derivation for representing dimensionless power output when this dependence is accounted for begins with substitution of Eq. 5-8 into 5-2, and observing the total area of the system A_{sys} is equal to XZ . This results in the proportional relationship:

$$U_D(X) = \frac{1}{r} XZU_D'' \quad 8-20$$

When parameters besides X are fixed, the differential thermal conductance may be represented

$$dU_D = \frac{1}{r} ZU_D'' dx \quad 8-21$$

Now rearrange Eq 3-37 to obtain

$$\dot{W}_{out} = T_S(\Psi_{IH}\gamma(\gamma_H^{-1} - 1) - \Psi_{IL}\gamma(\tau - \tau_I\gamma_H^{-1}))U_D \quad 8-22$$

This represents the power output for a section where all temperature ratios (T , τ , τ_I , γ , γ_H) are constant. When these vary as a function of x , the equation must be used as a differential relation.

Differential power output is then

$$d\dot{W}_{out} = T_S(\Psi_{IH}\gamma(\gamma_H^{-1} - 1) - \Psi_{IL}\gamma(\tau - \tau_I\gamma_H^{-1}))dU_D \quad 8-23$$

Insert Eq. 8-21 to obtain the differential relation

$$d\dot{W}_{out} = T_S(\Psi_{IH}\gamma(\gamma_H^{-1} - 1) - \Psi_{IL}\gamma(\tau - \tau_I\gamma_H^{-1}))\frac{1}{r}ZU_D'' dx \quad 8-24$$

Now the power output may be found for a system of length X (using lower case x as the variable of integration), constants are removed from the integral:

$$\dot{W}_{out}(X) = \frac{1}{r}ZU_D'' \int_0^X T_S(\Psi_{IH}\gamma(\gamma_H^{-1} - 1) - \Psi_{IL}\gamma(\tau - \tau_I\gamma_H^{-1}))dx \quad 8-25$$

This integral function is now taken through nondimensionalization. Substituting from Eq. 8-20 and introducing T_{SO} , Eq. 8-25 is cast as

$$\frac{\dot{W}_{out}(X)}{U_D(X)T_{SO}} = \dot{W}_{out}^*(X) = \frac{1}{X} \int_0^X \frac{T_S}{T_{SO}} (\Psi_{IH}\gamma(\gamma_H^{-1} - 1) - \Psi_{IL}\gamma(\tau - \tau_I\gamma_H^{-1})) dx \quad 8-26$$

Note that the total thermal conductance of the thermoelectric devices, U_D , retains a proportional dependency on X (Eq. 8-20). The result is that dimensionless power out, $\dot{W}_{out}^*(X)$, depicts the fact that power generation becomes less effective with increasing X . Substituting the definitions $x = a_2x^*$ and $X = a_2X^*$ into Eq. 8-26, including changing the limits of integration, reveals that it may be cast in completely dimensionless form as

$$\dot{W}_{out}^*(X^*) = \frac{1}{X^*} \int_0^{X^*} T_{RS} (\Psi_{IH}\gamma(\gamma_H^{-1} - 1) - \Psi_{IL}\gamma(\tau - \tau_I\gamma_H^{-1})) dx^* \quad 8-27$$

Equations 3-21 through 3-36 are called at each step, as well as Eq. 8-19 for updating ζ .

The power required by the system in fan or pump work is now considered. Eq. 8-3 is used to adapt the dimensionless parameter φ to each fluid stream:

$$\varphi_S = \frac{\mu_S^3 U_D''^2}{T_{SO} \rho_S^2 k_{fS}^3} \quad 8-28$$

$$\varphi_A = \frac{\mu_A^3 U_D''^2}{T_{SO} \rho_A^2 k_{fA}^3} \quad 8-29$$

Now Eq. 8-1 is used to write the nondimensional power requirement for both streams

$$\frac{\dot{W}_{req}(X)}{U_D(X)T_{SO}} = \dot{W}_{req}^* = \frac{1}{2} r \left(\left(\varphi f \epsilon_x \lambda \left(\frac{Re_d}{d_p^*} \right)^3 \right)_S + \left(\varphi f \epsilon_x \lambda \left(\frac{Re_d}{d_p^*} \right)^3 \right)_A \right) \quad 8-30$$

The dimensionless power required, \dot{W}_{req}^* , is not a function of X , which results from the fact that pressure drop is linear. When \dot{W}_{req}^* is taken out of nondimensional space by multiplying by U_D , the dependency of actual power requirement on the system length, X , is taken into account.

The difference between Eqs. 8-27 and 8-30 represents the net dimensionless power produced by the system:

$$\dot{W}_{net}^*(X^*) = \frac{1}{X^*} \int_0^{X^*} \mathbf{T}_{RS}(\Psi_{IH}\gamma(\gamma_H^{-1} - 1) - \Psi_{IL}\gamma(\tau - \tau_i\gamma_H^{-1})) dx^* - \frac{1}{2} r \left[\left(\varphi f \epsilon_x \lambda \left(\frac{Re_d}{d_p^*} \right)^3 \right)_S + \left(\varphi f \epsilon_x \lambda \left(\frac{Re_d}{d_p^*} \right)^3 \right)_A \right] \quad \mathbf{8-31}$$

This equation may be accurately solved using a first-order summation approach for the integral portion, with step size Δx^* recommended between 0.01 and 0.1. The net power output may then be calculated with the following discretization,

$$\dot{W}_{net}^*(X^*) \cong \left(\frac{1}{X^*} \sum_{i=1}^{\frac{X^*}{\Delta x^*}} \mathbf{T}_{RSi} \left(\Psi_{IH}\gamma_i(\gamma_{Hi}^{-1} - 1) - \Psi_{IL}\gamma_i(\tau_i - \tau_{ii}\gamma_{Hi}^{-1}) \right) \Delta x^* \right) - \frac{1}{2} r \left[\left(\varphi f \epsilon_x \lambda \left(\frac{Re_d}{d_p^*} \right)^3 \right)_S + \left(\varphi f \epsilon_x \lambda \left(\frac{Re_d}{d_p^*} \right)^3 \right)_A \right] \quad \mathbf{8-32}$$

where X^* is chosen such that $X^*/\Delta x^*$ yields an integer value.

The value of \dot{W}_{net}^* may now be used to model the payback time for any system of length X^* through substitution into Eq. 7-15 to obtain

$$n_{pb} = \left(\frac{1}{\omega i_{infl} - i_{equiv}} \right) \ln \left(\frac{(\omega i_{infl} - i_{equiv})(C_L r + C_{oneD} X^* Z^* (2p_{HS}^* r + p_{ins}^* (r - 1) + 1))}{8.76 \theta \chi_{\$} \dot{W}_{net}^* U_D^* T_{SO} A_{oneD} X^* Z^*} + 1 \right) \quad \mathbf{8-33}$$

The payback time, in years, is given through Eq. 8-33. For poor designs, no physical payback time may be obtained—indicating that the effects of inflation and the prevailing interest rate result in an investment that will never return its initial value in profit.

This section completes the analytical model of the proposed thermoelectric system with its accompanying economic value. The next section illustrates the use of the entire model on a complete system.

8.3 Solution Method: Minimizing Payback Time

A solution method is now presented to minimize payback time of an entire system.

Table 8-2: Parameters: Constant vs Design.

CONSTANT	DESIGN
T_{SO}	w_{xS}
T_{AO}	w_{zS}
$T_{S,ave} \cong T_{SO} - \frac{1}{8}(T_{SO} - T_{AO})$	t_{xS}
$T_{A,ave} \cong T_{AO} + \frac{1}{8}(T_{SO} - T_{AO})$	t_{zS}
\dot{m}_S	L_{finS}
ρ_S	u_{mS}
μ_S	w_{xA}
k_S	w_{zA}
c_{pS}	t_{xA}
L_{bS}	t_{zA}
ρ_A	L_{finA}
μ_A	u_{mA}
k_A	b
c_{pA}	Z
L_{bA}	X
Z_D	
$L_{ceramic}$	
$K_{ceramic}$	
$R_{contact}$	
U_D	
a_1	
a_2	
k_{sink}	
k_{bp}	
L_D	
p_{HS}	
p_{ins}	
C_{oneD}	
C_L	
i_{infl}	
i_{prev}	
ω	
χ_S	

The steps of this procedure are outlined as follows:

Step 1: Identify the constant and design parameters for the thermoelectric system. A likely categorization of this type is presented in Table 8-2.

Obtain values for fluid properties taken at an estimate of mean flow temperatures $T_{S,ave}$ and $T_{A,ave}$. Obtain characteristics of the thermoelectric device to be considered, cost estimates, and other parameters to be held constant. In this analysis, the mass flow of the hot stream, \dot{m}_S is considered a known parameter. This represents the fact that for a specific application, this parameter would be known and constraining. Choose values for the design variables. The value chosen for X will undergo a sub-optimization routine in nondimensional space. Table 8-3 presents combination parameters, for which values must also be obtained.

Table 8-3: Combination Parameters: Constant vs Design.

CONSTANT	DESIGN
$U_{IL}'' = U_{IH}'' = \frac{k_{cover}}{L_{cover} + k_{cover}R_{contact}''}$	$d_{pH} = \frac{2 w_{xH}w_{zH}}{(w_{xH} + w_{zH})}$
$U_{bp}'' = \frac{k_{bp}}{L_D}$	$d_{pL} = \frac{2 w_{xL}w_{zL}}{(w_{xL} + w_{zL})}$
$i_{equiv} = \frac{1 + i_{prev}}{1 + i_{infl}} - 1$	

Step 2: Nondimensionalize the known parameters and design parameters into the relevant dimensionless groups as shown in Table 8-4. Obtain values for these parameters. The nondimensional design variables will undergo an optimization routine.

Table 8-4: Dimensionless Groups: Constant vs Design.

CONSTANT	DESIGN
$T_o = \frac{T_{AO}}{T_{SO}}$	$\epsilon_{x,S} = 1 - \frac{W_{x,S}}{t_{x,S}}$
$M_S = \frac{\dot{m}_S}{a_1 \mu_S}$	$\epsilon_{z,S} = 1 - \frac{W_{z,S}}{t_{z,S}}$
$\kappa_S = \frac{k_{fin}}{k_S}$	$\epsilon_{x,A} = 1 - \frac{W_{x,A}}{t_{x,A}}$
$\kappa_A = \frac{k_{fin}}{k_A}$	$\epsilon_{z,A} = 1 - \frac{W_{z,A}}{t_{z,A}}$
$\zeta_o = T_{SO} Z_D$	$Re_{dA} = \frac{\rho_A u_{mA} d_{pL}}{\epsilon_{xH} \mu_H}$
$\Psi''_{IL} = \frac{U''_{IL}}{U''_D}$	$d_{pS}^* = d_{pS} \frac{U''_D}{k_{sink}}$
$\Psi''_{IH} = \frac{U''_{IH}}{U''_D}$	$d_{pA}^* = d_{pA} \frac{U''_D}{k_{sink}}$
$\Psi''_{bp} = \frac{U''_{bp}}{U''_D}$	$\lambda_S = \frac{L_{bS}}{d_{pS}}$
$\Pi_{uka} = \frac{k_{fin}}{a_1 U''_D}$	$\lambda_A = \frac{L_{bA}}{d_{pA}}$
$L_{bS}^* = \frac{L_{bS}}{a_1}$	$r = \frac{b}{a_1}$
$L_{bA}^* = \frac{L_{bA}}{a_1}$	$Z^* = \frac{Z}{a_1}$
$\varphi_S = \frac{\mu_S^3 U''_D{}^2}{T_{SO} \rho_S^2 k_{fS}^3}$	$X^* = \frac{X}{a_2}$
$\varphi_A = \frac{\mu_A^3 U''_D{}^2}{T_{SO} \rho_A^2 k_{fA}^3}$	
$\sigma_S = \frac{U''_D a_2}{c_{pS} \mu_S}$	
$\sigma_A = \frac{U''_D a_2}{c_{pA} \mu_A}$	

After the system is optimized, the design variables may be removed from nondimensional space to yield the true parameters of the final design.

Step 3: Use Eq. 8-10 to solve for hot stream Reynolds number. Solve for thermal conductance per area ratios Ψ_H'' , Ψ_L'' with Eq. 8-7. Use properties of the high temperature flow for the hot side (indicated with subscript S) and properties of the low temperature flow for the ambient side (indicated with subscript A). Obtain thermal conductance ratios Ψ_H , Ψ_{IH} , Ψ_L , Ψ_{IL} , and Ψ_{bp} with Eqs. 5-9 through 5-13.

Step 4: Use the friction factor tables to estimate the friction factor at the Reynolds numbers of each fluid stream based on ϵ_x , ϵ_z , λ , and Re_d . Friction factor tables are included in Appendix B.

Step 5: Solve Eq. 8-32 through the following numerical process:

- a) Use the relations developed in Chapter 3 to represent the temperature ratios τ , τ_b , γ , and γ_H as functions of $T = \frac{T_A}{T_S}$, $\zeta = Z_D T_S$ and the thermal conductance ratios Ψ_H , Ψ_{IH} , Ψ_L , Ψ_{IL} , and Ψ_{bp} . Equations from Chapter 3 are used in the following order:
 - a. 3-29 through 3-31
 - b. 3-27 (or 3-32)
 - c. 3.28
 - d. 3-25
 - e. 3-23 (or 3-24)
 - f. 3-21
 - g. 3-33 through 3-36

- b) Use any preferred method of solving systems of ordinary differential equations to find the profiles of T_{RS} , T_{RA} , using Eqs. 8-16 and 8-17. Boundary conditions are as given in Table 8-1. After each step, values are updated for T (Eq. 8-18) and ζ (Eq. 8-19).
- c) The discrete profiles of T_{RS} , τ , τ_b , γ , and γ_H are used in Eq. 8-32 to solve for the net dimensionless power harvested.

Step 6: Use Eq. 8-33 to solve for the payback time in years, n_{pb} of the system. Recall that for very poor designs, a physical payback value may not exist—indicating that the investment will never return its initial value in profit. If this occurs, decrease the value of X^* . However, a feasible value of X^* that ensures a real payback time is not guaranteed for all designs.

Step 7: Repeat steps 2 through 5 manipulating the value for X^* to find the value that minimizes payback time for the current design. This is a sub-optimization routine in one variable.

Step 8: Repeat steps two through seven with an optimization routine, perturbing the current design in ϵ_{xS} , ϵ_{xS} , ϵ_{xS} , ϵ_{xS} , Re_{dA} , d_{pS}^* , d_{pA}^* , λ_S , λ_A , r , and Z^* . Any optimization method may be used to search for the design with minimum payback time.

8.4 Cases Studies

The process of optimizing an overall system using the method outlined is presented for two different cases. Each final design represents an example where the payback time was brought from an unreasonable time to a feasible time through optimization of the initial design.

The model was optimized using a simulated annealing method with the eleven dimensionless design variables: ϵ_{xS} , ϵ_{xS} , ϵ_{xS} , ϵ_{xS} , Re_{dA} , d_{pS}^* , d_{pA}^* , λ_S , λ_A , r , and Z^* . The optimization routine itself was developed using *Mathematica 8.0*. This code is provided in Appendix A. Genetic algorithms or gradient-based methods may be used as well.

8.4.1 Case 1: Expensive Energy

The first case assumes that the thermoelectric harvester is made feasible primarily through the high cost of energy. An optimistic, but reasonable value of $Z_D = .002 \text{ K}^{-1}$ is chosen. The airstream temperature difference is initially 100°C . Physical dimensions are chosen for a theoretical device comparable to the ones tested in the experiments. (Table 8-5)

Table 8-5: First Optimized Case: Heat Path and Thermoelectric Device Parameters.

Parameter		Value
Mass flow rate of hot air stream. (kg/s)	\dot{m}_s	.03
Temperature of hot air stream/inlet temperature to conversion system. (K)	T_{SO}	400
Temperature of ambient air available for inlet of conversion system. (K)	T_{AO}	300
Z dimension of thermoelectric device (cm)	a_1	5
X dimension of thermoelectric device (cm)	a_2	5
Thickness of thermoelectric device/bypass insulation (mm)	L_D	4
Thickness of ceramic covers on thermoelectric device (mm)	L_{ceram}	1
Thermal conductivity of ceramic cover (W/mK)	k_{ceram}	100
Thermal conductance per area of thermoelectric device (W/m ² K)	U_D ''	400
Figure of merit Z_D for thermoelectric device (K ⁻¹)	Z_D	.002

Heat sink and cost information for this cost is presented in Table 8-6. This case seeks to demonstrate what the cost of electricity must be in order to provide a reasonable payback time of around 7 years. After some exploration, it was found that the nominal cost of electricity needed to be roughly \$1.00 per kilowatt-hour, which is roughly one order of magnitude greater than the current cost of electricity. This is the initial price of electricity used in this optimization.

The other cost values are chosen to be reasonable estimates of current prices. The price of thermoelectric devices is comparable to the price paid for the thermoelectric devices used in this research. The heat-sink cost and fixed cost of installation are both assumed to be on the order of \$1000. The cost of installation is set at \$2000. Installation costs much higher than that assumed here will render payback times unreasonably long, while lower installation costs will obviously improve upon the payback times calculated here.

Table 8-6: First Optimized Case: Heat Sink and Cost Parameters

Parameter		Value
Thermal conductivity of the heat sinks (W/mK)	k_{sink}	180
Effective thermal conductivity of bypass pathway (W/m ² K)	k_{bp}	.05
Thermal contact resistance between thermoelectric device and heat sinks. (Km ² /W)	R_c ''	4x10 ⁻⁵
Cost per thermoelectric device (\$)	C_D	50
Total fixed cost associated with installation of system (\$)	C_L	2000
Heat sink cost (\$/m ²)	p_{HS}	1000
Insulation cost (\$/m ²)	p_{ins}	10
Inflation rate	i_{infl}	.03
Prevailing interest rate	i_{prev}	.07
Ratio of rate of energy cost increase to inflation	ω	1.00
Initial price of energy (\$/kW-hour)	$\chi_{\$o}$	1.00
Proportion of time that system is in operation	θ	.71

Three starting points were chosen. Running the optimization routine with different starting points provides confidence that the final design, if agreed upon by all three routines, is not just a local optimum, but a global optimum. If the final designs are different, then the various local optima may be compared. The three starting designs in Table 8-7 have payback times of roughly 19, 55, and 25 years. These payback times are too long to be seriously considered from a mere economic standpoint. However, after running the simulated annealing algorithm, each final design has a calculated payback time close to the desired 7 years. Each optimization was programmed to use 600 total function calls (iterations of the process in Chapter 8.3) composed of 20 perturbations in 30 probability levels.

Table 8-7: Case 1 Starting and Ending Values for Design Variables. The payback time is the objective function to be minimized. Values for X^* are intentionally discretized in the final optimized designs.

	Starting			Ending		
	A	B	C	A	B	C
$\epsilon_{x,S}$.6	.3	.5	.21	.41	.60
$\epsilon_{z,S}$.6	.3	.3	.40	.43	.25
$\epsilon_{x,A}$.6	.3	.3	.39	.60	.58
$\epsilon_{z,A}$.6	.3	.5	.22	.22	.23
Re_{dA}	1000	300	500	950	585	843
Re_{dS}^\dagger	~40	~1200	~90	290	273	174
d_{pS}^*	.005	.0022	.005	.0024	.0022	.0024
d_{pA}^*	.01	.0022	.022	.0119	.0087	.0103
λ_S	20	3	20	6.4	5.7	7.9
λ_A	100	30	30	94	85	95
r	2	1.5	1.5	1.88	1.96	1.94
Z^*	50	30	30	69.6	43.1	33.0
X^* (Solved For)	2.85	3.80	2.00	3	5	6
Payback Time (yrs)	19.3	54.6	25.0	6.75	7.18	7.83

† Not a design variable. Calculated from Eq. 8-9.

In a simulated annealing algorithm, variables which are constraining are less obvious than when a gradient-based method is used. This is because the random method of design perturbation causes a constraining variable to undergo small fluctuations near its constraining value while the other variables continue to move toward their optimum values. When the final design is reached, constraining variables will be close to, but usually not exactly at, their constraining values.

The three final designs agree on certain variables. First, observe that although X^* and Z^* are quite different for each case, the number of devices to be included in the system for the three cases (calculated by Eq. 7-8) is very similar: 111, 110, and 102 respectively. It can be concluded that the total number of devices is more important than their spatial arrangement. The bypass ratio, r , is essentially constrained at its maximum value of 2 for each case. The length of the cool side fins (λ_A) (measured in dimensional fin diameters) is essentially constrained at the maximum allowed length of 100. The reason for this is discussed later in this section. The length of the hot side fins (λ_S) agree to within 1.5. If a plot similar to Fig. 4-8 were made for the low Re_{dS} number range observed in the optimized cases (174 ~ 290) the expected optimum fin lengths would be slightly longer than in Fig. 4-8 (where $Re_d = 500$ was used). Thus, the optimized fin lengths of 6.4 to 7.9 appear to correlate with the suggested optimum fin length in Chapter 4.3.

The dimensionless fin diameter, d_{pA}^* is similar for each case, being 4 to 5 times the hot fin diameter, d_{pS}^* . The hot side fin diameter is essentially constrained to its minimum of .022 for all three cases. This value was calculated from a dimensional minimum fin diameter of 1 mm. The hot side Reynolds number is similar for each case—well within the laminar range and several times smaller than the cold side Reynolds number. The cold side Reynolds number is in

the 600 to 900 range for each case. Finally, all three optimization cases agree that the porosity ϵ_{ZA} should be essentially constrained at the lower bound of 0.2.

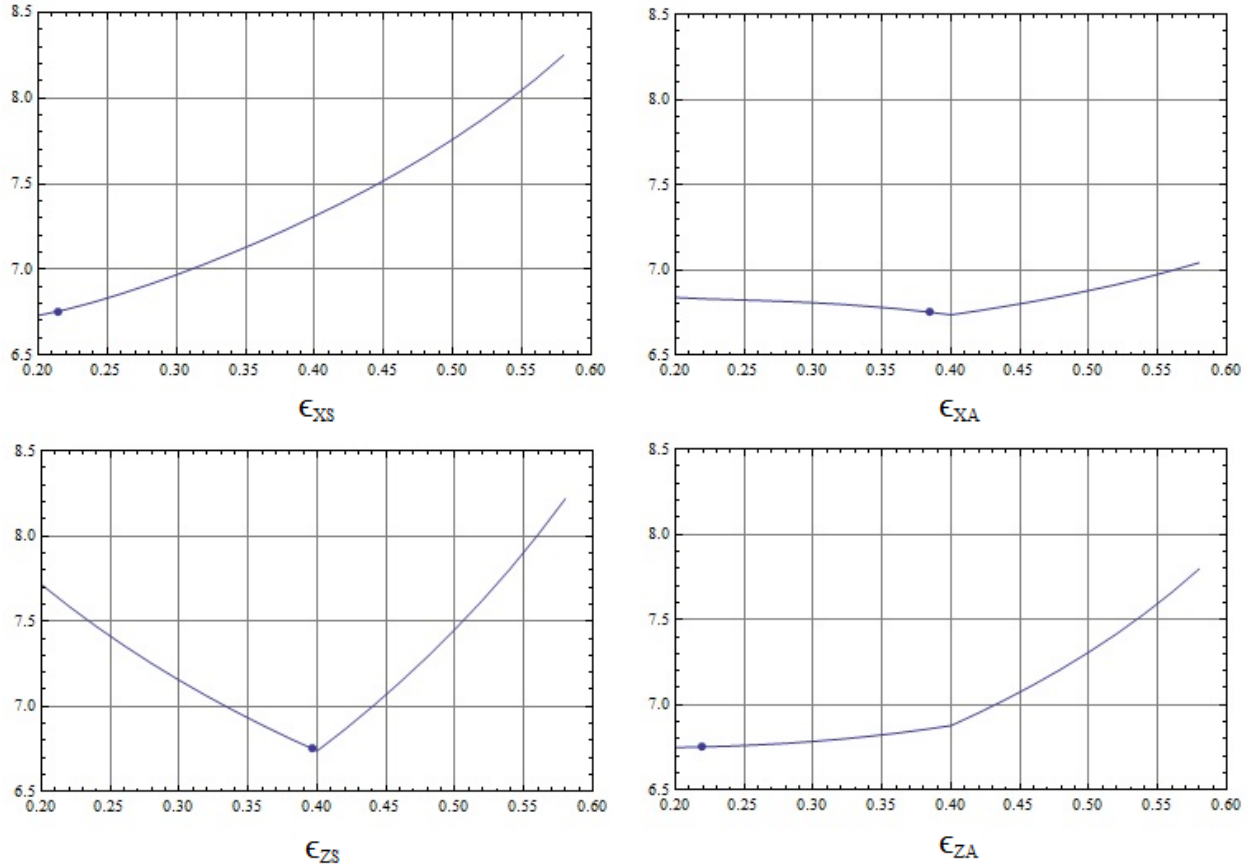


Figure 8-2: Sensitivity Plots for Heat Sink Porosities. The vertical axis of each plot is payback time in years. Case 1A.

The three porosities ϵ_{XS} , ϵ_{XA} and ϵ_{ZS} , which can only range between 0.2 and 0.8, do not display strong agreement. Sensitivity plots of porosities are included for the best case (design A in Table 8-7) in Fig. 8-2. For each plot, every variable is held constant, including X^* , except the one analyzed. The sensitivity plots for porosities and the other variables which follow allow for overall uncertainty in the objective to be estimated with respect to each variable. For example,

observing Fig. 8-2, an uncertainty of 0.05 in ϵ_{ZS} results in about half a year of payback increase, while the same uncertainty in ϵ_{XA} or ϵ_{ZA} produces a negligible change in payback time.

The sensitivity plot for ϵ_{XA} and ϵ_{ZS} sheds light on the behavior of the porosities in general. Because of the low resolution of the friction factor tables, values for porosities tend to get caught in local minimums formed by the piecewise nature of the linear interpolation used with the friction factor tables. Thus, the optimum values for all porosities tend to be clustered around 0.2, 0.4, and 0.6, which are specific values around which the tables were created. The sensitivity plots indicate that ϵ_{XA} is the least important porosity for this design. However, more specific conclusions require a higher resolution characterization of pressure losses as functions of porosity. The minimum in ϵ_{ZS} is especially suspect. It may be said that in general, the optimized porosities normal to the flow direction (ϵ_X) are lower than that of a heat sink optimized unto itself by Kim, Kim and Ortega (2006). This occurs in the thermoelectric system because concentrating the heat transfer is worth the pressure drop of tightly spaced fins.

Sensitivity plots for dimensionless fin diameter and normalized fin length for design A are given in Fig. 8-3. The strong slope of payback time with d_{pS}^* indicates that minimizing the diameter of the hot side fins is very important. The optimum observed in d_{pA}^* is likely attributable to the competing effects of poorer heat transfer at large diameters and high pressure drop at small diameters. Recall that the fin length on the cold side is 94 fin diameters. With such a tall channel, a small decrease in d_{pA}^* (to less than 0.01) can suddenly overwhelm the system with pressure drop. The fin length on the hot side (λ_S) displays an optimum as previously discussed. The plot indicates that the simulated annealing algorithm ended slightly above the optimum length of around 5, but that the difference in payback time is marginal.

Observe the plot of λ_A . The dimensionless fin length of the cool channel does not exhibit an optimum like that observed for λ_S . This is due to the fact that, while there is a finite mass flow for the hot stream, no such limitation exists for the cool stream. The system is free to intake any amount of ambient air. The optimization routine found that with very long fins (and therefore, a very large channel) the large mass flow of cool air is able to maintain a low temperature even while absorbing the heat transferred from the hot side. Maintaining a low temperature in the cool flow allows for the system to preserve the difference between T_S and T_A , allowing for a larger temperature difference than would be accomplished with short fins.

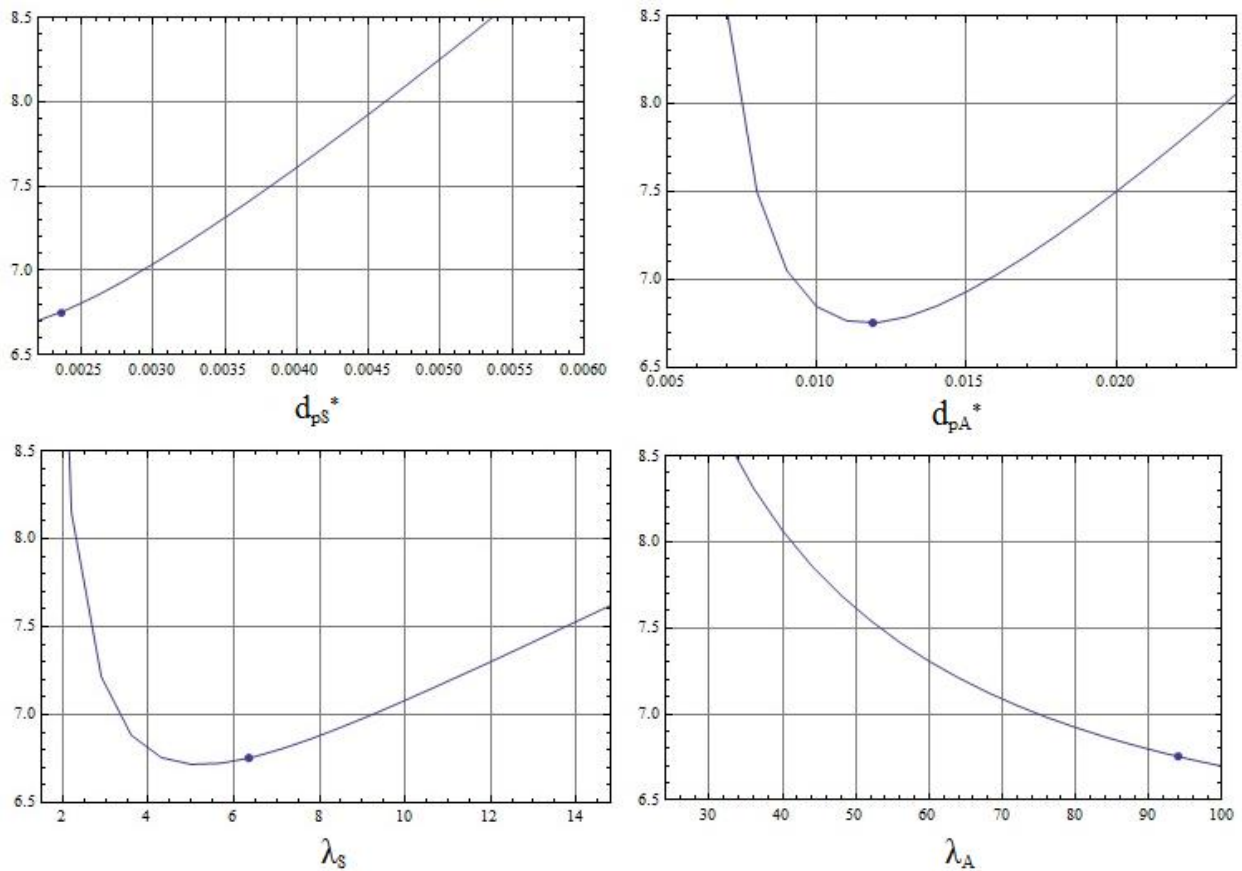


Figure 8-3: Sensitivity Plots for Fin Lengths and Diameters. The vertical axis of each plot is payback time in years. Case 1A.

It is expected that at some point, the added flow power required to drive such a large flow would cause diminishing returns beyond some optimum fin length. However, for this case, the optimum length for λ_A is larger than 100.

Figure 8-4 illustrates the effect of large fin length on the temperature of the cool fluid stream. Both fluid streams are shown as a function of system length x^* . The hot stream temperature decreases quickly, losing its exergy content. In contrast, the cool stream increases from ambient temperature very gradually, owing to its high thermal capacitance.

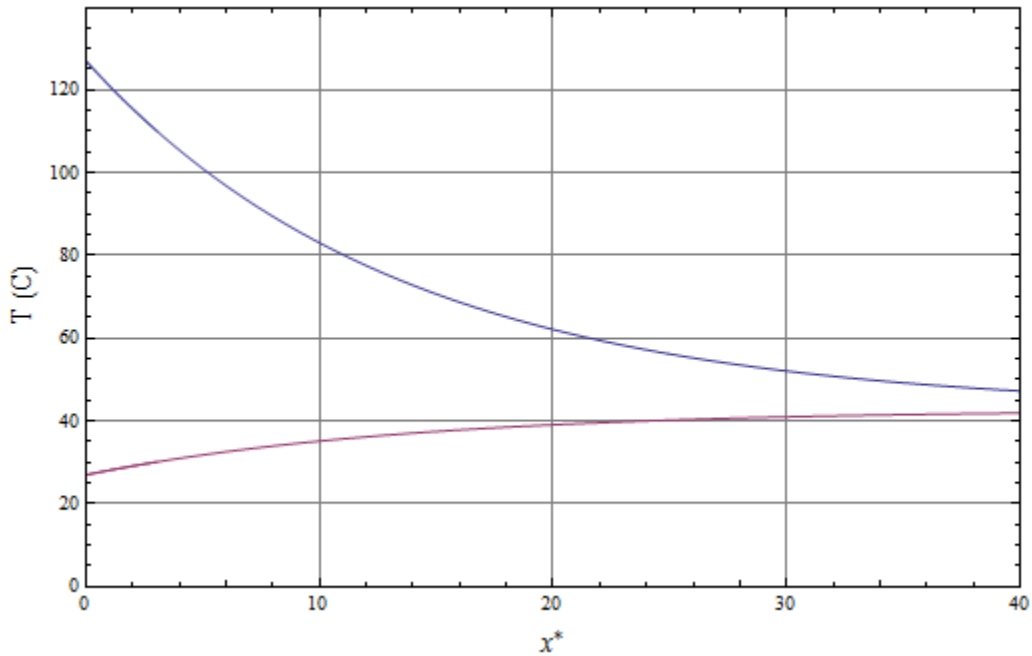


Figure 8-4: Temperature Profiles of Fluid Streams. The upper curve is the hot stream temperature, T_S . The lower curve is the cool stream temperature, T_A . Case 1A.

Sensitivity plots for the remaining design variables are shown in Fig. 8-5. The bypass ratio, r , is essentially constrained at its maximum value of 2. As argued in Chapter 5, an optimum bypass ratio must exist, but it is usually greater than 2 when airstreams are used as the

working fluid. The cool side Reynolds number, Re_{dA} , exhibits an optimum due to the competing effects of heat transfer and pressure drop. The optimum is broad, however. Comparable performance is obtained over a range of 600 to 1000. The different values for Re_{dA} in Table 8-7 illustrate this range. The optimum for Z^* is very shallow on the right side. It is surmised from Table 8-7 that subtle changes in the other variables shift the location of this optimum significantly.

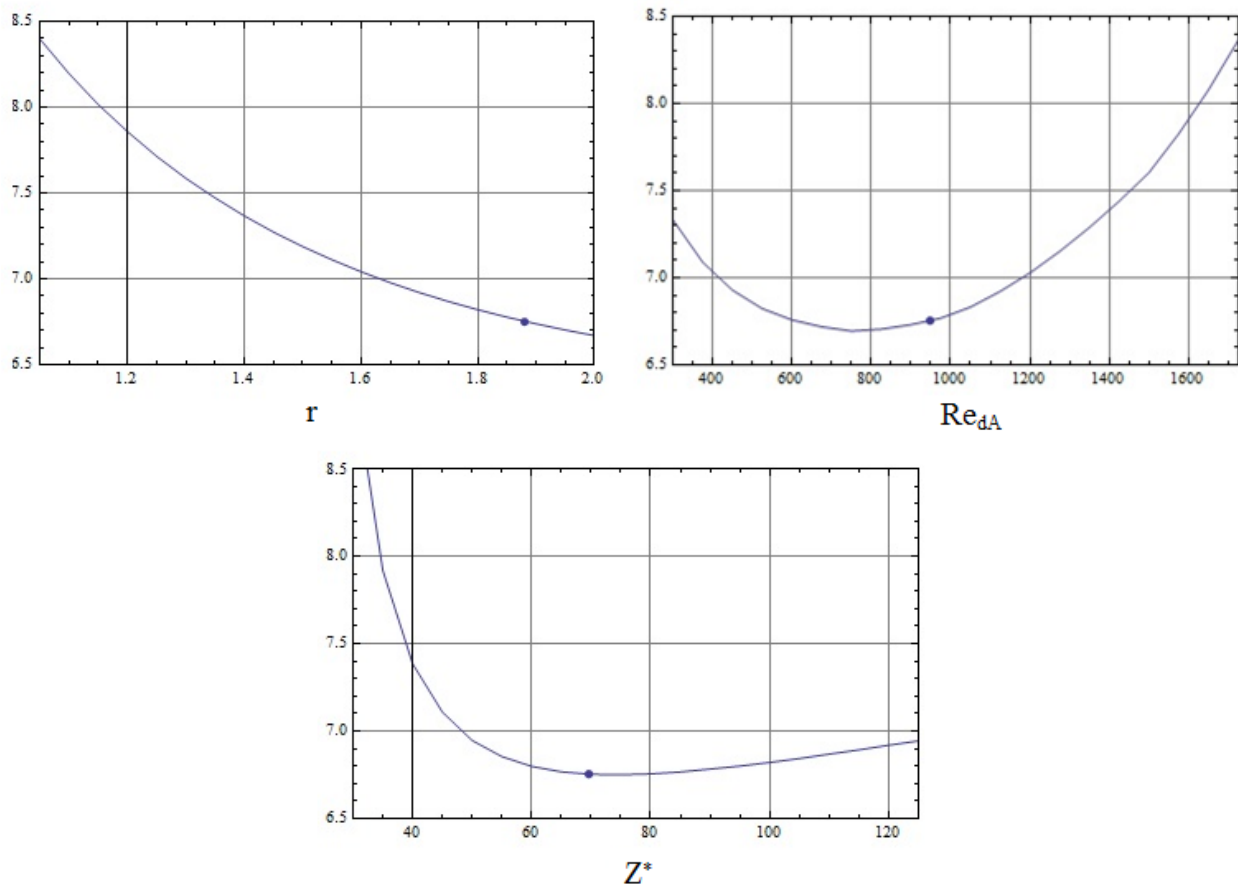


Figure 8-5: Sensitivity Plots for Bypass Ratio, Reynolds Number, and Z^* . The vertical axis of each plot is payback time in years. Case 1A.

Consider Fig. 8-6, which shows the total power output and the calculated payback time as a function of the length of the system, X^* .

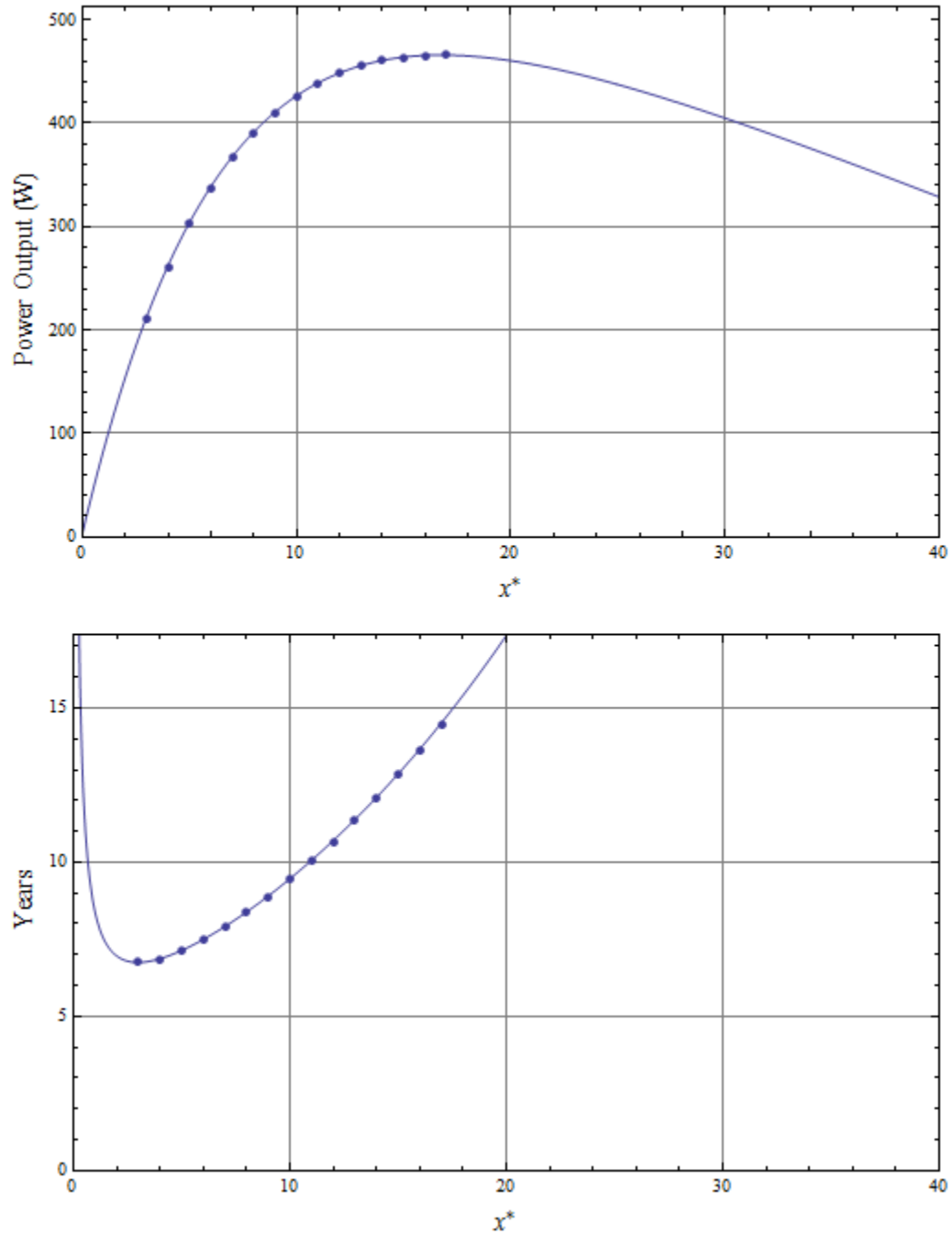


Figure 8-6: Power Output and Payback Time vs X^* . The individual points represent discrete design points with the system length being an integer value of device lengths. Case 1A.

The fully optimized design with minimized payback time exhibits an X^* value of 3 and a Z^* value of 69.6 (Table 8-7). This means that the entire system is 69.6 device lengths (3.48 m) wide and only 3 device lengths (15 cm) in the flow direction. Increasing the length of the system in the flow direction to 17 device lengths (0.85 m) increases the total net power it can generate, but increases the initial cost and the payback time as well. Beyond $X^* = 17$, the increase in pump power required to move air through the channel is larger than the increase in power generated from the waning source stream.

The design points between the minimum payback and maximum power harvest represent some compromise between these two objectives. Recall, however, that in this analysis, payback time is the objective function on which the optimization routine was based. The maximum power case was calculated by simply extending X^* on the optimized design. Observe that small sacrifices in payback time result in comparatively large increases in power output. For example, if the system is extended to 5 device lengths, the payback time increases about 4% (~7 years), while the power harvest increases about 42% (~300 Watts).

The fan power requirement is also best illustrated versus the system length, X^* (Fig. 8-7). Fan power increases linearly with increasing X^* , while the gross power harvest increases rapidly before leveling off as the hot fluid stream cools. The net power harvest is the difference between the gross power and required fan power. At the minimum payback time design ($X^* = 3$), the fan power is 10.5% of the gross power output. At the maximum power design ($X^* = 17$), the fan power is 23.1% of the gross power output.

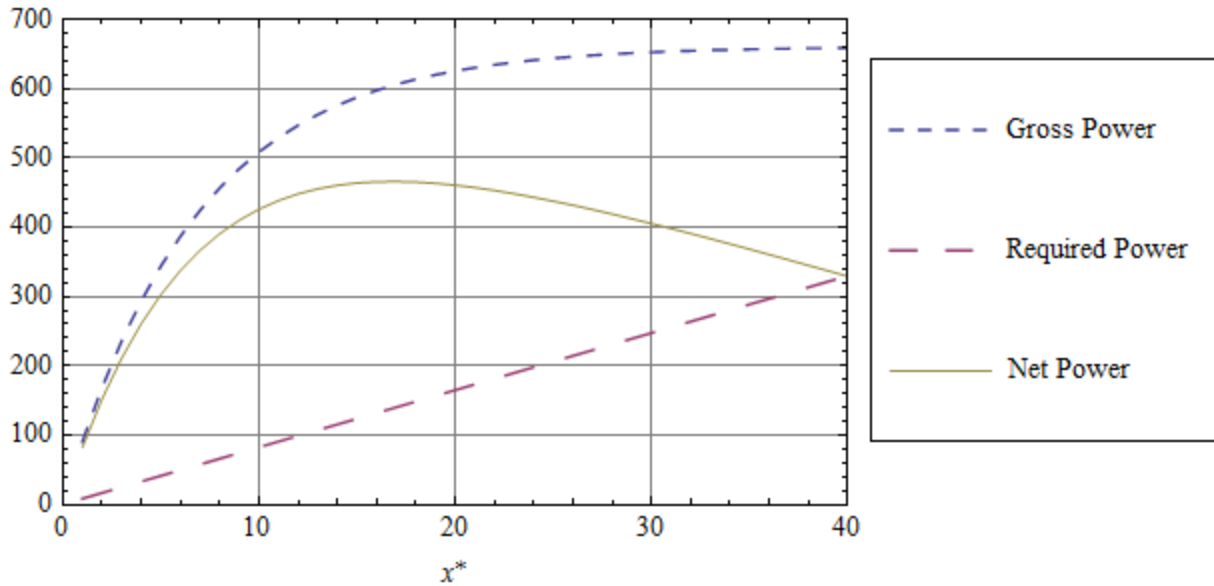


Figure 8-7: Gross, Required, and Net Power vs X^* . Case 1A.

Table 8-8 is a summary output for the optimized case. Cost parameters are included that allow for comparison between the minimum payback time design and the maximum power output design. The model suggests that 210 watts may be obtainable for about \$8600, and that 465 watts may be obtainable for nearly \$40,000. These numbers are independent of the price of energy. Recall that the payback times shown are calculated using \$1.00 per kW-hr as the initial price of electricity. This was in order to answer the question, “At what energy price does the thermoelectric harvester become feasible?”. At current energy prices (\$0.08 to \$0.15 per kW-hr) (EIA), the payback times would be much longer or nonexistent.

Table 8-8: Final Optimized Variables and Cost Parameters. Case 1A.

Minimum Payback Time Case:

Power Output	210.821 (W)
Total Devices	111.
Total Cost	8595.7 (\$)
Payback Time	6.753 (yrs)
X^*	3

Maximum Power Output Case:

Power Output	465.821 (W)
Total Devices	629.
Total Cost	39375.6 (\$)
Payback Time	14.4786 (yrs)
X^*	17

System Parameters

Z^*	69.5504
r	1.87974
Hot Side	
Re_{ds}	290.214
d_{ps}^*	0.00236029
λ_s	6.35531
ϵ_{xs}	0.214216
ϵ_{zs}	0.396287
Ambient Side	
Re_{dA}	948.429
d_{pA}^*	0.0118636
λ_A	93.9463
ϵ_{xA}	0.384795
ϵ_{zA}	0.218681

The results indicates that under circumstances of electricity cost at \$1.00 per kilowatt-hour, a 100°C temperature difference in air streams may begin to represent a viable source for obtaining DC power with a thermoelectric system.

8.4.2 Case 2: Large Temperature Difference

The second case assumes that the use of the thermoelectric harvester is made feasible primarily through the high quality of the temperature difference between the fluid streams. A conservative value for Z_D of 0.0007 K^{-1} is used. The price of electricity is set to \$0.15 per kW-hr. This is higher than the price of electricity in the United States in general, but accurately represents what many US residents in population-dense areas pay, including the New England states and California (EIA). The mass flow rate of the available airstream is arbitrarily chosen to be 1/10 of that in the last case. Other heat path and thermoelectric device parameters are the same as in the previous case, which are listed in Table 8-9.

Table 8-9: Second Optimized Case: Heat Path and Thermoelectric Device Parameters.

Parameter		Value
Mass flow rate of hot air stream. (kg/s)	\dot{m}_s	.003
Temperature of hot air stream/inlet temperature to conversion system. (K)	T_{SO}	650
Temperature of ambient air available for inlet of conversion system. (K)	T_{AO}	300
Z dimension of thermoelectric device (cm)	a_1	5
X dimension of thermoelectric device (cm)	a_2	5
Thickness of thermoelectric device/bypass insulation (mm)	L_D	4
Thickness of ceramic covers on thermoelectric device (mm)	L_{ceram}	1
Thermal conductivity of ceramic cover (W/mK)	k_{ceram}	100
Thermal transport coefficient of thermoelectric device ($\text{W}/\text{m}^2\text{K}$)	U_D''	400
Figure of merit Z_D for thermoelectric device (K^{-1})	Z_D	.0007

Heat sink and cost information for this case is presented in Table 8-10. This case seeks to demonstrate what the necessary temperature of the source stream must be in order to provide a

reasonable payback time of about 7 years. After some exploration, it was found that the initial temperature of the available fluid streams needed to be roughly 350°C above ambient. In most cases, waste heat or exhaust streams of such a high temperature would be more efficiently used in a fluid cycle to generate power instead of a thermoelectric system. However, the need for such a high temperature provides an important point of reference for demonstrating the challenges of economic waste heat recovery using the current technology in commercially available thermoelectric devices.

Some of cost values are more optimistic than in the first case. Each thermoelectric device costs \$30, and the total installation cost is reduced to \$1000. The cost of energy is projected to rise slightly faster than inflation ($\omega = 1.05$), and the system runs continuously without stopping ($\theta = 1$). The other cost parameters are the same as in the first case.

Table 8-10: Second Optimized Case: Heat Sink and Cost Parameters.

Parameter		Value
Thermal conductivity of the heat sinks (W/mK)	k_{sink}	180
Effective thermal conductivity of bypass pathway (W/m ² K)	k_{bp}	.05
Thermal contact resistance between thermoelectric device and heat sinks. (Km ² /W)	R_c ''	4x10 ⁻⁵
Cost per thermoelectric device (\$)	C_D	30
Total fixed cost associated with installation of system (\$)	C_L	1000
Heat sink cost (\$/m ²)	p_{HS}	1000
Insulation cost (\$/m ²)	p_{ins}	10
Inflation rate	i_{infl}	.03
Prevailing interest rate	i_{prev}	.07
Ratio of rate of energy cost increase to inflation	ω	1.05
Initial price of energy (\$/kW-hour)	χ_s	0.15
Proportion of time that system is in operation	θ	1

As in the first case, three starting points were chosen. The three starting designs in Table 8-11 have payback times of 38, 154, and 145 years respectively. After running the simulated annealing algorithm for each case, payback times close to the desired 7 years were obtained for each design. Each optimization was programmed to use 900 total function calls (iterations of the process in Chapter 8.3) composed of 30 perturbations in 30 probability levels.

Table 8-11: Case 2 Starting and Ending Values for Design Variables. The payback time is the objective function to be minimized. Values for X^* are intentionally discretized in the final optimized designs.

	Starting				Ending		
	A	B	C		A	B	C
$\epsilon_{x,S}$.6	.2	.4		0.36	0.20	0.22
$\epsilon_{z,S}$.6	.2	.4		0.44	0.34	0.41
$\epsilon_{x,A}$.6	.2	.2		0.27	0.31	0.49
$\epsilon_{z,A}$.6	.2	.2		0.34	0.40	0.37
Re_{dA}	1000	50	500		822	520	534
Re_{dS}^\dagger	~10	~860	~24		290	503	336
d_{pS}^*	.005	.0022	.005		.0023	.0023	.0025
d_{pA}^*	.01	.0022	.022		.0092	.0062	.0057
λ_S	14	0.5	14		1.43	1.11	1.58
λ_A	100	10	10		94	86	100
r	2	1	1.5		1.96	1.81	1.95
Z^*	24	9	15		13.7	18.1	17.5
X^* (Solved For)	2.00	0.45‡	0.35		8	6	7
Payback Time (yrs)	38.3	154‡	145		7.47	7.45	6.93

†Not a design variable. Calculated from Eq. 8-9.

‡Taken after one design iteration. Initial design is infeasible.

As in the first case, there are differences in X^* and Z^* , but it is observed through Eq. 7-8 that the total number of devices predicted by each case is very similar: 56, 60, and 63 respectively. The bypass ratio is again nearly 2 for all cases. The cool side fin length is approaches the limit of 100. The bypass ratio and λ_A for design B are far enough from the

constraint to indicate that either these variables were actually not constraining, or that their influence became small as they approached their upper limits. All three cases agree that the fin length on the hot side (λ_s), should be much shorter than that observed in the previous case. This would seem to disagree with the optimum fin lengths observed in Fig. 4-8. However, direct comparison with that plot is misleading due to the high temperature of the stream. A plot analogous to Fig. 4-8 for the temperatures involved in this case would likely have a much different A value than that used in Fig. 4-8. It is concluded that the optimum fin length decreases with increasing temperature difference between the fin base and the fluid stream.

The dimensionless fin diameter on the cool side, d_{pA}^* is similar for each case, being several times the dimensionless diameter on the hot side, d_{pS}^* . The hot side diameter is essentially constrained at its minimum value of 0.0022. Both Reynolds numbers generally follow the trends of the first case. As in the first case, drawing conclusions from the optimized porosity values is difficult, underscoring the need for a higher resolution method of characterizing the friction factor.

Figure 8-8 shows the temperature of the fluid streams for the best performing design (design *C*). Similar characteristics to the previous case are observed due to the high thermal capacitance of the cool stream.

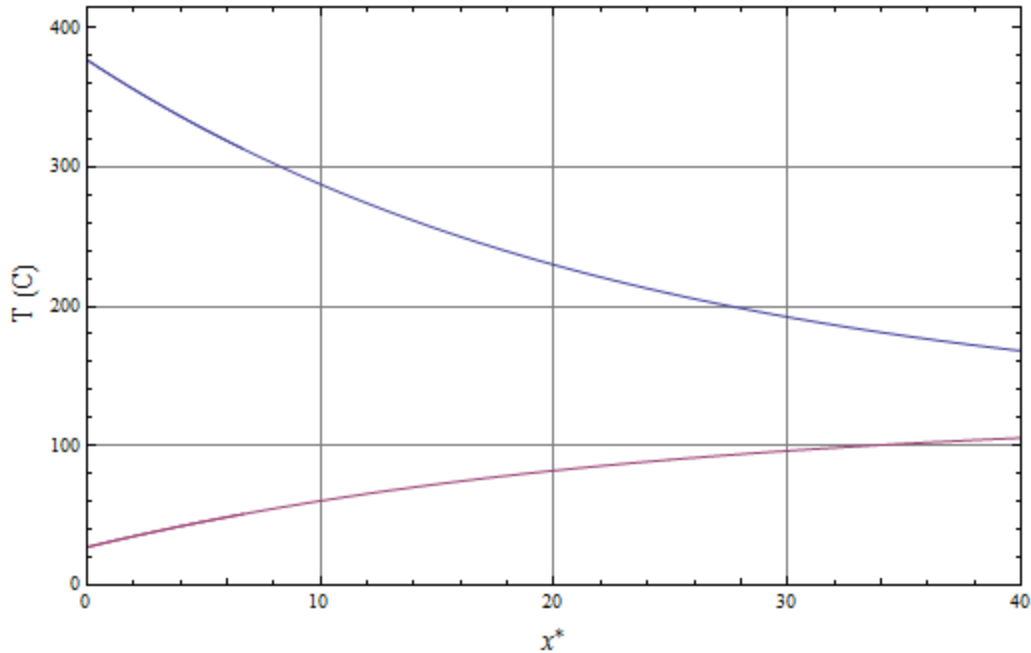


Figure 8-8: Temperature Profiles of Fluid Streams. The upper curve is the hot stream temperature, T_S . The lower curve is the cool stream temperature, T_A . Case 2C.

The fully optimized design with minimized payback time exhibits an X^* value of 7 and a Z^* value of 17.5. This means that the entire system is 17.5 device lengths (.875 m) wide and 7 device lengths (.30 m) in the flow direction. Increasing the length of the system in the flow direction to 29 device lengths (1.45 m) increases the total net power that it can generate, but increases the initial cost and payback time as well. It is interesting to note that if X^* is 18 or greater, the system will be longer in the flow direction than it is wide. This is in contrast to the previous case. This is attributable to the much lower mass flow rate, resulting in the fact that Z^* may be much smaller while still maintaining the optimum Reynolds number and fin length. The characteristics of the power output and the payback time follow the same pattern as in the previous case.

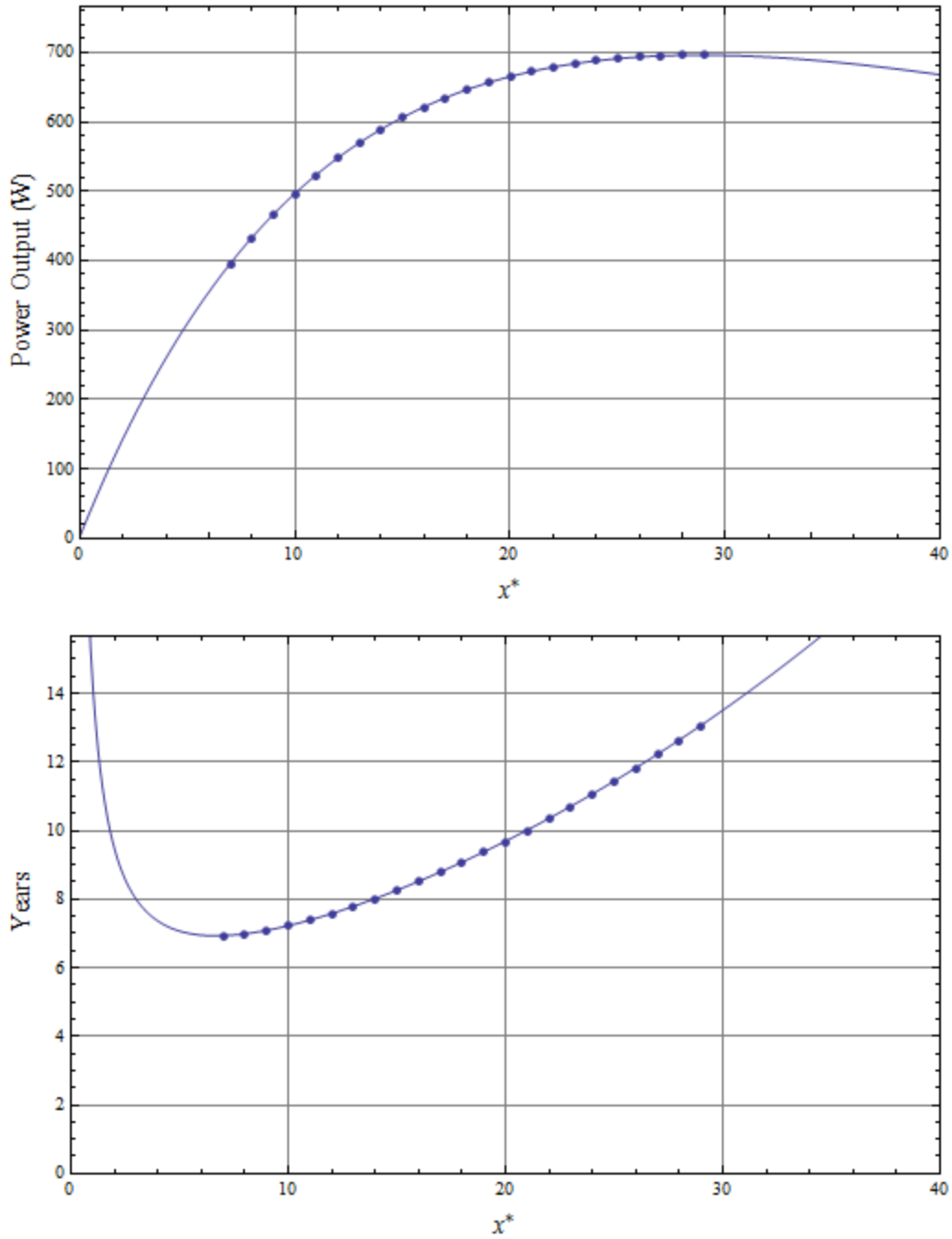


Figure 8-9: Power Output and Payback Time vs X^* . The individual points represent discrete design points with the system length being an integer value of device lengths. Case 2C.

The design points between the minimum payback and maximum power harvest represent some compromise between these two objectives. Like the previous case, small increases in payback time yield comparatively large increases in net power output.

Table 8-12: Final Optimized Variables and Cost Parameters. Case 2C.

Minimum Payback Time Case:

Power Output	394.606 (W)
Total Devices	63.
Total Cost	3505.71 (\$)
Payback Time	6.93449 (yrs)
X*	7

Maximum Power Output Case:

Power Output	696.013 (W)
Total Devices	261.
Total Cost	11380.8 (\$)
Payback Time	13.049 (yrs)
X*	29

System Parameters

Z*	17.5488
r	1.94987

Hot Side

Re _{ds}	336.383
d _{ps} *	0.00249083
λ _s	1.5757
ε _{xs}	0.219962
ε _{zs}	0.406218

Ambient Side

Re _{da}	533.967
d _{pa} *	0.00570157
λ _a	99.797
ε _{xa}	0.487101
ε _{za}	0.370016

Table 8-12 is a summary for this case. Cost parameters are included that allow for comparison between the minimum payback time design and the maximum power output design.

The results indicate that a thermoelectric power conversion system with a source temperature airstream of 350°C may begin to represent an economically viable option for obtaining DC power at the upper end of current energy prices.

9 CONCLUSION

9.1 Summary

It has been shown in this research that a differential approach to characterizing thermoelectric behavior results in a governing equation for thermodynamic efficiency (Eq. 2-11) that is comparable to that presented by Gordon (1991) (Eq. 2-28). The differential approach is a versatile method. For example, assumptions could be relaxed or empirical corrections could be included on a differential level, and the resulting differential equation for the temperature profile observed.

It was shown that the heat rate approximations developed in Chapter 2 closely matched an exact analytical solution. These heat rates may be used to construct an algebraically involved, but closed-form analytical solution of a thermoelectric power harvesting system with five thermal pathways surrounding the thermoelements.

A classical analytical solution for heat transfer through fin arrays was coupled with an empirical Nusselt number correlation (Eq. 4-23). This combination was fully nondimensionalized with parameters pertinent to a thermoelectric waste heat harvesting system (Eq. 8-7). Pressure drop through fin arrays was characterized through the definition of a modified Darcy-type friction factor (Eq. 4-29). Through modeling as a porous medium, a nonlinear momentum equation and empirically-derived constants published by other researchers were used to solve for friction factor based on four dimensionless characteristics of a given heat sink. A

tabular function consisting of 5888 friction factors was generated, enabling pressure drop calculations without the need for a differential equation solver.

The concept of incorporating bypass insulation was presented. The method of treating bypass insulation in the model was supported through numerical validation. The economical concept behind bypass insulation was introduced.

A test station was designed and constructed to obtain experimental data. The test station simulated a thermoelectric harvesting system of a single device. Power output measurements for two types of devices were taken under two radically different heat sinks and bypass ratios. It was shown that the model predicted the power outputs very well, provided that preliminary experiments were performed to characterize the thermoelectric device.

A system of modeling payback time was derived from first principles, incorporating the time value of money. Equations were presented enabling the design of a system with the objective of minimizing payback time. The economic motivation of incorporating bypass solution was analytically confirmed.

A numerical approach to characterizing spatial effects on the fluid streams was developed, allowing the modeling of a finite heat source and the loss in available energy as heat is drawn through the system. The solution method of optimizing the design was presented in detail and conducted for two cases that demonstrate examples of conditions under which a thermoelectric system of the type considered will yield a target payback time of about 7 years.

Throughout all the mathematical modeling, an original system of nondimensionalization was maintained. The entire system of dimensionless grouping evolved gradually throughout the development of the research and was specifically designed to be as useful, organized, and

intuitive as possible (though this may be difficult to believe at first reading). The system allows optimization to be performed in condensed, dimensionless space.

Physical design characteristics of an optimized system are surmised from a tailored simulated annealing approach on a two case studies of optimized systems. Discussion and interpretations of the results concerning optimized design variables was offered.

The model predicted that an optimized physical system of thermoelectric energy conversion of the type described could exhibit a payback time of roughly seven years for an energy cost of \$.15 per kilowatt-hour, a temperature difference of 350°C and optimistic assumptions regarding startup costs and neglecting maintenance expenses. In addition, a physical system utilizing a temperature difference of 100 °C could exhibit a similar payback time if an optimistic, but reasonable Z_D value is assumed, and the nominal price of energy rose to \$1.00 per kilowatt-hour. Airstreams were considered in both cases.

The limitations on the model, such as bypass insulation ratio and the need for high thermal capacitance in the ambient fluid stream, may function as catalysts for the refining of the general design presented here. Suggestions include adapting the model to the bypass insulation configuration of Fig. 5-4, or introducing some method of drawing in new ambient air along the flow direction of the system in order to maintain temperature difference without large fan power. Ideas for further research on system design are noted throughout the thesis and summarized in the final section of this chapter.

9.2 Conclusions on Optimized Design

The optimized cases provide valuable information regarding design characteristics of a thermoelectric energy harvesting system. With this information, this research may take new directions that improve those aspects of the system that are most critical to its performance. The two cases in the previous section together suggest several things about this type of thermoelectric energy harvester:

1. Like heat engines in general, thermodynamic efficiency is greatly increased with the quality of the temperature difference available. Cost-effective thermoelectric energy recovery of waste streams less than 100°C greater than the ambient is difficult.
2. For source fluid streams with a large mass flow, the optimized system may be only a few devices in the streamwise direction, X , but much longer in width, Z . For a large mass flow rate of 0.03 kg/s, the optimized system will be 30 to 70 devices wide and only 3 to 6 devices in the streamwise direction (see Table 8-7). For source fluid streams with small mass flows, this aspect ratio of the system will be less pronounced or may reverse to become longer in the streamwise direction. For a low mass flow rate of .003 kg/s, the optimized system will be 13 to 18 device lengths wide and 6 to 8 device lengths in the flow direction (Table 8-11).
3. For air as the working fluid, insulation bypass ratios should be larger than 2. Although an optimum bypass ratio almost certainly exists (See Chapter 5), it is larger than the method developed in this research can model accurately. When used to model larger bypass ratios, the model predicts an optimum bypass ratio of 4.0 for a typical case. This is expected to be an overestimation (See Fig. 7-3).

4. Both heat sinks for the thermoelectric harvester proposed should have low porosities (0.2 to 0.4) in both directions. This is in contrast to heat sinks that are optimized unto themselves for minimum thermal resistance, which have high porosity (0.8) normal to the flow direction (Kim, Kim, and Ortega). Low porosities increase fan work required to move fluid through the fin array, making this design not ideal for many other applications. However, the optimized cases indicate that the need for very dense fin systems to focus high amounts of heat transfer through the thermoelectric devices outweighs the drawbacks of lower porosities. (See Tables 8-7 and 8-11).
5. Fin diameter for the hot stream should be very small (constrained at 1 mm for both case studies). This is attributed to the need to maximize surface area and increase thermal conductance to the thermoelectric devices despite the higher fan work requirements associated with smaller fin diameters.
6. Fin length for the hot side will only be several fin diameters ($1 \lesssim \lambda_s \lesssim 8$). The dimensionless fin lengths observed for the hot side appear to agree generally with those found to maximize the ratio of heat transfer to pressure drop (see Section 4-3).
7. Fin diameter for the cool side exhibits an optimum diameter of 2 to 5 times the fin diameter on the hot side. This would indicate medium-sized fins of 2-5 mm in diameter. The fin diameter is calculated with Eq. 4-22. For square fins it is equal to the fin width.
8. The fin length/channel height for the cool stream should be very large. Both case studies indicate that the system is highly benefitted by fins that are at least 100 diameters long. Although this creates larger fan power requirements, it has one highly beneficial effect. The very large channel accommodates a high-volume flow fluid stream. By virtue of its bulk, this stream possesses such thermal capacitance that it does not increase in

temperature nearly as much as the other stream *decreases* in temperature along the flow direction. Because this stream maintains its temperature well, the temperature difference across the device is better preserved along the flow direction. This effect strongly suggests that innovative methods of introducing new ambient air along the flow direction are advisable, which would help to preserve the temperature difference between the air streams without requiring a channel as large as suggested by these two cases.

9.3 Further Recommended Research

Efficiency Relation. The efficiency relation developed in this research through a differential solution to a thermoelement temperature profile (Eq. 2-11) should be further explored and scrutinized. Further exploration on the effects of electrical load on the device and incorporation of these into an improved efficiency function is both an experimental and analytical task. Improving the accuracy of this relation will be very beneficial to the analytical model.

Model Improvement. The schematic of Fig. 3-2 serves as the basis for the general model. In practice, value for the interfacial thermal conductances, U_{IL} , U_{IH} were found to be very large compared to the primary thermal conductances, U_L , U_H . A different version of the heat path schematic may be explored which neglects these thermal conductances in favor of relaxing other assumptions, such as the single node approximation.

Pressure Drop Characterization. The extension of estimating pressure drop based on the modified momentum equation for flow through a porous medium is a very basic approximation which extrapolates 16 experiments to an enormous design space. Resolution is poor with respect to porosities, which resulted in inconclusive results with regard to an optimum set of porosities

for each fin array. In addition, fin aspect ratio was not taken into account, and accuracy of the porous momentum equation at Reynolds numbers as low as 10 and as high as 5000 is not empirically confirmed. Further research on accurately predicting pressure drop through large arrays of square fin heat sinks, especially in a tabular or correlational format, would benefit the research.

Experimental Continuation. Experiments recommended include the creation of a test station specifically to characterize the parameters Z_D and U_D of a thermoelectric device in a more direct manner than that performed in this research. Such tests could validate manufacturer data as well as determine the effects of temperature on these parameters. Experimental methods of determining the electrical resistance of a device and of observing behavior over a range of loading ratios would be valuable in determining the accuracy of the efficiency relation used in this research as well as discovering the source of discrepancy observed between manufacturer data and the characterization of the devices performed in this research. In addition, a robust prototype system that includes many thermoelectric devices together with bypass insulation is recommended to further validate the model.

Bypass Insulation Modeling. In Chapter 5, the limitations of the model in accurately characterizing bypass ratio are discussed. It was demonstrated that the model predicted significantly reduced payback times for systems utilizing bypass insulation, but that the optimum bypass ratio for many cases is beyond what the model developed in this research can accurately employ. Spatial effects of large bypass insulation will tend to reduce the average temperature difference across the thermoelectric devices below the average temperature difference of the entire system. If this effect could be characterized through analytical means, the model could be extended to arbitrarily large bypass ratios, increasing its utility.

REFERENCES

- Caputo, R. 2009, "The End of Cheap Oil", *Hitting the Wall: A Vision of a Secure Energy Future*, Morgan & Claypool, San Rafael, CA.
- Cengel, Y.A., and Boles, M.A., 2008, *Thermodynamics: An Engineering Approach*, Sixth Edition, McGraw-Hill, New York.
- CIA (Central Intelligence Agency), *The World Factbook* (online version), <https://www.cia.gov/library/publications/the-world-factbook/geos/us.html>. Accessed 5/31/2011.
- Churchill, S.W., and M. Bernstein, *Journal of Heat Transfer*, **99**, 300, 1977. In (Incropera).
- EIA (U.S. Energy Information Administration), "Average Retail Price of Electricity to Ultimate Customers by End-Use Sector, by State", March 11, 2011. www.eia.gov/cneaf/electricity/epm/table5_6_a.html. Accessed 7/3/2011.
- Encyclopaedia Britannica, "Thomas Johann Seebeck," 2011. <http://www.britannica.com/EBchecked/topic/532353/Thomas-Johann-Seebeck>. Accessed 5/31/2011.
- Gordon, J.M., 1991, "Generalized Power Versus Efficiency Characteristics of Heat Engines: The Thermoelectric Generator as an Instructive Illustration," *American Journal of Physics*, **59**(6), pp. 551-555.
- Hilpert, R., *Forsch. Geb. Ingenieurwes.*, **4**, 215, 1933. In (Incropera).
- Incropera, F.P., Dewitt, D.P., Bergman, T.L., and Lavine, A.S., 2007, *Fundamentals of Heat and Mass Transfer*. Sixth Edition, John Wiley & Sons Inc., Hoboken, NJ.
- Jaluria, Y., 1998, *Design and Optimization of Thermal Systems*. First Edition, McGraw-Hill, New York.
- Kim, D., Kim, S.J., and Ortega, A., 2004, "Compact Modeling of Fluid Flow and Heat Transfer in Pin Fin Heat Sinks", *Journal of Electronic Packaging*, **126**, pp. 342-350.
- Koh, J.C.Y., and Colony, R., 1986, "Heat Transfer of Microstructures for Integrated Circuits," *Int. Comm. Heat Mass Transfer*, **13**, pp. 89-98.

Marlow Industries, Inc., TG12-8 Thermoelectric Generator Technical Data Sheet, <http://www.marlow.com/media/marlow/product/downloads/tg12-8-011/TG12-8.pdf>. Accessed 5/31/2011.

Masuoka, T., and Takatsu, Y., 1997, "Author's Reply", *Int. Journal of Heat and Mass Transfer*, **40**, pp. 2499-2500.

Rowe, D.M., Editor, 2006, "General Principles and Basic Considerations", *Thermoelectrics Handbook*, Vol. II, CRC Press, Taylor & Francis Group, Boca Raton, FL.

Thermal Electronics Corp., Specifications: TEG Module TEG1-12611-6.0, <http://www.espressomilkcooler.com/SpecTEG1-12611-6.0.pdf>, Accessed 5/31/2011.

You, H.I. and Chang, C.H., 1997, "Determination of Flow Properties in Non-Darcian Flow", *Journal of Heat Transfer*, **119**, 190-192.

Zukauskas, A., "Heat Transfer from Tubes in Cross Flow," in J. P. Hartnett and T.F. Irvine, Jr. Eds., *Advances in Heat Transfer*, Vol. 8, Academic Press, New York, 1972. In (Incropera).

APPENDIX A. MODEL AND OPTIMIZATION MATHEMATICA CODE

The following code was written in *Wolfram Mathematica 8.0*. The best-performing design of Case 1 is presented (Case A). Sample output and history plots pertaining to the simulated annealing algorithm are included. Although extensive comments have been inserted for clarity, a working knowledge of *Mathematica* is necessary for following the program in detail.

Design Case 1A: Expensive Energy, Low Temp Gradient

System Parameters and System Model Equations

```
(***** Constant Parameters *****)

a1 = .05; (* m *)
a2 = .05; (* m *)
UDflux = 400; (* W/m2K (UD) *)
kbp = .05; (* W/mK (Effective k of bypass insulation) *)
wbp = .004;
(* m (Thickness of thermoelectric device/bypass insulation, notated LD in thesis) *)
Z = .002; (* K-1, ZD value *)
Lceram = .001; (* m *)
kceram = 100; (* W/mK *)
Rcontactflux = 4 * 10-5; (* Km2/W (Thermal contact resistance, Rc) *)
ksink = 180; (* W/mK *)

mdotS = .03; (* kg/s, mass flow of source *)

xHS = 1000; (* $/m2 (notated pHS in thesis) *)
xins = 10; (* $/m2 (notated pins in thesis) *)
CD = 50; (* $ Cost per device *)
CL = 2000; (* $ Cost of installation *)
iinfl = .03; (* yr-1 inflation interest rate *)
iprev = .07; (* yr-1 prevailing interest rate *)
ω = 1.00; (* ratio of cost of energy increase to inflation increase *)
xenergy = 1.00; (* $/kW-hour *)

TS = 400; (* K (T80) *)
TA = 300; (* K (T20) *)

(***** Property Curve Fits for Atmospheric Air at 1 Atmosphere
(deg C) *****)
kaircurve[T] := (-3.31568 * 10-5 T2 + 8.03864 * 10-2 T + 24.1372) * 10-3;
ρaircurve[T] := 1.41783 * 10-11 T4 - 2.11288 * 10-8 T3 + 1.28112 * 10-5 T2 - 4.55736 * 10-3 T + 1.27961;
μaircurve[T] := (-1.93427 * 10-4 T2 + 4.75191 * 10-1 T + 1.71954 * 102) * 10-7;
cpaircurve[T] := ((-4.37192 * 10-10) T3 + (5.66285 * 10-7) T2 - (4.98838 * 10-7) T + 1.00599) * 103;
```

```

(* Estimate average temperature through channel *)

kairS = kaircurve [ (TS - 273.15) + ( (TS-TA) / 2 - 273.15 ) ]; (* W/mK (krs) *)

rhoairS = rhoaircurve [ (TS - 273.15) + ( (TS-TA) / 2 - 273.15 ) ]; (* kg/m^3 (rhoS) *)

muairS = muaircurve [ (TS - 273.15) + ( (TS-TA) / 2 - 273.15 ) ]; (* kg/s*m (muS) *)

cpairS = cpaircurve [ (TS - 273.15) + ( (TS-TA) / 2 - 273.15 ) ]; (* J/kg*K (cpg) *)

kairA = kaircurve [ (TA - 273.15) + ( (TS-TA) / 2 - 273.15 ) ]; (* W/mK (kra) *)

rhoairA = rhoaircurve [ (TA - 273.15) + ( (TS-TA) / 2 - 273.15 ) ]; (* kg/m^3 (rhoA) *)

muairA = muaircurve [ (TA - 273.15) + ( (TS-TA) / 2 - 273.15 ) ]; (* kg/s*m (muA) *)

cpairA = cpaircurve [ (TA - 273.15) + ( (TS-TA) / 2 - 273.15 ) ]; (* J/kg*K (cpa) *)

(***** Dimensionless Parameters *****)

MS = (mdotS) / (a1 * muairS);

go = TS Z;

xS = (ksink) / (kairS);
xA = (ksink) / (kairA);

muka = (ksink) / (a1 * UDflux);

Lbstar = 0.1;

```



```

(*****  $\epsilon_{IH}$ ",  $\epsilon_{IL}$ ", and  $\epsilon_{bp}$ " are defined *****)

$$\pi 1 = \frac{1}{R_{contactflux} UDflux};$$


$$\pi 2 = \frac{k_{ceram}}{UDflux L_{ceram}};$$


$$\epsilon_{IHflux} = (\pi 1^{-1} + \pi 2^{-1})^{-1};$$


$$\epsilon_{ILflux} = (\pi 1^{-1} + \pi 2^{-1})^{-1};$$


$$\epsilon_{bpflux} = \frac{k_{bp}}{w_{bp} * UDflux};$$

(*****)

To = TA / TS;


$$\phi S = \frac{\mu_{air} S^3 UDflux^2}{TS \rho_{air} S^2 k_{sink}^3};$$


$$\phi A = \frac{\mu_{air} A^3 UDflux^2}{TS \rho_{air} A^2 k_{sink}^3};$$


$$\chi_{HSstar} = \frac{\chi_{HS} a_1 a_2}{CD};$$


$$\chi_{insstar} = \frac{\chi_{ins} a_1 a_2}{CD};$$


$$i_{real} = \frac{1 + i_{prev}}{1 + i_{infl}} - 1;$$


$$\theta = .71;$$


$$c_A = \frac{a_2 UDflux}{c_{pairA} \mu_{airA}};$$


$$c_S = \frac{a_2 UDflux}{c_{pairS} \mu_{airS}};$$


(***** Hot side Reynolds number is a function of MS and other design variables *****)

RedS[r_, Zstar_,  $\epsilon_{xS}$ _,  $\epsilon_{xA}$ _,  $\epsilon_{zS}$ _,  $\epsilon_{zA}$ _,  $\lambda_S$ _,  $\lambda_A$ _,  $\phi_{pstarS}$ _,  $\phi_{pstarA}$ _, RedA_] :=  $\frac{MS}{Zstar \epsilon_{xS} \lambda_S};$ 

```

(****** The constants in the Nusselt Number Correlation are defined,
based on Reynolds number *****)

$$C1[Red_] := \begin{cases} .36283 & 0 < Red \leq 1512; \\ .04433 & Red > 1512 \end{cases};$$

$$m[Red_] := \begin{cases} .54219 & 0 < Red \leq 1512; \\ .82934 & Red > 1512 \end{cases};$$

(****** Equations for \bar{h}_R and \bar{h}_L as functions of 10 design variables *****)

$\bar{h}Hflux[Zstar_, \epsilon xS_, \epsilon xA_, \epsilon zS_, \epsilon zA_, \lambda S_, \lambda A_, dpstarS_, dpstarA_, RedA_] :=$

$$\left(\frac{mka}{Lbstar} \right) \left[2 \sqrt{\frac{(\epsilon xS + \epsilon zS - \epsilon xS \epsilon zS) C1\left[\frac{MS}{Zstar \epsilon xS \lambda S}\right] \left(\frac{MS}{Zstar \epsilon xS \lambda S}\right)^{m\left[\frac{MS}{Zstar \epsilon xS \lambda S}\right]}}{\kappa S}} (1 - \epsilon xS) (1 - \epsilon zS) \right. \\ \left. \frac{\text{Tanh}\left[2 \lambda S \sqrt{\left(1 / \kappa S (\epsilon xS + \epsilon zS - \epsilon xS \epsilon zS) C1\left[\frac{MS}{Zstar \epsilon xS \lambda S}\right] \left(\frac{MS}{Zstar \epsilon xS \lambda S}\right)^{m\left[\frac{MS}{Zstar \epsilon xS \lambda S}\right]}\right)}\right]}{(\epsilon xS + \epsilon zS - \epsilon xS \epsilon zS)^2 C1\left[\frac{MS}{Zstar \epsilon xS \lambda S}\right] \left(\frac{MS}{Zstar \epsilon xS \lambda S}\right)^{m\left[\frac{MS}{Zstar \epsilon xS \lambda S}\right]}} \right]}{\kappa S} \right] / \\ \left(\frac{dpstarS mka}{Lbstar} + 2 \sqrt{\frac{(\epsilon xS + \epsilon zS - \epsilon xS \epsilon zS) C1\left[\frac{MS}{Zstar \epsilon xS \lambda S}\right] \left(\frac{MS}{Zstar \epsilon xS \lambda S}\right)^{m\left[\frac{MS}{Zstar \epsilon xS \lambda S}\right]}}{\kappa S}} (1 - \epsilon xS) (1 - \epsilon zS) \right. \\ \left. \frac{\text{Tanh}\left[2 \lambda S \sqrt{\left(1 / \kappa S (\epsilon xS + \epsilon zS - \epsilon xS \epsilon zS) C1\left[\frac{MS}{Zstar \epsilon xS \lambda S}\right] \left(\frac{MS}{Zstar \epsilon xS \lambda S}\right)^{m\left[\frac{MS}{Zstar \epsilon xS \lambda S}\right]}\right)}\right]}{(\epsilon xS + \epsilon zS - \epsilon xS \epsilon zS)^2 C1\left[\frac{MS}{Zstar \epsilon xS \lambda S}\right] \left(\frac{MS}{Zstar \epsilon xS \lambda S}\right)^{m\left[\frac{MS}{Zstar \epsilon xS \lambda S}\right]}} \right]}{\kappa S} \right);$$

$$\begin{aligned}
& \mathbb{F}Lflux[Zstar_ , \epsilon xS_ , \epsilon xA_ , \epsilon zS_ , \epsilon zA_ , \lambda S_ , \lambda A_ , dpstarS_ , dpstarA_ , RedA_] := \\
& \left(\frac{\mu ka}{Lbstar} \right) \\
& \left(2 \sqrt{\frac{(\epsilon xA + \epsilon zA - \epsilon xA \epsilon zA) C1[RedA] (RedA)^{m[RedA]}}{\kappa A}} (1 - \epsilon xA) (1 - \epsilon zA) \right. \\
& \quad \left. \text{Tanh} \left[2 \lambda A \sqrt{\frac{(\epsilon xA + \epsilon zA - \epsilon xA \epsilon zA) C1[RedA] (RedA)^{m[RedA]}}{\kappa A}} \right] + \right. \\
& \quad \left. \frac{(\epsilon xA + \epsilon zA - \epsilon xA \epsilon zA)^2 C1[RedA] (RedA)^{m[RedA]}}{\kappa A} \right) \Bigg/ \\
& \left(\frac{dpstarA \mu ka}{Lbstar} + 2 \sqrt{\frac{(\epsilon xA + \epsilon zA - \epsilon xA \epsilon zA) C1[RedA] (RedA)^{m[RedA]}}{\kappa A}} (1 - \epsilon xA) (1 - \epsilon zA) \right. \\
& \quad \left. \text{Tanh} \left[2 \lambda A \sqrt{\frac{(\epsilon xA + \epsilon zA - \epsilon xA \epsilon zA) C1[RedA] (RedA)^{m[RedA]}}{\kappa A}} \right] + \right. \\
& \quad \left. \frac{(\epsilon xA + \epsilon zA - \epsilon xA \epsilon zA)^2 C1[RedA] (RedA)^{m[RedA]}}{\kappa A} \right) ;
\end{aligned}$$

(***** Equations for \mathbb{F}_H and \mathbb{F}_L as functions of 11 design variables *****)

$$\mathbb{F}H[r_ , Zstar_ , \epsilon xS_ , \epsilon xA_ , \epsilon zS_ , \epsilon zA_ , \lambda S_ , \lambda A_ , dpstarS_ , dpstarA_ , RedA_] := r \mathbb{F}Hflux[Zstar_ , \epsilon xS_ , \epsilon xA_ , \epsilon zS_ , \epsilon zA_ , \lambda S_ , \lambda A_ , dpstarS_ , dpstarA_ , RedA_]$$

$$\mathbb{F}L[r_ , Zstar_ , \epsilon xS_ , \epsilon xA_ , \epsilon zS_ , \epsilon zA_ , \lambda S_ , \lambda A_ , dpstarS_ , dpstarA_ , RedA_] := r \mathbb{F}Lflux[Zstar_ , \epsilon xS_ , \epsilon xA_ , \epsilon zS_ , \epsilon zA_ , \lambda S_ , \lambda A_ , dpstarS_ , dpstarA_ , RedA_]$$

$$\mathbb{F}IH = \mathbb{F}IHflux;$$

$$\mathbb{F}IL = \mathbb{F}ILflux;$$

$$\mathbb{F}bp[r_] := \mathbb{F}bpflux (r - 1);$$

(***** System model equations from Chapter 3 as functions of T_2 TA/TS *****)

$$DDo[T_] := \left(1 + \frac{\mathbb{F}Hfixed \mathbb{F}IL - \mathbb{F}IH \mathbb{F}Lfixed}{\mathbb{F}bpfixed (\mathbb{F}Lfixed + \mathbb{F}Hfixed) + \mathbb{F}Lfixed (\mathbb{F}Hfixed + \mathbb{F}IH)} \right);$$

$$CCo[T_] := 2 \mathbb{F}IH \left(1 + \frac{\mathbb{F}Lfixed \mathbb{F}IH}{\mathbb{F}bpfixed (\mathbb{F}Lfixed + \mathbb{F}Hfixed) + \mathbb{F}Hfixed \mathbb{F}Lfixed} \right)^{-1};$$

$$\begin{aligned}
\text{BBo}[T] &:= \frac{\xi}{2} \left(\frac{\xi \text{Lfixed} \xi \text{Hfixed} \xi \text{IH} (1 - T)}{\xi \text{Lfixed} (\xi \text{IH} + \xi \text{Hfixed}) + \xi \text{bpfixed} (\xi \text{Lfixed} + \xi \text{Hfixed})} \right); \\
\text{Y1o}[T] &:= \left(\frac{1}{2 (\text{DDo}[T] - 1)} \right. \\
&\quad \left. (4 \text{DDo}[T] + \text{CCo}[T] - \sqrt{(4 \text{DDo}[T] + \text{CCo}[T])^2 - 4 (\text{DDo}[T] - 1) (1 + \text{BBo}[T] + \text{CCo}[T] + 3 \text{DDo}[T])})} \right)^2 \\
\text{Yoo}[T] &:= \frac{(\text{Y1o}[T] - 1) * 2}{\xi \xi \text{IH}}; \\
\text{Woo}[T] &:= \left(\frac{2}{\xi \xi \text{IL}} \right) \left(1 - \left(2 - \sqrt{1 + \frac{1}{2} \xi \xi \text{IH} \text{Yoo}[T]} \right)^2 \right); \\
\text{Xoo}[T] &:= \frac{4}{\xi} \left(-1 + \sqrt{1 + \frac{\xi}{2} \xi \text{IH} \text{Yoo}[T]} \right); \\
\text{Xool}[T] &:= \frac{4}{\xi} \left(1 - \sqrt{1 - \frac{\xi}{2} \xi \text{IL} \text{Woo}[T]} \right); \\
\text{Zoo}[T] &:= T + \frac{\xi \text{IL}}{\xi \text{Lfixed}} \text{Woo}[T] + \frac{\xi \text{bpfixed}}{\xi \text{Lfixed}} (\text{Xoo}[T] + \text{Yoo}[T] + \text{Woo}[T]); \\
\tau\text{o}[T] &:= \frac{\text{Zoo}[T] + \text{Woo}[T]}{\text{Xoo}[T] + \text{Zoo}[T] + \text{Woo}[T]}; \\
\tau\text{Io}[T] &:= \frac{\text{Zoo}[T]}{\text{Xoo}[T] + \text{Yoo}[T] + \text{Zoo}[T] + \text{Woo}[T]}; \\
\gamma\text{o}[T] &:= \text{Xoo}[T] + \text{Zoo}[T] + \text{Woo}[T]; \\
\gamma\text{Ho}[T] &:= \frac{\text{Xoo}[T] + \text{Zoo}[T] + \text{Woo}[T]}{\text{Xoo}[T] + \text{Yoo}[T] + \text{Zoo}[T] + \text{Woo}[T]};
\end{aligned}$$

Module For Calculating X* and Payback Time

```

(***** The module "Actualretailprice" serves as a function of 11 design
variables with the output of optimum X* value that minimizes payback time,
and the minimized payback time. *****)

Actualretailprice[r_, Zstar_, exS_, exA_, ezS_, ezA_, λS_, λA_, dpstarS_, dpstarA_, RedA_] :=

Module[{rfixed = r, Zstarfixed = Zstar, Xstarfixed = 0, exSfixed = exS, exAfixed = exA,
ezSfixed = ezS, ezAfixed = ezA, λSfixed = λS, λAfixed = λA, dpstarSfixed = dpstarS,
dpstarAfixed = dpstarA, RedAfixed = RedA, ActualPaybacktimevalue = 0, i = 1, count = 1},

```

$$\text{RedSfixed} = \frac{\text{MS}}{\text{Zstar} \epsilon x S \lambda S};$$

$g = g^0;$

(* The function "friction" is a previously defined function of four variables
($\text{Re}_d, \epsilon x, \epsilon z, \lambda$), active in the Mathematica kernel,
which uses linear interpolation on the set of friction factor tables *)

(* If a Reynolds number above 5000 is encountered, use the friction factor for 5000 *)
 $\text{frictionSfixed} = \text{If}[\text{RedSfixed} > 5000, \text{friction}[5000, \epsilon x\text{Sfixed}, \epsilon z\text{Sfixed}, \lambda\text{Sfixed}],$
 $\text{friction}[\text{RedSfixed}, \epsilon x\text{Sfixed}, \epsilon z\text{Sfixed}, \lambda\text{Sfixed}]];$
 $\text{frictionAfixed} = \text{If}[\text{RedAfixed} > 5000, \text{friction}[5000, \epsilon x\text{Afixed}, \epsilon z\text{Afixed}, \lambda\text{Afixed}],$
 $\text{friction}[\text{RedAfixed}, \epsilon x\text{Afixed}, \epsilon z\text{Afixed}, \lambda\text{Afixed}]];$

(* The function "zHflux" is evaluated at the input values for the 10 design variables,
and the result stored in "zHarea" (Both represent \mathbb{R} .)*)

$\text{zHarea} = \text{zHflux}[\text{Zstarfixed}, \epsilon x\text{Sfixed}, \epsilon x\text{Afixed}, \epsilon z\text{Sfixed}, \epsilon z\text{Afixed}, \lambda\text{Sfixed},$
 $\lambda\text{Afixed}, \text{dpstarSfixed}, \text{dpstarAfixed}, \text{RedAfixed}];$
 $\text{zLarea} = \text{zLflux}[\text{Zstarfixed}, \epsilon x\text{Sfixed}, \epsilon x\text{Afixed}, \epsilon z\text{Sfixed}, \epsilon z\text{Afixed}, \lambda\text{Sfixed},$
 $\lambda\text{Afixed}, \text{dpstarSfixed}, \text{dpstarAfixed}, \text{RedAfixed}];$

(* The function "zH" is evaluated at the input values for the 11 design variables,
and the result stored in "zHfixed" (Both represent \mathbb{R} .)*)

$\text{zHfixed} = \text{zH}[\text{rfixed}, \text{Zstarfixed}, \epsilon x\text{Sfixed}, \epsilon x\text{Afixed}, \epsilon z\text{Sfixed}, \epsilon z\text{Afixed}, \lambda\text{Sfixed},$
 $\lambda\text{Afixed}, \text{dpstarSfixed}, \text{dpstarAfixed}, \text{RedAfixed}];$
 $\text{zLfixed} = \text{zL}[\text{rfixed}, \text{Zstarfixed}, \epsilon x\text{Sfixed}, \epsilon x\text{Afixed}, \epsilon z\text{Sfixed}, \epsilon z\text{Afixed}, \lambda\text{Sfixed},$
 $\lambda\text{Afixed}, \text{dpstarSfixed}, \text{dpstarAfixed}, \text{RedAfixed}];$
 $\text{zbpfixed} = \text{zbp}[\text{rfixed}];$

(* Arrays are defined which provide storage for the temperature ratios $T_{RA}, T_{RS},$
 $T, W_{\text{net}}, W_{\text{gross}}, T_B, T_A, \tau, \tau_I, \gamma, \gamma_H, \eta_{\text{pb}},$ and x^* *)

$\text{Clear}[x\text{star}];$
 $\text{cbx} = .05;$
 $\text{TEGmax} = 40;$
 $\text{Wcum} = \text{Range}[0, \text{TEGmax}, \text{cbx}];$
 $\text{BigTA} = \text{Range}[0, \text{TEGmax}, \text{cbx}];$
 $\text{BigTS} = \text{Range}[0, \text{TEGmax}, \text{cbx}];$
 $\text{BigT} = \text{Range}[0, \text{TEGmax}, \text{cbx}];$
 $\text{Wetar} = \text{Range}[0, \text{TEGmax}, \text{cbx}];$
 $\text{Wpiece} = \text{Range}[0, \text{TEGmax}, \text{cbx}];$

```

TSpoints = Range[0, TEGmax, dx];
TApoints = Range[0, TEGmax, dx];
rpoints = Range[0, TEGmax, dx];
rIpoints = Range[0, TEGmax, dx];
γpoints = Range[0, TEGmax, dx];
γHpoints = Range[0, TEGmax, dx];
RealPaybacktime = Range[0, TEGmax, dx];

Paybacktime = Range[0, TEGmax, dx];

x = Range[0, TEGmax, dx];
total = Count[x, _];

(* All initial elements are set to 0 *)
For[k = 1, k ≤ total, k++,

    Wcum[k] = 0;
    BigTA[k] = 0;
    BigTS[k] = 0;
    BigT[k] = 0;
    Wstar[k] = 0;
    Wpiece[k] = 0;
    TSpoints[k] = 0;
    TApoints[k] = 0;
    rpoints[k] = 0;
    rIpoints[k] = 0;
    γpoints[k] = 0;
    γHpoints[k] = 0;
    RealPaybacktime[k] = 0;
    Paybacktime[k] = 0;
];

(* Boundary Conditions for  $T_{RA}$ ,  $T_{RS}$  profiles *)
BigTA[1] = 1;
BigTS[1] = 1;
BigT[1] = To;
TSpoints[1] = TS;
TApoints[1] = TA;

(* Convenient counters *)
count = 1;
countevery = 100;

(****** The model is solved for  $x^* = 0$ ,
the first element in each array ******)

```

```

rpoints[1] = (Zoo[BigT[1]] + Woo[BigT[1]]) /
(Xoo[BigT[1]] + Zoo[BigT[1]] + Woo[BigT[1]]) ;
rIpoints[1] = Zoo[BigT[1]] /
(Xoo[BigT[1]] + Yoo[BigT[1]] + Zoo[BigT[1]] + Woo[BigT[1]]) ;
rYpoints[1] = Xoo[BigT[1]] + Zoo[BigT[1]] + Woo[BigT[1]] ;
rHpoints[1] = (Xoo[BigT[1]] + Zoo[BigT[1]] + Woo[BigT[1]]) /
(Xoo[BigT[1]] + Yoo[BigT[1]] + Zoo[BigT[1]] + Woo[BigT[1]]) ;

(* Wgross *)
Wpiece[1] =
((xIH rpoints[1] ((rHpoints[1])^-1 - 1) -
xIL rpoints[1] (rpoints[1] - rIpoints[1] (rHpoints[1])^-1))) dx;

(* Wnet *)
Wcum[1] = 1/dx Wpiece[1] - 1/2 phiS rfixed frictionSfixed exSfixed lambdaSfixed RedSfixed^3 /
dpstarSfixed^3 -
1/2 phiA rfixed frictionAfixed exAfixed lambdaAfixed RedAfixed^3 /
dpstarAfixed^3 ;

(* npb *)
Paybacktime[1] =
(1 / (omega iinfl - ireal) *
Log[
((omega iinfl - ireal)
(CL rfixed + CD dx Zstarfixed (2 xHSstar rfixed + xinsstar (rfixed - 1) + 1)) /
(8.76 theta Wcum[1] Udflex a1 a2 Zstarfixed dx TS xenergy)) + 1] ;

(***** LOOP. The model is solved for all other values of
x* *****)
(* Note, "xstar" is not x* as used in the thesis,
it represents which position in the array is being solved. If x* is 5,
and the step size, "dx", is .1, then xstar is 50 *)

For[xstar = 2, xstar <= total, xstar++,

(* Chapter 3 model equations called upon *)
rpoints[xstar - 1] = (Zoo[BigT[xstar - 1]] + Woo[BigT[xstar - 1]]) /
(Xoo[BigT[xstar - 1]] + Zoo[BigT[xstar - 1]] + Woo[BigT[xstar - 1]]);
rIpoints[xstar - 1] = Zoo[BigT[xstar - 1]] /
(Xoo[BigT[xstar - 1]] + Yoo[BigT[xstar - 1]] + Zoo[BigT[xstar - 1]] + Woo[BigT[xstar - 1]]);
rYpoints[xstar - 1] = Xoo[BigT[xstar - 1]] + Zoo[BigT[xstar - 1]] + Woo[BigT[xstar - 1]] ;

```

```

γHpoints[xstar - 1] = (Xoo[BigT[xstar - 1]] + Zoo[BigT[xstar - 1]] + Woo[BigT[xstar - 1]]) /
  (Xoo[BigT[xstar - 1]] + Yoo[BigT[xstar - 1]] + Zoo[BigT[xstar - 1]] + Woo[BigT[xstar - 1]]);

(* 1st Order Euler method used to solve each step of the profile of T2S, T3S *)
BigTA[xstar] = BigTA[xstar - 1] +  $\frac{cA \ \xi \ Larea}{\epsilon x \ Afixed \ \lambda \ Afixed \ RedAfixed}$ 
   $\left( \frac{\tau Ipoints[xstar - 1] \ \gamma points[xstar - 1]}{BigT[xstar - 1] \ \gamma Hpoints[xstar - 1]} - 1 \right) BigTA[xstar - 1] \ * \ dx;$ 
BigTS[xstar] = BigTS[xstar - 1] +  $\frac{cS \ \xi \ Harea}{\epsilon x \ Sfixed \ \lambda \ Afixed \ RedSfixed}$   $\left( \frac{\gamma points[xstar - 1]}{\gamma Hpoints[xstar - 1]} - 1 \right)$ 
  BigTS[xstar - 1] \ * \ dx;

(* Update g *)
g = g0 BigTS[xstar];

(* Wcross *)
Wpiece[xstar] = Wpiece[xstar - 1] +
   $\left( (\xi IH \ \gamma points[xstar - 1] \ (\gamma Hpoints[xstar - 1])^{-1} - 1) - \xi IL \ \gamma points[xstar - 1] \right.$ 
   $\left. (\tau points[xstar - 1] - \tau Ipoints[xstar - 1] \ (\gamma Hpoints[xstar - 1])^{-1}) \right) BigTS[xstar] \ dx;$ 

(* Wnet *)
Wcum[xstar] =  $\frac{1}{dx \ * \ xstar}$  Wpiece[xstar] -
   $\frac{1}{2} \phi S \ rfixed \ frictionSfixed \ \epsilon x \ Sfixed \ \lambda \ Sfixed \ \frac{RedSfixed^3}{\rho pstarSfixed^3} -$ 
   $\frac{1}{2} \phi A \ rfixed \ frictionAfixed \ \epsilon x \ Afixed \ \lambda \ Afixed \ \frac{RedAfixed^3}{\rho pstarAfixed^3};$ 

(* npb *)
Paybacktime[xstar] =
   $\left( \frac{1}{\omega \ iinfl - ireal} \right)$ 
  Log[
     $((\omega \ iinfl - ireal) (CLrfixed + CD(xstar \ dx) \ Zstarfixed (2 \ \chi HSstar \ rfixed +$ 
     $\chi instar (rfixed - 1) + 1))) /$ 
     $(8.76 \ \theta \ Wcum[xstar] \ UDflux \ a1 \ a2 \ Zstarfixed (xstar \ dx) \ TS \ \chi energy) + 1];$ 

(* Update T = TA/TS *)
BigT[xstar] = To  $\frac{BigTA[xstar]}{BigTS[xstar]}$ ;

(* Calculate new TA, TS *)
TSpoints[xstar] = TS + BigTS[xstar];
TApoints[xstar] = TA + BigTA[xstar];

```



```

count++;

If[count = countevery + 1, count = 1, countevery = countevery];

]

(****** END LOOP ******)

(* Search through the array of payback times. If any contain an imaginary componenet,
reset the payback time to 106 to tag it as infeasible *)
(* Values in "Paybacktime" are sorted into a new array, "RealPaybacktime" *)

For[i = 1, i ≤ total, i++,
  If[Im[Paybacktime[i]] ≠ 0, RealPaybacktime[i] = 106, RealPaybacktime[i] = Paybacktime[i]
];

(* Search through the payback times. When the lowest payback time is found,
this position, "j" is the same as the "xstar" that minimizes payback time *)
j = 2;
While[(RealPaybacktime[j] ≤ RealPaybacktime[j - 1] ∨ RealPaybacktime[j] == 106) && j < total,
  j++;
];

(* Use "j" to define "Xstarfixed", or the X* with minimum payback time *)
Xstarfixed = j dx;

(* Save the optimum payback time value *)
ActualPaybacktimevalue = RealPaybacktime[j];

(* Module Output *)
{ActualPaybacktimevalue, Xstarfixed}

]

```

Optimization Routine

```
(* The module works as shown below: The first value in the output is payback time,
the second is X* *)
```

```
Actualretailprice[2, 8, .8, .8, .2, .2, 4, 50, .005, .003, 400]
{109.543, 9.06}
```

■ Simulated Annealing Algorithm

```
(* "b" is defined as the first output, payback time, and "hxstar" is the second output,
optimum X* *)
```

```
b[x11_, x10_, x9_, x8_, x7_, x6_, x5_, x4_, x3_, x2_, x1_] :=
  Actualretailprice[x11, x10, x9, x8, x7, x6, x5, x4, x3, x2, x1][1]
hxstar[x11_, x10_, x9_, x8_, x7_, x6_, x5_, x4_, x3_, x2_, x1_] :=
  Actualretailprice[x11, x10, x9, x8, x7, x6, x5, x4, x3, x2, x1][2]
```

```
ntemps = 30; (* Number of 'annealing temperatures' *)
n = 20; (* Number of iterations at each temperature *)
totalcalls = ntempn; (* total number of function calls *)
Pso = 0.5; (* Initial probability of choosing a worse design *)
Pff = .0001; (* Final probability of choosing a worse design *)
```

```
(* Step sizes for each variable *)
```

```
 $\Delta 1 = 200$ ; (*  $\Delta \text{ReyA}$  *)
 $\Delta 2 = .0004$ ; (*  $\Delta \text{dpA}$  *)
 $\Delta 3 = .0004$ ; (*  $\Delta \text{dpS}$  *)
 $\Delta 4 = 10$ ; (*  $\Delta \lambda A$  *)
 $\Delta 5 = 2$ ; (*  $\Delta \lambda S$  *)
 $\Delta 6 = .04$ ; (*  $\Delta \epsilon ZA$  *)
 $\Delta 7 = .04$ ; (*  $\Delta \epsilon ZS$  *)
 $\Delta 8 = .04$ ; (*  $\Delta \epsilon \lambda A$  *)
 $\Delta 9 = .04$ ; (*  $\Delta \epsilon \lambda S$  *)
 $\Delta 10 = 2$ ; (*  $\Delta Z^*$  *)
 $\Delta 11 = .2$ ; (*  $\Delta F$  *)
```

```
(* Define arrays to store the values of each iteration *)
```

```
x1 = Range[1, ntempn + 1];
x2 = Range[1, ntempn + 1];
x3 = Range[1, ntempn + 1];
x4 = Range[1, ntempn + 1];
x5 = Range[1, ntempn + 1];
x6 = Range[1, ntempn + 1];
x7 = Range[1, ntempn + 1];
```

```

x8 = Range[1, nntemps + 1];
x9 = Range[1, nntemps + 1];
x10 = Range[1, nntemps + 1];
x11 = Range[1, nntemps + 1];
bpoints = Range[1, nntemps + 1];
Xstarpoints = Range[1, nntemps + 1];

```

```

(* Initial Design Variables *)
x1[1] = 1000; (* Starting ReyA *)
x2[1] = .01; (* Starting dpAstar *)
x3[1] = .005; (* Starting dpSstar *)
x4[1] = 100; (* Starting λA *)
x5[1] = 20; (* Starting λS *)
x6[1] = .6; (* Starting εZA *)
x7[1] = .6; (* Starting εZS *)
x8[1] = .6; (* Starting eXA *)
x9[1] = .6; (* Starting eXS *)
x10[1] = 50; (* Starting Z* *)
x11[1] = 2; (* Starting r *)

```

■ Perform Iterations

```

(* Define starting and final 'annealing temperatures' and step fraction *)
Ts =  $\frac{-1}{\text{Log}[Pso]}$ ;
Tf =  $\frac{-1}{\text{Log}[Pf]}$ ;
F =  $\left( \frac{Tf}{Ts}, \frac{1}{nntemps-1} \right)$ ;
Fn = 1;

(* Calculate First value in arrays *)
bpoints[1] = b[x11[1], x10[1], x9[1], x8[1], x7[1], x6[1], x5[1], x4[1], x3[1], x2[1], x1[1]];
Xstarpoints[1] = bxstar[x11[1], x10[1], x9[1], x8[1], x7[1], x6[1], x5[1], x4[1],
  x3[1], x2[1], x1[1]];
ΔEavg = 0;
ΔEcum = 0;

(* Some convenient variables *)
q = 2;
i = 2;
accept = True;

```

```
(****** Double Loop, "roll" indicates the number of temperatures,
"count" indicates the number of iterations at each temperature *****)
```

```
For[roll = 1, roll ≤ ntemps, roll++,
```

```
For[count = 2, count ≤ n + 1, count++,
```

```
(* Randomly perterb the current design *)
```

```
x1cand = x1[i - 1] + Random[Real, {-1, 1}] Δ1;
x2cand = x2[i - 1] + Random[Real, {-1, 1}] Δ2;
x3cand = x3[i - 1] + Random[Real, {-1, 1}] Δ3;
x4cand = x4[i - 1] + Random[Real, {-1, 1}] Δ4;
x5cand = x5[i - 1] + Random[Real, {-1, 1}] Δ5;
x6cand = x6[i - 1] + Random[Real, {-1, 1}] Δ6;
x7cand = x7[i - 1] + Random[Real, {-1, 1}] Δ7;
x8cand = x8[i - 1] + Random[Real, {-1, 1}] Δ8;
x9cand = x9[i - 1] + Random[Real, {-1, 1}] Δ9;
x10cand = x10[i - 1] + Random[Real, {-1, 1}] Δ10;
x11cand = x11[i - 1] + Random[Real, {-1, 1}] Δ11;
```

```
(* If any variables are outside their bounds, modify the perterbation*)
```

```
While[x1cand ≤ 10,
```

```
  x1cand = x1[i - 1] + Random[Real, {-1, 1}] Δ1; (* ReyA *)
```

```
]
```

```
;
```

```
While[x2cand ≤ .002222222 ∨ x2cand > .1,
```

```
  x2cand = x2[i - 1] + Random[Real, {-1, 1}] Δ2; (* dp*A *)
```

```
]
```

```
;
```

```
While[x3cand ≤ .002222222 ∨ x3cand > .1,
```

```
  x3cand = x3[i - 1] + Random[Real, {-1, 1}] Δ3; (* dp*S *)
```

```
]
```

```
;
```

```
While[x4cand ≤ .5 ∨ x4cand > 100,
```

```
  x4cand = x4[i - 1] + Random[Real, {-1, 1}] Δ4; (* λA *)
```

```
]
```

```
;
```

```
While[x5cand ≤ .5 ∨ x5cand > 100,
```

```
  x5cand = x5[i - 1] + Random[Real, {-1, 1}] Δ5; (* λS *)
```

```

]
;
While[x6cand ≤ .2 ∨ x6cand > .8,
  x6cand = x6[i-1] + Random[Real, {-1, 1}] Δ6; (* ∈ZA *)
]
;
While[x7cand ≤ .2 ∨ x7cand > .8,
  x7cand = x7[i-1] + Random[Real, {-1, 1}] Δ7; (* ∈ZS *)
]
;
While[x8cand ≤ .2 ∨ x8cand > .8,
  x8cand = x8[i-1] + Random[Real, {-1, 1}] Δ8; (* ∈XA *)
]
;
While[x9cand ≤ .2 ∨ x9cand > .8,
  x9cand = x9[i-1] + Random[Real, {-1, 1}] Δ9; (* ∈XS *)
]
;
While[x10cand ≤ 1,
  x10cand = x10[i-1] + Random[Real, {-1, 1}] Δ10; (* ∈Z* *)
]
;
While[x11cand ≤ 1 ∨ x11cand > 2,
  x11cand = x11[i-1] + Random[Real, {-1, 1}] Δ11; (* ∈r *)
]
;

(* This forces the Z* value to be modified such than the design uses an
integer quantity of total thermoelectric devices *)
x10cand = x11cand Round[ $\frac{x10cand}{x11cand}$ ];

(* "holdit" gathers both module outputs in a single function call,
saving computation time *)
holdit = Actualretailprice[x11cand, x10cand, x9cand, x8cand, x7cand, x6cand,
  x5cand, x4cand, x3cand, x2cand, x1cand];

(* candidate for payback time *)
bcand = holdit[1];

(* 'Energy difference' parameter in annealing algorithm *)
ΔE = bcand - hpoints[i-1];

(* Absolute value *)
ΔEabs = Abs[ΔE];

```

```

(* If this is the first design perturbation (i = 2) then automatically
accept the design *)
If[i == 2, ΔEavg = Abs[ΔE]];

(* Probability of accepting the design if it is poorer than the current design *)
Ps = Exp[ $\frac{-\Delta E_{abs}}{\Delta E_{avg} (T_s)}$ ];

(* If the design is better than the current design, or is the first perturbation,
accept it. If it is poorer, only accept it if "Ps" is greater than a random
number between 0 and 1 *)
If[ΔE ≤ 0, accept = True, accept = Ps ≥ Random[Real, {0, 1}]];
If[i == 2, accept = True];

(* If the design is accepted, save it to the next element in each master array *)
If[accept == True, {bpoints[i] = bcand, x1[i] = x1cand, x2[i] = x2cand, x3[i] = x3cand,
x4[i] = x4cand, x5[i] = x5cand, x6[i] = x6cand, x7[i] = x7cand, x8[i] = x8cand,
x9[i] = x9cand, x10[i] = x10cand, x11[i] = x11cand},
{bpoints[i] = bpoints[i - 1], x1[i] = x1[i - 1], x2[i] = x2[i - 1], x3[i] = x3[i - 1],
x4[i] = x4[i - 1], x5[i] = x5[i - 1], x6[i] = x6[i - 1], x7[i] = x7[i - 1],
x8[i] = x8[i - 1], x9[i] = x9[i - 1], x10[i] = x10[i - 1], x11[i] = x11[i - 1]}];

(* Accepted designs will contribute to the running "ΔEavg" *)
If[accept == True, ΔEcum = ΔEcum + ΔEabs, ΔEcum = ΔEcum];
If[accept == True, q = q + 1, q = q];


$$\Delta E_{avg} = \frac{\Delta E_{cum}}{q - 1};$$


thexstar = Actualretailprice[x11[i], x10[i], x9[i], x8[i], x7[i], x6[i], x5[i],
x4[i], x3[i], x2[i], x1[i]][2];

(* Print the output for each iteration *)
Print[Style[{ $\frac{MS}{x9[i] x10[i] x5[i]}$ , " " x1[i], " " x2[i], " " x3[i], " " x4[i],
" " x5[i], " " x6[i], " " x7[i], " " x8[i], " " x9[i], " " x10[i], " " x11[i],
" " bpoints[i], " " thexstar}, FontSize → 12]]

```

```

    i++;

]
;
(***** End the "count" loop *****)

(***** Update the 'annealing temperature' *****)
Tsnew = F Ts;
Ts = Tsnew;

(***** After completing this loop,
the following output allows for the variables to be visually matched to
their values *****)
Print[
Style[
" ReS      ReA      dp^A      dp^S      λA      λS      εzA
  εzS      εxA      εxS      Z*      r      Yrs      X*",
FontSize → 12]];

(* Print an approximate percentage completion *)
Print[Round[100  $\frac{\text{roll}}{\text{ntemps}}$ ], "% Complete"];

];

(***** End the "roll" loop *****)

(* These three parameters are stored with more descriptive variable names for
convenience *)
thezstar = x10[i - 1];
ther = x11[i - 1];
years = bpoints[i - 1];

{44.1731, 1016.36 , 0.0102514 , 0.00535515 , 97.9066 , 20.4399 ,
 0.634366 , 0.565804 , 0.638621 , 0.62614 , 48.6071 , 1.8695 , 24.9473 , 2.65 }
{41.3553, 933.895 , 0.0099647 , 0.00514383 , 89.8035 , 20.654 , 0.646411 ,
 0.583612 , 0.61349 , 0.628034 , 51.2258 , 1.97022 , 23.0261 , 2.55 }
{46.8402, 991.878 , 0.0101322 , 0.00476864 , 99.4193 , 18.7939 ,
 0.668799 , 0.620289 , 0.653331 , 0.604694 , 51.622 , 1.98546 , 25.695 , 2.65 }
{46.8402, 991.878 , 0.0101322 , 0.00476864 , 99.4193 , 18.7939 ,
 0.668799 , 0.620289 , 0.653331 , 0.604694 , 51.622 , 1.98546 , 25.695 , 2.65 }

```

{44.5676, 939.56 , 0.00984397 , 0.00456335 , 95.6382 , 20.1184 , 0.629071 ,
0.628313 , 0.688859 , 0.595723 , 51.4459 , 1.9054 , 21.8324 , 2.65 }

{42.8608, 791.748 , 0.00973323 , 0.0046355 , 93.7863 , 20.1905 ,
0.590025 , 0.636602 , 0.688519 , 0.63097 , 50.3258 , 1.93561 , 19.516 , 2.95 }

{46.2144, 824.592 , 0.00979034 , 0.00447749 , 90.4286 , 19.2752 ,
0.609247 , 0.62053 , 0.707064 , 0.617135 , 49.9863 , 1.78523 , 20.4539 , 2.8 }

{44.3171, 713.368 , 0.00980384 , 0.00450458 , 92.8248 , 20.0908 , 0.609643 ,
0.65495 , 0.676989 , 0.638201 , 48.3594 , 1.72712 , 20.9905 , 2.95 }

{46.1141, 590.142 , 0.0100121 , 0.00412268 , 88.2405 , 19.8974 , 0.60654 ,
0.638214 , 0.712487 , 0.606141 , 49.4086 , 1.59383 , 20.4023 , 2.75 }

{50.2739, 756.743 , 0.0103139 , 0.00377538 , 90.8985 , 19.0842 , 0.580412 ,
0.643088 , 0.728699 , 0.579951 , 49.3854 , 1.59308 , 18.9989 , 2.75 }

{55.3026, 695.906 , 0.0104185 , 0.0035499 , 95.6549 , 18.3853 , 0.569203 ,
0.664408 , 0.710827 , 0.542709 , 49.7992 , 1.65997 , 16.4764 , 2.9 }

{57.1823, 773.448 , 0.0107126 , 0.00354964 , 89.7839 , 18.8973 ,
0.547989 , 0.640646 , 0.72015 , 0.508074 , 50.0518 , 1.47211 , 17.4154 , 2.5 }

{49.822, 647.152 , 0.0106324 , 0.00394027 , 96.4059 , 20.3332 , 0.511171 ,
0.61839 , 0.724509 , 0.534034 , 50.7939 , 1.49394 , 17.5702 , 2.55 }

{49.1021, 829.869 , 0.0103315 , 0.00415198 , 91.0591 , 21.2211 ,
0.544848 , 0.590239 , 0.697757 , 0.509219 , 51.7886 , 1.6706 , 16.3647 , 2.4 }

{50.289, 868.538 , 0.00993597 , 0.00414474 , 84.5987 , 22.2833 , 0.516574 ,
0.586332 , 0.716281 , 0.486105 , 50.4456 , 1.80163 , 15.6514 , 2.4 }

{49.7858, 808.714 , 0.0098282 , 0.00430765 , 82.8456 , 20.7545 ,
0.528038 , 0.608946 , 0.697421 , 0.52228 , 50.9197 , 1.95845 , 15.3993 , 2.6 }

{50.3271, 737.75 , 0.00971261 , 0.004266 , 80.8677 , 20.2314 , 0.535234 ,
0.593055 , 0.733415 , 0.533295 , 50.607 , 1.80739 , 16.4642 , 2.6 }

{50.3271, 737.75 , 0.00971261 , 0.004266 , 80.8677 , 20.2314 , 0.535234 ,
0.593055 , 0.733415 , 0.533295 , 50.607 , 1.80739 , 16.4642 , 2.6 }

{50.3271, 737.75 , 0.00971261 , 0.004266 , 80.8677 , 20.2314 , 0.535234 ,
0.593055 , 0.733415 , 0.533295 , 50.607 , 1.80739 , 16.4642 , 2.6 }

{45.4673, 780.032 , 0.00945231 , 0.0045475 , 89.7785 , 21.0117 ,
0.511548 , 0.57032 , 0.706329 , 0.552223 , 52.0874 , 1.79612 , 16.2577 , 2.5 }

ReS	ReA	dp^A	dp^S	λA	λS		
εxA	εxS	εxA	εxS	Z^	r	Yrs	X^

3 * Complete

{343.349, 860.131 , 0.012112 , 0.00256759 , 93.909 , 4.96208 , 0.247997 ,
0.346533 , 0.388264 , 0.227496 , 70.8979 , 1.91616 , 6.92897 , 3.45 }

{343.349, 860.131 , 0.012112 , 0.00256759 , 93.909 , 4.96208 , 0.247997 ,
0.346533 , 0.388264 , 0.227496 , 70.8979 , 1.91616 , 6.92897 , 3.45 }

{343.349, 860.131 , 0.012112 , 0.00256759 , 93.909 , 4.96208 , 0.247997 ,
0.346533 , 0.388264 , 0.227496 , 70.8979 , 1.91616 , 6.92897 , 3.45 }

{343.349, 860.131 , 0.012112 , 0.00256759 , 93.909 , 4.96208 , 0.247997 ,


```

0.346533 , 0.388264 , 0.227496 , 70.8979 , 1.91616 , 6.92897 , 3.45 }
{343.349, 860.131 , 0.012112 , 0.00256759 , 93.909 , 4.96208 , 0.247997 ,
0.346533 , 0.388264 , 0.227496 , 70.8979 , 1.91616 , 6.92897 , 3.45 }
{343.349, 860.131 , 0.012112 , 0.00256759 , 93.909 , 4.96208 , 0.247997 ,
0.346533 , 0.388264 , 0.227496 , 70.8979 , 1.91616 , 6.92897 , 3.45 }
{343.349, 860.131 , 0.012112 , 0.00256759 , 93.909 , 4.96208 , 0.247997 ,
0.346533 , 0.388264 , 0.227496 , 70.8979 , 1.91616 , 6.92897 , 3.45 }
{426.641, 922.765 , 0.0117912 , 0.00262017 , 94.8036 , 4.41387 , 0.249855 ,
0.361295 , 0.390057 , 0.208581 , 69.9599 , 1.89081 , 6.92873 , 3.6 }
{426.641, 922.765 , 0.0117912 , 0.00262017 , 94.8036 , 4.41387 , 0.249855 ,
0.361295 , 0.390057 , 0.208581 , 69.9599 , 1.89081 , 6.92873 , 3.6 }
{426.641, 922.765 , 0.0117912 , 0.00262017 , 94.8036 , 4.41387 , 0.249855 ,
0.361295 , 0.390057 , 0.208581 , 69.9599 , 1.89081 , 6.92873 , 3.6 }
{426.641, 922.765 , 0.0117912 , 0.00262017 , 94.8036 , 4.41387 , 0.249855 ,
0.361295 , 0.390057 , 0.208581 , 69.9599 , 1.89081 , 6.92873 , 3.6 }
{426.641, 922.765 , 0.0117912 , 0.00262017 , 94.8036 , 4.41387 , 0.249855 ,
0.361295 , 0.390057 , 0.208581 , 69.9599 , 1.89081 , 6.92873 , 3.6 }
{426.641, 922.765 , 0.0117912 , 0.00262017 , 94.8036 , 4.41387 , 0.249855 ,
0.361295 , 0.390057 , 0.208581 , 69.9599 , 1.89081 , 6.92873 , 3.6 }
{426.641, 922.765 , 0.0117912 , 0.00262017 , 94.8036 , 4.41387 , 0.249855 ,
0.361295 , 0.390057 , 0.208581 , 69.9599 , 1.89081 , 6.92873 , 3.6 }
{426.641, 922.765 , 0.0117912 , 0.00262017 , 94.8036 , 4.41387 , 0.249855 ,
0.361295 , 0.390057 , 0.208581 , 69.9599 , 1.89081 , 6.92873 , 3.6 }
{426.641, 922.765 , 0.0117912 , 0.00262017 , 94.8036 , 4.41387 , 0.249855 ,
0.361295 , 0.390057 , 0.208581 , 69.9599 , 1.89081 , 6.92873 , 3.6 }
{426.641, 922.765 , 0.0117912 , 0.00262017 , 94.8036 , 4.41387 , 0.249855 ,
0.361295 , 0.390057 , 0.208581 , 69.9599 , 1.89081 , 6.92873 , 3.6 }
{290.214, 948.429 , 0.0118636 , 0.00236029 , 93.9463 , 6.35531 , 0.218681 ,
0.396287 , 0.384795 , 0.214216 , 69.5504 , 1.87974 , 6.75362 , 3.1 }
{290.214, 948.429 , 0.0118636 , 0.00236029 , 93.9463 , 6.35531 , 0.218681 ,
0.396287 , 0.384795 , 0.214216 , 69.5504 , 1.87974 , 6.75362 , 3.1 }

ReS      ReA      dp^A      dp^S      λA      λS
εxA      εxS      εxA      εxS      Z^*      r      Yrs      X^*

100 * Complete

```

Results

- Plots

```

(* The total number of times the model was solved is stored in i-1 *)
Print["Total Function Calls  ", i - 1];

(* History plots of each design variable *)
plotx1 = ListPlot[x1, Joined → True, PlotRange → {Min[x1], Max[x1]}, Frame → True,
  GridLines → Automatic, PlotLabel → "ReGR"];
plotx2 = ListPlot[x2, Joined → True, PlotRange → {Min[x2], Max[x2]}, Frame → True,
  GridLines → Automatic, PlotLabel → "dPA"];
plotx3 = ListPlot[x3, Joined → True, PlotRange → {Min[x3], Max[x3]}, Frame → True,
  GridLines → Automatic, PlotLabel → "dPS"];
plotx4 = ListPlot[x4, Joined → True, PlotRange → {Min[x4], Max[x4]}, Frame → True,
  GridLines → Automatic, PlotLabel → "λA"];
plotx5 = ListPlot[x5, Joined → True, PlotRange → {Min[x5], Max[x5]}, Frame → True,
  GridLines → Automatic, PlotLabel → "λS"];
plotx6 = ListPlot[x6, Joined → True, PlotRange → {Min[x6], Max[x6]}, Frame → True,
  GridLines → Automatic, PlotLabel → "εZA"];
plotx7 = ListPlot[x7, Joined → True, PlotRange → {Min[x7], Max[x7]}, Frame → True,
  GridLines → Automatic, PlotLabel → "εZS"];
plotx8 = ListPlot[x8, Joined → True, PlotRange → {Min[x8], Max[x8]}, Frame → True,
  GridLines → Automatic, PlotLabel → "εXA"];
plotx9 = ListPlot[x9, Joined → True, PlotRange → {Min[x9], Max[x9]}, Frame → True,
  GridLines → Automatic, PlotLabel → "εXS"];
plotx10 = ListPlot[x10, Joined → True, PlotRange → {Min[x10], Max[x10]}, Frame → True,
  GridLines → Automatic, PlotLabel → "Z"];
plotx11 = ListPlot[x11, Joined → True, PlotRange → {Min[x11], Max[x11]}, Frame → True,
  GridLines → Automatic, PlotLabel → "r"];

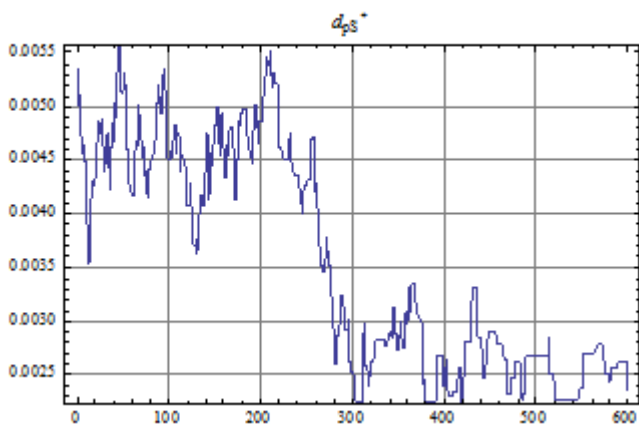
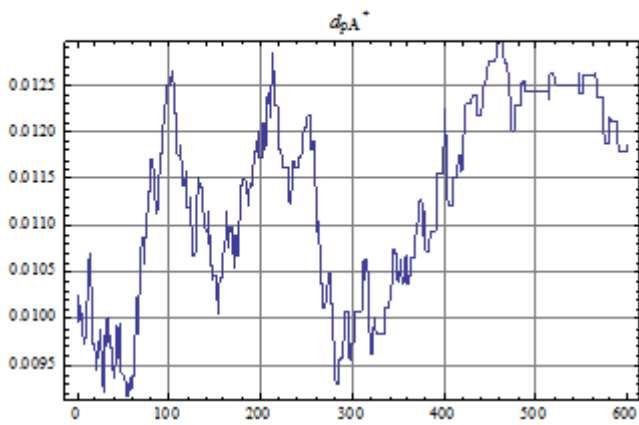
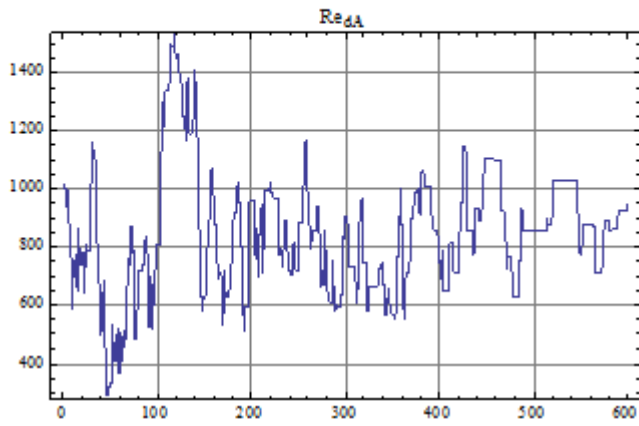
(* History plot of payback time *)
objectiveplot = ListPlot[bpoints, Joined → True, PlotRange → {Min[bpoints], Max[bpoints]},
  Frame → True, GridLines → Automatic, PlotLabel → "Payback Years"];

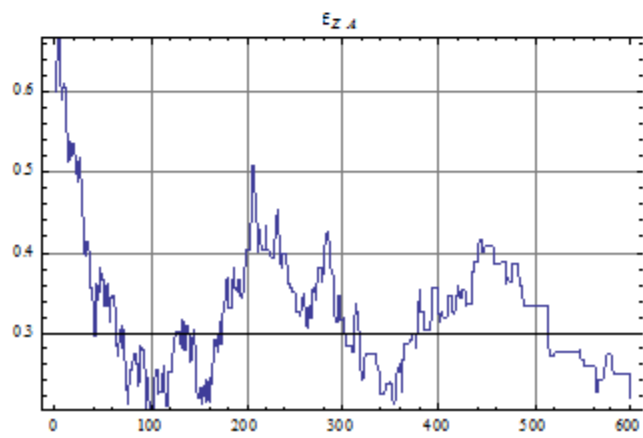
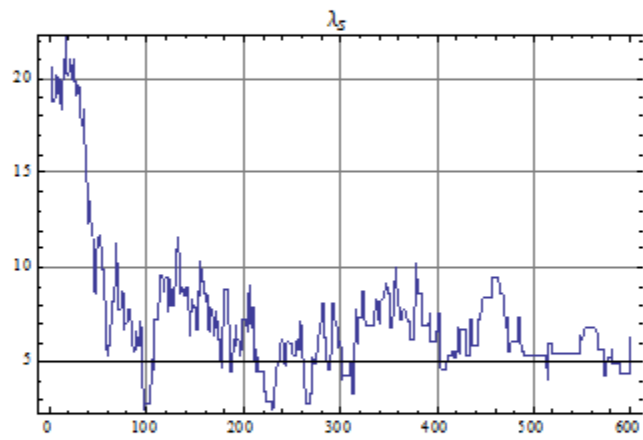
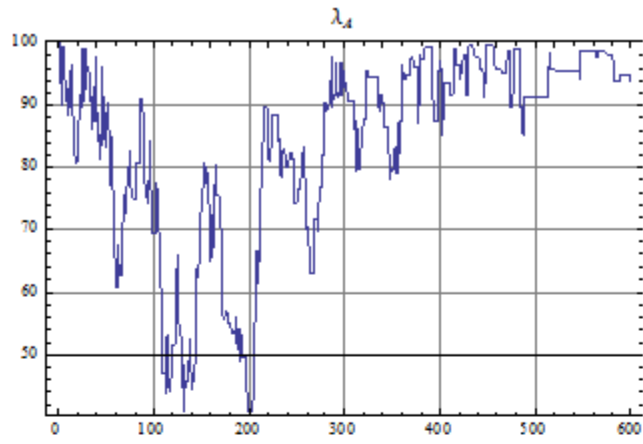
plotx1
plotx2
plotx3
plotx4
plotx5
plotx6
plotx7
plotx8
plotx9
plotx10
plotx11

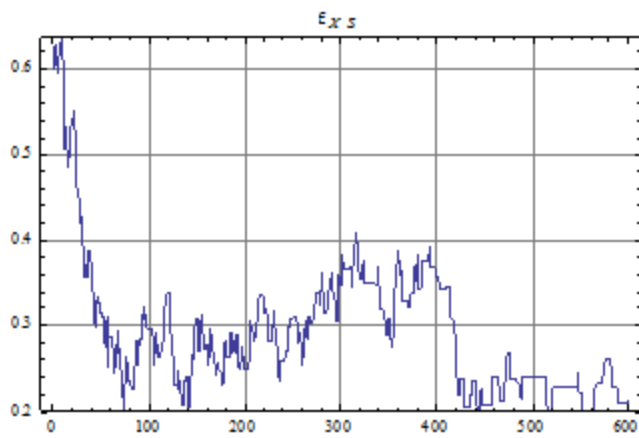
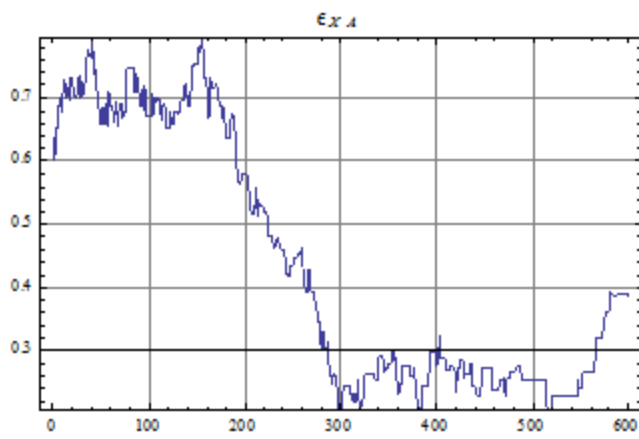
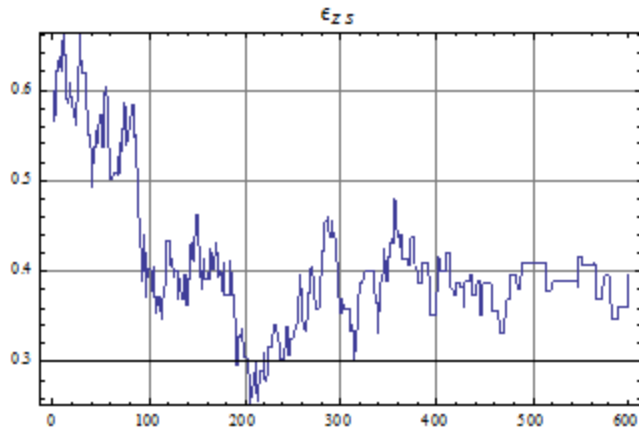
```

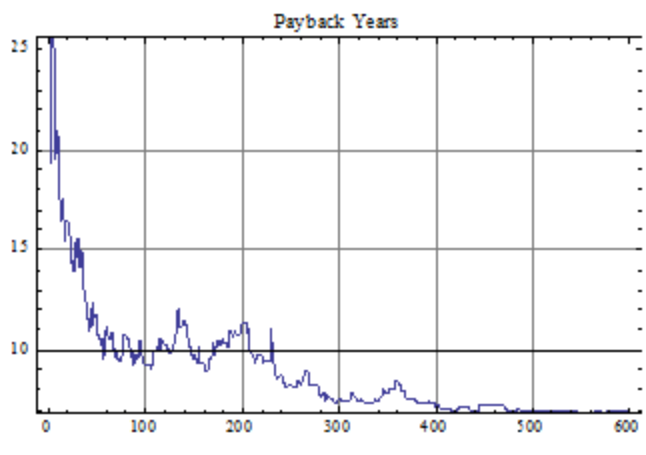
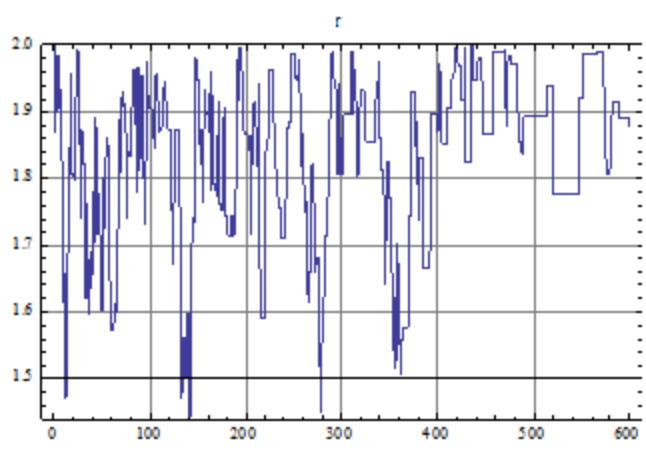
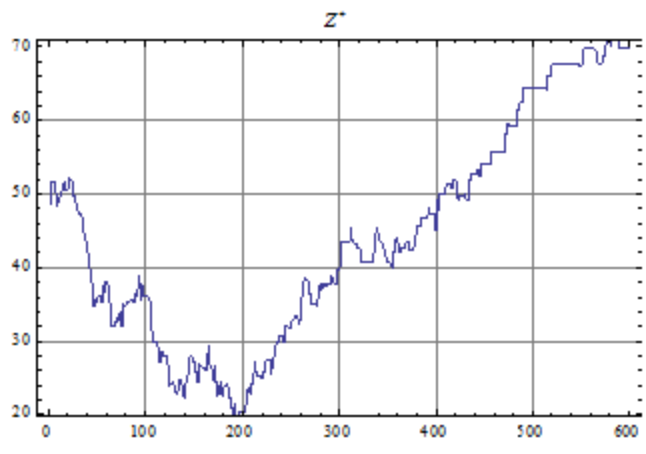
objectiveplot

Total Function Calls 601









- Results

```

(* Convenient descriptors *)
scale = dx-1;
portion = 1;

(* "DimWork" will store the dimensional power calculated from the dimensionless power *)
DimWork = Range[1, total];

(* Wnet* is used to calculate Wnet *)
For[a = 1, a ≤ total, a++,
  DimWork[a] = Wcum[a] UDflux a1 a1 TS  $\left( \frac{\text{thezstar}}{\text{ther}} \right)$  (dx a);
];

maxpowerlocation;

(* Search through the array to find the x* location with maximum power *)
For[a = 1, a ≤ total, a++,
  If[DimWork[a] == Max[DimWork], maxpowerlocation = a];
];

(* The actual x* value is the array location multiplied by the step size *)
themaxpowerxstar = maxpowerlocation dx;

(* Values for x* are discretized to represent physical design points *)
discretexvalues = Range[Max[Floor[thezstar], 1], Round[themaxpowerxstar], 1];
discretexpoints = dx-1 discretexvalues;

(* Define arrays to store the Wnet and npb values *)
discretepowerpoints = Range[1, Count[discretexvalues, _]];
discretepaybackpoints = Range[1, Count[discretexvalues, _]];

(* Import the values for Wnet and npb into the arrays *)
For[t = 1, t ≤ Count[discretexvalues, _], t++,
  discretepowerpoints[t] = DimWork[discretexpoints[t]]; (* SHOULD NOT BE +1 *)
  discretepaybackpoints[t] = Paybacktime[discretexpoints[t]]; (* SHOULD NOT BE +1 *)
];

(* The array locations of the maximum Wnet and minimum npb are stored *)
For[ab = 1, ab ≤ Count[discretexvalues, _], ab++,
  If[discretepowerpoints[ab] == Max[discretepowerpoints], discretexstarpower = ab];
  If[discretepaybackpoints[ab] == Min[discretepaybackpoints], discretexstarpay = ab];
];

```

```
(* Plots showing Power and payback time*)
plot2 = ListLinePlot[{x[1 ;; xstar - 1], DimWork[1 ;; xstar - 1]}',
  PlotRange -> {{0, portion TEGmax}, {0, 1.1 Max[DimWork]}}, Frame -> True,
  FrameLabel -> {Style["x", FontSize -> 14], Style["Power Output (W)", FontSize -> 14]},
  GridLines -> Automatic];
plot4 = ListLinePlot[{x[1 ;; xstar - 1], Paybacktime[1 ;; xstar - 1]}',
  PlotRange -> {{0, portion TEGmax}, {0, 1.2 Max[discretipaybackpoints]}},
  Frame -> True, FrameLabel -> {Style["x", FontSize -> 14], Style["Years", FontSize -> 14]},
  GridLines -> Automatic];
```

(* Plots showing discretized design points beginning with minimum payback time and ending with maximum power output *)

```
discreteplotpower =
  ListPlot[
    {discretexvalues[discretexstarpay ;;], discretepowerpoints[discretexstarpay ;;]}',
    PlotRange -> {{0, portion TEGmax}, {0, 1.1 Max[DimWork]}}, Frame -> True,
    FrameLabel -> {Style["x", FontSize -> 14], Style["Power Output (W)", FontSize -> 14]},
    GridLines -> Automatic, PlotStyle -> PointSize[.01]};

discreteplotpayback =
  ListPlot[
    {discretexvalues[discretexstarpay ;;], discretipaybackpoints[discretexstarpay ;;]}',
    PlotRange -> {{0, portion TEGmax}, {0, 1.2 Max[discretipaybackpoints]}},
    Frame -> True, FrameLabel -> {Style["x", FontSize -> 14], Style["Years", FontSize -> 14]},
    GridLines -> Automatic, PlotStyle -> PointSize[.01]};
```

```
Show[plot2, discreteplotpower]
Show[plot4, discreteplotpayback]
```

(* Plots showing the temperature profiles of T_S and T_A *)

```
plot5 =
  ListLinePlot[{{x[1 ;; Round[scale thexstar]], TSpoints[1 ;; Round[scale thexstar]] - 273}' ,
    {x[1 ;; Round[scale thexstar]], TApoints[1 ;; Round[scale thexstar]] - 273}'},
  PlotRange -> {{0, portion TEGmax}, {0, 1.1 (TSpoints[1] - 273)}}, Frame -> True,
  FrameLabel -> {Style["x", FontSize -> 14], Style["T (C)", FontSize -> 14]},
  GridLines -> Automatic];
plot6 = ListLinePlot[{{x[1 ;; xstar - 1], TSpoints[1 ;; xstar - 1] - 273}' ,
  {x[1 ;; xstar - 1], TApoints[1 ;; xstar - 1] - 273}'},
  PlotRange -> {{thexstar, portion TEGmax}, {0, 1.1 (TSpoints[1] - 273)}}, Frame -> True,
  FrameLabel -> {Style["x", FontSize -> 14], Style["T (C)", FontSize -> 14]},
  GridLines -> Automatic];
```



```

Show[plot5, plot6]

(***** Table Outputs *****)

(* Minimum payback time case *)

Print["Minimum Payback Time Case: "];

Print["Power Output      ", discretpowerpoints[discretexstarpay], " (W)"];
Print["Total Devices     ",  $\frac{\text{discretexvalues[discretexstarpay] thezstar}}{\text{ther}}$ ];
Print[" Total Cost       ",
      CL + CD  $\left( \frac{\text{discretexvalues[discretexstarpay] thezstar}}{\text{ther}} \right) (2 \chi\text{HSstar ther} + \chi\text{insstar (ther - 1) + 1),$ 
      " ($)"];
Print[" Payback Time     ", Paybacktime[ $\frac{\text{discretexvalues[discretexstarpay]}}{\text{dx}}$ ], " (yrs)"];
Print["          X*      ", discretexvalues[discretexstarpay]];

Print[" "];

(* Maximum power output case *)

Print["Maximum Power Output Case: "];

Print["Power Output      ", discretpowerpoints[discretexstarpower], " (W)"];
Print["Total Devices     ",  $\frac{\text{discretexvalues[discretexstarpower] thezstar}}{\text{ther}}$ ];
Print[" Total Cost       ",
      CL + CD  $\left( \frac{\text{discretexvalues[discretexstarpower] thezstar}}{\text{ther}} \right)$ 
       $(2 \chi\text{HSstar ther} + \chi\text{insstar (ther - 1) + 1),$  " ($)"];
Print[" Payback Time     ", Paybacktime[ $\frac{\text{discretexvalues[discretexstarpower]}}{\text{dx}}$ ], " (yrs)"];
Print["          X*      ", discretexvalues[discretexstarpower]];

Print[" "];

Print["System Parameters"];

Print["          Z*      ", thezstar];
Print["          r        ", ther];

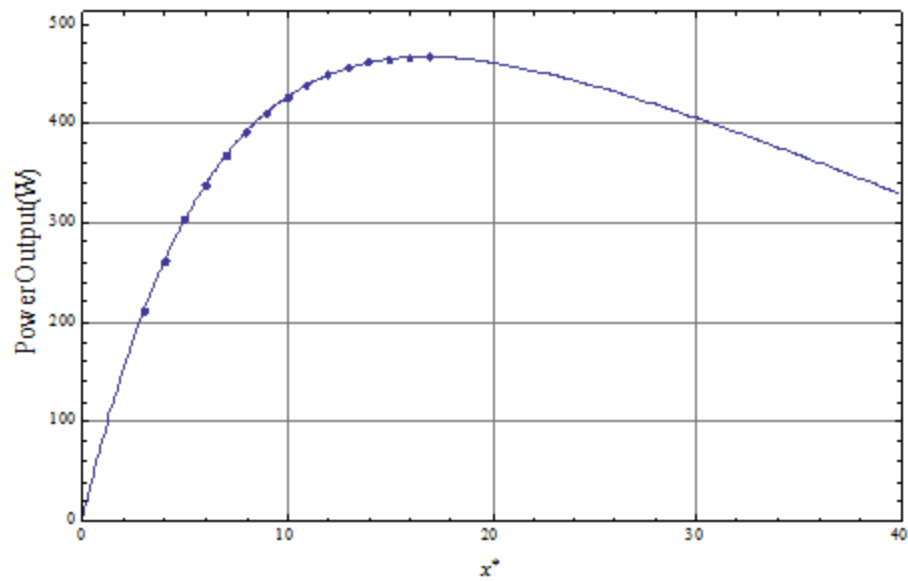
```

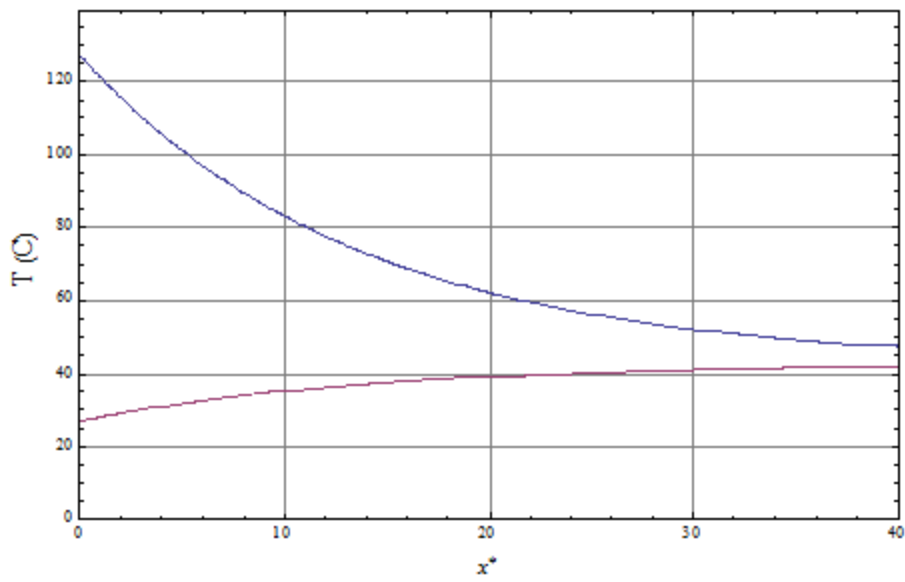
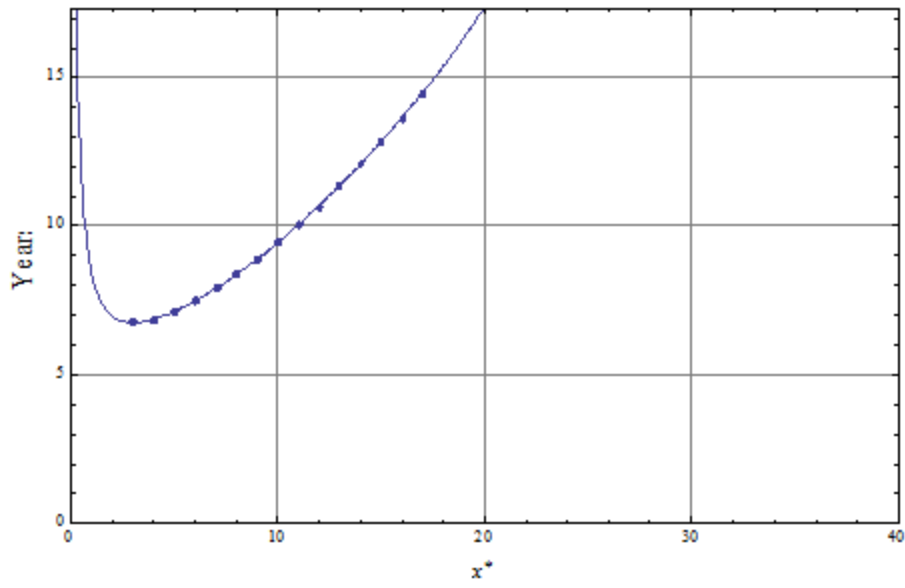
```

Print[" Hot Side"];
Print[" Reds ", RedSfixed];
Print[" dps* ", x3[i - 1]];
Print[" λs ", x5[i - 1]];
Print[" εxS ", x9[i - 1]];
Print[" εzS ", x7[i - 1]];

Print[" Ambient Side"];
Print[" Reda ", x1[i - 1]];
Print[" dpa* ", x2[i - 1]];
Print[" λA ", x4[i - 1]];
Print[" εxA ", x8[i - 1]];
Print[" εzA ", x6[i - 1]];

```





Minimum Payback Time Case:
 Power Output 210.821 (W)
 Total Devices 111.
 Total Cost 8595.7 (\$)
 Payback Time 6.753 (yrs)
 x^* 3

Maximum Power Output Case:

Power Output	465.821 (W)
Total Devices	629.
Total Cost	39375.6 (\$)
Payback Time	14.4786 (yrs)
X*	17

System Parameters

Z*	69.5504
r	1.87974
Hot Side	
Re _{ds}	290.214
d _{ps} *	0.00236029
λ _s	6.35531
ε _{xs}	0.214216
ε _{zs}	0.396287
Ambient Side	
Re _{da}	948.429
d _{pa} *	0.0118636
λ _a	93.9463
ε _{xa}	0.384795
ε _{za}	0.218681

APPENDIX B. FRICTION FACTOR TABLES

Friction factor tables for $f = \frac{\left(\frac{\rho u_m^2}{2 d_p \epsilon_x^2}\right)}{\frac{dP}{dx}}$

u_m : volume averaged velocity through channel.

dP/dx : pressure drop along flow direction.

ρ : fluid density.

d_p : hydraulic diameter of fins: $d_p = \frac{2w_x w_z}{w_x + w_z}$

ϵ_x : heat sink porosity normal to the flow direction: $\epsilon_x = 1 - \frac{w_z}{t_z}$

ϵ_z : heat sink porosity parallel to the flow direction: $\epsilon_z = 1 - \frac{w_x}{t_x}$

λ : dimensionless fin length: $\lambda = \frac{L}{d_p}$

Friction factor, f , cont.

$\epsilon_x = 0.2$

$\epsilon_z = 0.2$

Re_d	λ														
	.5	.75	1	1.5	2	2.5	3	4	5	6	8	10	15	20	100
10	14.6	12.5	11.6	10.7	10.3	10.	9.87	9.69	9.58	9.52	9.43	9.39	9.33	9.3	9.25
15	9.73	8.36	7.72	7.13	6.85	6.69	6.59	6.46	6.39	6.35	6.29	6.26	6.23	6.21	6.17
20	7.3	6.28	5.8	5.35	5.14	5.02	4.94	4.85	4.8	4.76	4.72	4.7	4.67	4.66	4.63
25	5.84	5.02	4.64	4.28	4.11	4.02	3.96	3.88	3.84	3.81	3.78	3.76	3.74	3.73	3.71
30	4.87	4.19	3.87	3.57	3.43	3.35	3.3	3.24	3.2	3.18	3.15	3.14	3.12	3.11	3.09
40	3.66	3.15	2.91	2.68	2.58	2.52	2.48	2.43	2.41	2.39	2.37	2.36	2.34	2.34	2.32
50	2.93	2.52	2.33	2.15	2.06	2.02	1.99	1.95	1.93	1.91	1.9	1.89	1.88	1.87	1.86
75	1.96	1.69	1.56	1.44	1.38	1.35	1.33	1.3	1.29	1.28	1.27	1.26	1.26	1.25	1.24
100	1.48	1.27	1.17	1.08	1.04	1.02	1.	0.982	0.971	0.964	0.956	0.951	0.946	0.943	0.937
150	0.99	0.852	0.787	0.727	0.698	0.682	0.672	0.659	0.652	0.648	0.642	0.639	0.635	0.633	0.629
200	0.747	0.643	0.595	0.549	0.528	0.515	0.507	0.498	0.493	0.489	0.485	0.483	0.48	0.478	0.475
250	0.602	0.518	0.479	0.442	0.425	0.415	0.409	0.401	0.397	0.394	0.391	0.389	0.387	0.385	0.383
300	0.505	0.435	0.402	0.371	0.357	0.348	0.343	0.337	0.333	0.331	0.328	0.326	0.324	0.323	0.321
400	0.383	0.33	0.306	0.282	0.271	0.265	0.261	0.256	0.253	0.252	0.25	0.248	0.247	0.246	0.245
500	0.311	0.268	0.248	0.229	0.22	0.215	0.212	0.208	0.206	0.204	0.202	0.201	0.2	0.2	0.198
750	0.213	0.184	0.171	0.158	0.152	0.148	0.146	0.143	0.142	0.141	0.14	0.139	0.138	0.138	0.137
1000	0.165	0.143	0.132	0.122	0.118	0.115	0.113	0.111	0.11	0.109	0.108	0.108	0.107	0.107	0.106
1500	0.116	0.101	0.0935	0.0866	0.0833	0.0815	0.0803	0.0788	0.078	0.0774	0.0768	0.0764	0.0759	0.0757	0.0752
2000	0.0917	0.0798	0.0741	0.0688	0.0662	0.0648	0.0638	0.0627	0.062	0.0616	0.0611	0.0608	0.0604	0.0602	0.0598
2500	0.0771	0.0672	0.0625	0.0581	0.0559	0.0547	0.0539	0.053	0.0524	0.0521	0.0516	0.0514	0.0511	0.0509	0.0506
3000	0.0672	0.0588	0.0547	0.0509	0.0491	0.048	0.0473	0.0465	0.046	0.0457	0.0453	0.0451	0.0448	0.0447	0.0444
4000	0.0549	0.0482	0.045	0.0419	0.0405	0.0396	0.0391	0.0384	0.038	0.0378	0.0375	0.0373	0.0371	0.037	0.0367
5000	0.0474	0.0418	0.0391	0.0365	0.0353	0.0346	0.0341	0.0336	0.0332	0.033	0.0328	0.0326	0.0324	0.0323	0.0321

Friction factor, f , cont.

$\epsilon_x = 0.4$

$\epsilon_z = 0.2$

Re_d	λ														
	.5	.75	1	1.5	2	2.5	3	4	5	6	8	10	15	20	100
10	11.7	8.13	6.59	5.27	4.7	4.4	4.22	4.01	3.9	3.84	3.76	3.72	3.67	3.65	3.62
15	7.84	5.42	4.4	3.51	3.14	2.94	2.82	2.68	2.61	2.56	2.51	2.48	2.45	2.44	2.42
20	5.88	4.07	3.3	2.64	2.36	2.21	2.12	2.01	1.96	1.92	1.89	1.87	1.84	1.83	1.82
25	4.71	3.26	2.64	2.11	1.89	1.77	1.69	1.61	1.57	1.54	1.51	1.5	1.48	1.47	1.45
30	3.93	2.72	2.21	1.76	1.58	1.48	1.41	1.35	1.31	1.29	1.26	1.25	1.23	1.23	1.21
40	2.95	2.04	1.66	1.33	1.19	1.11	1.06	1.01	0.984	0.968	0.949	0.939	0.927	0.922	0.913
50	2.36	1.64	1.33	1.06	0.951	0.89	0.854	0.812	0.79	0.776	0.761	0.753	0.744	0.739	0.732
75	1.58	1.1	0.891	0.714	0.638	0.598	0.573	0.545	0.53	0.521	0.511	0.506	0.499	0.497	0.492
100	1.19	0.827	0.672	0.539	0.482	0.452	0.433	0.412	0.401	0.394	0.386	0.382	0.377	0.375	0.371
150	0.797	0.556	0.453	0.364	0.326	0.305	0.293	0.279	0.271	0.266	0.261	0.258	0.255	0.254	0.251
200	0.601	0.421	0.343	0.276	0.248	0.232	0.223	0.212	0.206	0.203	0.199	0.196	0.194	0.193	0.191
250	0.484	0.34	0.278	0.224	0.201	0.188	0.18	0.172	0.167	0.164	0.161	0.159	0.157	0.156	0.155
300	0.406	0.286	0.234	0.189	0.169	0.159	0.152	0.145	0.141	0.139	0.136	0.135	0.133	0.132	0.131
400	0.308	0.218	0.179	0.145	0.13	0.122	0.117	0.112	0.109	0.107	0.105	0.104	0.102	0.102	0.101
500	0.249	0.177	0.146	0.119	0.107	0.1	0.0963	0.0918	0.0893	0.0878	0.0861	0.0851	0.084	0.0835	0.0827
750	0.171	0.123	0.102	0.0836	0.0754	0.071	0.0682	0.0651	0.0633	0.0623	0.061	0.0604	0.0596	0.0592	0.0586
1000	0.132	0.0962	0.0802	0.066	0.0597	0.0563	0.0541	0.0517	0.0503	0.0495	0.0485	0.048	0.0474	0.0471	0.0466
1500	0.0934	0.069	0.0581	0.0483	0.0439	0.0415	0.04	0.0383	0.0373	0.0367	0.036	0.0356	0.0351	0.0349	0.0345
2000	0.0739	0.0554	0.047	0.0394	0.036	0.0341	0.0329	0.0316	0.0308	0.0303	0.0297	0.0294	0.029	0.0289	0.0285
2500	0.0622	0.0472	0.0403	0.0341	0.0313	0.0297	0.0287	0.0275	0.0269	0.0264	0.026	0.0257	0.0254	0.0252	0.0249
3000	0.0544	0.0417	0.0358	0.0305	0.0281	0.0267	0.0258	0.0248	0.0242	0.0239	0.0234	0.0232	0.0229	0.0228	0.0225
4000	0.0446	0.0347	0.0302	0.026	0.024	0.0229	0.0222	0.0214	0.0209	0.0206	0.0203	0.0201	0.0198	0.0197	0.0195
5000	0.0387	0.0305	0.0268	0.0232	0.0216	0.0206	0.0201	0.0193	0.0189	0.0187	0.0184	0.0182	0.018	0.0179	0.0177

Friction factor, f , cont.

$\epsilon_x = 0.6$

$\epsilon_z = 0.2$

Re_d	λ														
	.5	.75	1	1.5	2	2.5	3	4	5	6	8	10	15	20	100
10	13.7	7.7	5.34	3.49	2.76	2.4	2.19	1.97	1.86	1.8	1.73	1.69	1.66	1.64	1.62
15	9.17	5.14	3.57	2.33	1.85	1.61	1.47	1.32	1.24	1.2	1.16	1.13	1.11	1.1	1.08
20	6.88	3.86	2.68	1.75	1.39	1.21	1.1	0.991	0.935	0.903	0.869	0.852	0.833	0.826	0.815
25	5.5	3.09	2.15	1.4	1.11	0.968	0.884	0.795	0.75	0.724	0.697	0.683	0.668	0.663	0.654
30	4.59	2.58	1.79	1.17	0.93	0.809	0.739	0.664	0.627	0.605	0.582	0.571	0.558	0.554	0.546
40	3.44	1.93	1.35	0.882	0.7	0.609	0.557	0.501	0.473	0.456	0.439	0.43	0.421	0.417	0.412
50	2.75	1.55	1.08	0.708	0.563	0.49	0.448	0.403	0.38	0.367	0.353	0.346	0.339	0.336	0.331
75	1.84	1.04	0.725	0.476	0.379	0.33	0.302	0.272	0.257	0.248	0.238	0.234	0.229	0.227	0.224
100	1.38	0.782	0.547	0.36	0.287	0.251	0.229	0.206	0.195	0.188	0.181	0.178	0.174	0.172	0.17
150	0.922	0.525	0.369	0.245	0.196	0.171	0.156	0.141	0.133	0.129	0.124	0.121	0.119	0.118	0.116
200	0.693	0.397	0.28	0.187	0.15	0.131	0.12	0.108	0.102	0.0989	0.0952	0.0933	0.0913	0.0904	0.0892
250	0.556	0.32	0.227	0.152	0.122	0.107	0.0982	0.0887	0.0838	0.081	0.078	0.0764	0.0748	0.0741	0.0731
300	0.464	0.269	0.191	0.129	0.104	0.091	0.0836	0.0756	0.0715	0.0691	0.0665	0.0652	0.0638	0.0632	0.0623
400	0.35	0.205	0.147	0.0996	0.0807	0.071	0.0653	0.0592	0.056	0.0542	0.0522	0.0512	0.05	0.0496	0.0489
500	0.282	0.167	0.12	0.0822	0.0669	0.059	0.0544	0.0494	0.0468	0.0452	0.0436	0.0427	0.0418	0.0414	0.0408
750	0.191	0.115	0.0844	0.0588	0.0484	0.043	0.0398	0.0362	0.0344	0.0333	0.0321	0.0315	0.0308	0.0305	0.03
1000	0.145	0.0896	0.0664	0.0471	0.0391	0.0349	0.0324	0.0296	0.0282	0.0273	0.0264	0.0259	0.0253	0.025	0.0247
1500	0.101	0.0639	0.0484	0.0353	0.0297	0.0268	0.025	0.023	0.0219	0.0213	0.0206	0.0202	0.0198	0.0196	0.0193
2000	0.0783	0.051	0.0393	0.0293	0.025	0.0227	0.0213	0.0197	0.0188	0.0183	0.0177	0.0174	0.017	0.0169	0.0166
2500	0.065	0.0433	0.0339	0.0256	0.0221	0.0202	0.019	0.0176	0.0169	0.0165	0.016	0.0157	0.0154	0.0152	0.015
3000	0.0562	0.0381	0.0302	0.0232	0.0201	0.0185	0.0175	0.0163	0.0156	0.0152	0.0148	0.0146	0.0143	0.0141	0.0139
4000	0.0453	0.0316	0.0255	0.0201	0.0177	0.0163	0.0155	0.0146	0.014	0.0137	0.0133	0.0131	0.0129	0.0128	0.0126
5000	0.0387	0.0276	0.0226	0.0182	0.0161	0.015	0.0143	0.0135	0.0131	0.0128	0.0124	0.0123	0.012	0.0119	0.0117

Friction factor, f_s cont.

$\epsilon_x = 0.8$

$\epsilon_z = 0.2$

Re_d	λ														
	.5	.75	1	1.5	2	2.5	3	4	5	6	8	10	15	20	100
10	17.3	8.31	5.04	2.62	1.74	1.32	1.09	0.853	0.741	0.679	0.616	0.585	0.555	0.544	0.529
15	11.6	5.55	3.36	1.75	1.16	0.883	0.728	0.571	0.496	0.454	0.412	0.392	0.372	0.364	0.354
20	8.67	4.16	2.52	1.31	0.873	0.664	0.548	0.43	0.373	0.342	0.311	0.295	0.28	0.274	0.267
25	6.93	3.33	2.02	1.05	0.7	0.533	0.44	0.345	0.3	0.275	0.25	0.237	0.225	0.221	0.215
30	5.78	2.78	1.69	0.878	0.585	0.445	0.367	0.289	0.251	0.23	0.209	0.199	0.188	0.185	0.18
40	4.33	2.08	1.27	0.661	0.441	0.336	0.277	0.218	0.19	0.174	0.158	0.15	0.143	0.14	0.136
50	3.47	1.67	1.02	0.53	0.354	0.27	0.223	0.176	0.153	0.14	0.127	0.121	0.115	0.113	0.11
75	2.31	1.12	0.68	0.357	0.239	0.182	0.151	0.119	0.104	0.0955	0.0868	0.0827	0.0785	0.0769	0.0749
100	1.73	0.838	0.512	0.27	0.181	0.139	0.115	0.0909	0.0794	0.073	0.0665	0.0633	0.0601	0.059	0.0574
150	1.15	0.561	0.345	0.183	0.123	0.0948	0.079	0.0627	0.0549	0.0506	0.0461	0.044	0.0418	0.041	0.0399
200	0.864	0.423	0.261	0.139	0.0944	0.0729	0.0609	0.0486	0.0427	0.0394	0.036	0.0343	0.0327	0.032	0.0312
250	0.691	0.34	0.21	0.113	0.0771	0.0598	0.0501	0.0401	0.0353	0.0326	0.0299	0.0285	0.0272	0.0267	0.026
300	0.575	0.285	0.177	0.0956	0.0655	0.051	0.0429	0.0345	0.0304	0.0281	0.0258	0.0247	0.0235	0.0231	0.0225
400	0.431	0.215	0.135	0.0738	0.0511	0.0401	0.0338	0.0274	0.0243	0.0225	0.0207	0.0198	0.0189	0.0186	0.0181
500	0.345	0.174	0.11	0.0607	0.0424	0.0335	0.0284	0.0232	0.0206	0.0192	0.0177	0.0169	0.0162	0.0159	0.0155
750	0.23	0.118	0.076	0.0432	0.0308	0.0246	0.0211	0.0175	0.0157	0.0147	0.0136	0.0131	0.0125	0.0123	0.012
1000	0.173	0.0907	0.0591	0.0344	0.0249	0.0202	0.0175	0.0146	0.0132	0.0124	0.0116	0.0111	0.0107	0.0105	0.0102
1500	0.116	0.063	0.0421	0.0255	0.019	0.0157	0.0138	0.0118	0.0107	0.0101	0.00951	0.00919	0.00884	0.0087	0.0085
2000	0.088	0.0491	0.0336	0.021	0.016	0.0134	0.0119	0.0103	0.00949	0.009	0.00848	0.00822	0.00792	0.0078	0.00762
2500	0.0714	0.0408	0.0284	0.0183	0.0142	0.012	0.0108	0.00943	0.00873	0.00831	0.00786	0.00763	0.00737	0.00727	0.0071
3000	0.0604	0.0352	0.0249	0.0164	0.0129	0.0111	0.01	0.00883	0.00821	0.00785	0.00745	0.00724	0.007	0.00691	0.00675
4000	0.0468	0.0283	0.0205	0.014	0.0113	0.00988	0.00902	0.00806	0.00756	0.00726	0.00692	0.00674	0.00654	0.00646	0.00631
5000	0.0387	0.0241	0.0179	0.0126	0.0103	0.00913	0.00841	0.00759	0.00716	0.0069	0.0066	0.00644	0.00626	0.00619	0.00605

Friction factor, f , cont.

$\epsilon_x = 0.2$

$\epsilon_z = 0.4$

Re_d	λ														
	.5	.75	1	1.5	2	2.5	3	4	5	6	8	10	15	20	100
10	4.58	2.59	1.81	1.19	0.943	0.82	0.748	0.672	0.633	0.611	0.587	0.575	0.562	0.556	0.549
15	3.06	1.75	1.23	0.816	0.652	0.568	0.52	0.467	0.441	0.426	0.409	0.401	0.391	0.388	0.382
20	2.31	1.33	0.944	0.631	0.506	0.442	0.405	0.365	0.345	0.333	0.32	0.314	0.306	0.303	0.299
25	1.86	1.08	0.77	0.519	0.418	0.367	0.337	0.304	0.287	0.277	0.267	0.261	0.255	0.253	0.249
30	1.55	0.913	0.655	0.444	0.36	0.316	0.291	0.263	0.249	0.24	0.231	0.226	0.221	0.219	0.216
40	1.18	0.703	0.51	0.351	0.286	0.253	0.233	0.212	0.2	0.194	0.187	0.183	0.179	0.177	0.174
50	0.953	0.577	0.423	0.295	0.242	0.215	0.199	0.181	0.171	0.166	0.16	0.157	0.153	0.152	0.149
75	0.655	0.409	0.306	0.219	0.183	0.164	0.152	0.139	0.133	0.129	0.124	0.122	0.119	0.118	0.116
100	0.508	0.325	0.247	0.181	0.153	0.138	0.129	0.119	0.113	0.11	0.106	0.104	0.102	0.101	0.0993
150	0.361	0.24	0.188	0.142	0.122	0.112	0.105	0.0976	0.0936	0.0911	0.0882	0.0867	0.0849	0.0841	0.0827
200	0.289	0.198	0.158	0.122	0.107	0.0983	0.093	0.0869	0.0836	0.0815	0.0792	0.0779	0.0763	0.0756	0.0744
250	0.246	0.172	0.14	0.11	0.0972	0.0901	0.0856	0.0804	0.0775	0.0757	0.0737	0.0725	0.0712	0.0705	0.0694
300	0.217	0.155	0.127	0.102	0.0907	0.0845	0.0805	0.076	0.0734	0.0718	0.07	0.069	0.0677	0.0671	0.0661
400	0.181	0.133	0.111	0.0914	0.0824	0.0773	0.0741	0.0703	0.0682	0.0669	0.0653	0.0644	0.0634	0.0629	0.0619
500	0.159	0.12	0.102	0.0849	0.0772	0.0729	0.0701	0.0669	0.065	0.0639	0.0625	0.0617	0.0607	0.0603	0.0594
750	0.13	0.101	0.0881	0.0757	0.0699	0.0667	0.0646	0.062	0.0606	0.0597	0.0586	0.058	0.0572	0.0568	0.0561
1000	0.114	0.0916	0.0809	0.0708	0.0661	0.0634	0.0616	0.0595	0.0583	0.0575	0.0566	0.0561	0.0554	0.0551	0.0544
1500	0.0984	0.0814	0.0733	0.0656	0.062	0.0599	0.0585	0.0568	0.0559	0.0553	0.0545	0.0541	0.0535	0.0533	0.0527
2000	0.0898	0.0758	0.0692	0.0628	0.0597	0.058	0.0568	0.0554	0.0546	0.0541	0.0534	0.0531	0.0526	0.0524	0.0519
2500	0.0844	0.0723	0.0665	0.061	0.0583	0.0567	0.0557	0.0545	0.0538	0.0533	0.0528	0.0524	0.052	0.0518	0.0514
3000	0.0806	0.0698	0.0646	0.0597	0.0573	0.0559	0.055	0.0539	0.0532	0.0528	0.0523	0.052	0.0516	0.0514	0.051
4000	0.0755	0.0665	0.0621	0.0579	0.0559	0.0547	0.054	0.053	0.0525	0.0521	0.0517	0.0514	0.0511	0.0509	0.0506
5000	0.0722	0.0643	0.0605	0.0568	0.055	0.054	0.0533	0.0525	0.052	0.0517	0.0513	0.0511	0.0508	0.0506	0.0503

Friction factor, f , cont.

$$\epsilon_x = 0.4$$

$$\epsilon_z = 0.4$$

Re_d	λ														
	.5	.75	1	1.5	2	2.5	3	4	5	6	8	10	15	20	100
10	9.09	5.03	3.45	2.22	1.74	1.5	1.36	1.22	1.14	1.1	1.06	1.04	1.01	1.	0.988
15	6.06	3.36	2.32	1.49	1.17	1.01	0.919	0.821	0.772	0.744	0.714	0.699	0.683	0.676	0.667
20	4.55	2.53	1.75	1.13	0.887	0.767	0.697	0.623	0.586	0.565	0.542	0.531	0.518	0.514	0.507
25	3.64	2.03	1.41	0.91	0.717	0.62	0.564	0.504	0.475	0.457	0.439	0.43	0.42	0.416	0.41
30	3.04	1.7	1.18	0.765	0.603	0.522	0.475	0.425	0.4	0.386	0.37	0.362	0.354	0.351	0.346
40	2.28	1.29	0.894	0.583	0.461	0.4	0.364	0.326	0.307	0.296	0.284	0.278	0.272	0.269	0.266
50	1.83	1.04	0.723	0.474	0.376	0.327	0.298	0.267	0.252	0.242	0.233	0.228	0.223	0.221	0.217
75	1.23	0.703	0.495	0.328	0.262	0.229	0.209	0.188	0.177	0.171	0.164	0.161	0.157	0.155	0.153
100	0.924	0.536	0.381	0.255	0.205	0.179	0.164	0.148	0.14	0.135	0.13	0.127	0.124	0.123	0.121
150	0.624	0.37	0.267	0.182	0.148	0.13	0.12	0.108	0.103	0.0991	0.0953	0.0934	0.0912	0.0903	0.0889
200	0.475	0.287	0.209	0.145	0.119	0.106	0.0974	0.0885	0.0839	0.0811	0.0781	0.0765	0.0748	0.0741	0.0729
250	0.386	0.237	0.175	0.123	0.102	0.0906	0.0839	0.0765	0.0727	0.0703	0.0678	0.0664	0.0649	0.0643	0.0632
300	0.326	0.203	0.152	0.108	0.0902	0.0806	0.0749	0.0685	0.0651	0.0631	0.0609	0.0597	0.0583	0.0578	0.0568
400	0.253	0.161	0.123	0.0895	0.0755	0.068	0.0635	0.0584	0.0557	0.0541	0.0522	0.0512	0.0501	0.0496	0.0488
500	0.209	0.136	0.105	0.0782	0.0666	0.0604	0.0566	0.0523	0.05	0.0486	0.047	0.0462	0.0452	0.0447	0.044
750	0.151	0.103	0.0814	0.0627	0.0545	0.05	0.0472	0.044	0.0423	0.0412	0.04	0.0393	0.0385	0.0382	0.0375
1000	0.123	0.0859	0.0695	0.0548	0.0482	0.0446	0.0424	0.0398	0.0384	0.0375	0.0365	0.0359	0.0352	0.0349	0.0343
1500	0.0937	0.0685	0.057	0.0465	0.0418	0.0391	0.0374	0.0355	0.0344	0.0337	0.0329	0.0324	0.0319	0.0316	0.0311
2000	0.0793	0.0596	0.0506	0.0422	0.0384	0.0362	0.0349	0.0332	0.0323	0.0317	0.031	0.0307	0.0302	0.03	0.0295
2500	0.0706	0.0542	0.0466	0.0396	0.0363	0.0344	0.0333	0.0318	0.031	0.0305	0.0299	0.0296	0.0292	0.029	0.0285
3000	0.0647	0.0505	0.0439	0.0377	0.0348	0.0332	0.0321	0.0309	0.0302	0.0297	0.0292	0.0289	0.0285	0.0283	0.0279
4000	0.0571	0.0457	0.0404	0.0353	0.0329	0.0316	0.0307	0.0297	0.0291	0.0287	0.0282	0.0279	0.0276	0.0274	0.0271
5000	0.0524	0.0427	0.0381	0.0338	0.0317	0.0306	0.0298	0.0289	0.0284	0.028	0.0276	0.0274	0.0271	0.0269	0.0266

Friction factor, f , cont.

$\epsilon_x = 0.6$

$\epsilon_z = 0.4$

Re_d	λ														
	.5	.75	1	1.5	2	2.5	3	4	5	6	8	10	15	20	100
10	13.2	6.75	4.34	2.51	1.82	1.49	1.3	1.11	1.01	0.957	0.902	0.875	0.847	0.836	0.822
15	8.79	4.51	2.9	1.68	1.22	1.	0.875	0.744	0.68	0.645	0.607	0.589	0.57	0.563	0.553
20	6.59	3.39	2.18	1.27	0.924	0.756	0.661	0.563	0.515	0.488	0.46	0.446	0.432	0.427	0.419
25	5.27	2.71	1.75	1.02	0.744	0.61	0.534	0.455	0.416	0.394	0.372	0.361	0.349	0.345	0.339
30	4.39	2.27	1.47	0.854	0.624	0.512	0.448	0.382	0.35	0.332	0.313	0.303	0.294	0.29	0.285
40	3.3	1.71	1.11	0.647	0.474	0.39	0.342	0.292	0.267	0.253	0.239	0.232	0.225	0.222	0.218
50	2.64	1.37	0.891	0.523	0.384	0.316	0.278	0.238	0.218	0.207	0.195	0.189	0.183	0.181	0.178
75	1.76	0.922	0.603	0.358	0.265	0.219	0.193	0.165	0.152	0.144	0.136	0.132	0.128	0.126	0.124
100	1.32	0.698	0.46	0.275	0.205	0.17	0.15	0.129	0.119	0.113	0.106	0.103	0.1	0.0989	0.0971
150	0.882	0.473	0.316	0.192	0.144	0.121	0.107	0.0927	0.0855	0.0814	0.077	0.0748	0.0725	0.0716	0.0703
200	0.663	0.361	0.244	0.151	0.114	0.0962	0.0857	0.0745	0.0689	0.0657	0.0623	0.0605	0.0587	0.058	0.0569
250	0.533	0.294	0.2	0.126	0.0962	0.0814	0.0728	0.0636	0.059	0.0563	0.0534	0.052	0.0504	0.0498	0.0488
300	0.446	0.249	0.171	0.109	0.084	0.0715	0.0642	0.0563	0.0523	0.05	0.0475	0.0462	0.0449	0.0443	0.0435
400	0.338	0.193	0.135	0.0877	0.0688	0.0591	0.0533	0.0472	0.044	0.0421	0.0401	0.0391	0.0379	0.0375	0.0368
500	0.274	0.16	0.113	0.075	0.0595	0.0515	0.0468	0.0416	0.039	0.0374	0.0357	0.0348	0.0338	0.0334	0.0327
750	0.189	0.115	0.0837	0.0578	0.047	0.0413	0.0379	0.0342	0.0322	0.031	0.0297	0.029	0.0282	0.0279	0.0274
1000	0.147	0.092	0.0688	0.049	0.0406	0.0361	0.0334	0.0304	0.0288	0.0278	0.0267	0.0261	0.0255	0.0252	0.0247
1500	0.106	0.0694	0.0536	0.0399	0.0339	0.0307	0.0287	0.0265	0.0253	0.0245	0.0237	0.0232	0.0227	0.0224	0.022
2000	0.0853	0.0579	0.0459	0.0352	0.0305	0.0279	0.0263	0.0245	0.0235	0.0228	0.0221	0.0217	0.0213	0.0211	0.0207
2500	0.0731	0.051	0.0412	0.0323	0.0284	0.0262	0.0248	0.0232	0.0224	0.0218	0.0212	0.0208	0.0204	0.0202	0.0199
3000	0.065	0.0464	0.0379	0.0303	0.0269	0.025	0.0238	0.0224	0.0216	0.0211	0.0205	0.0202	0.0198	0.0197	0.0193
4000	0.0549	0.0404	0.0338	0.0277	0.025	0.0234	0.0224	0.0213	0.0206	0.0202	0.0197	0.0195	0.0191	0.019	0.0187
5000	0.0488	0.0368	0.0312	0.0261	0.0238	0.0224	0.0216	0.0206	0.02	0.0196	0.0192	0.019	0.0187	0.0185	0.0183

Friction factor, f , cont.

$\epsilon_x = 0.8$

$\epsilon_z = 0.4$

Re_d	λ																
	.5	.75	1	1.5	2	2.5	3	4	5	6	8	10	15	20	100		
10	17.3	7.98	4.67	2.26	1.39	0.991	0.769	0.546	0.441	0.384	0.326	0.299	0.271	0.262	0.249		
15	11.5	5.33	3.12	1.51	0.935	0.666	0.517	0.368	0.298	0.26	0.221	0.203	0.184	0.178	0.169		
20	8.63	4.	2.34	1.14	0.706	0.503	0.392	0.279	0.227	0.198	0.168	0.155	0.141	0.136	0.129		
25	6.9	3.2	1.88	0.913	0.568	0.405	0.316	0.226	0.184	0.16	0.137	0.126	0.115	0.111	0.106		
30	5.75	2.67	1.57	0.764	0.476	0.34	0.266	0.19	0.155	0.135	0.116	0.107	0.0972	0.0939	0.0896		
40	4.31	2.01	1.18	0.577	0.361	0.259	0.203	0.146	0.119	0.104	0.0895	0.0825	0.0754	0.0729	0.0696		
50	3.44	1.61	0.948	0.465	0.292	0.21	0.165	0.119	0.0976	0.0858	0.0738	0.0681	0.0624	0.0603	0.0577		
75	2.29	1.08	0.638	0.316	0.2	0.145	0.114	0.0836	0.069	0.0609	0.0528	0.0489	0.045	0.0436	0.0417		
100	1.72	0.812	0.484	0.242	0.154	0.112	0.0892	0.0658	0.0547	0.0485	0.0422	0.0393	0.0363	0.0352	0.0337		
150	1.14	0.546	0.328	0.167	0.108	0.0796	0.064	0.048	0.0403	0.0361	0.0317	0.0297	0.0276	0.0268	0.0258		
200	0.855	0.413	0.251	0.129	0.0847	0.0633	0.0513	0.039	0.0331	0.0299	0.0265	0.0249	0.0232	0.0226	0.0218		
250	0.683	0.334	0.204	0.107	0.0708	0.0535	0.0437	0.0337	0.0288	0.0261	0.0233	0.022	0.0206	0.0201	0.0194		
300	0.569	0.281	0.173	0.0918	0.0615	0.0469	0.0386	0.0301	0.026	0.0236	0.0212	0.0201	0.0189	0.0184	0.0178		
400	0.426	0.214	0.134	0.0729	0.0499	0.0386	0.0322	0.0256	0.0223	0.0205	0.0186	0.0177	0.0167	0.0163	0.0158		
500	0.341	0.174	0.111	0.0615	0.0428	0.0336	0.0284	0.0229	0.0202	0.0186	0.017	0.0162	0.0154	0.015	0.0146		
750	0.229	0.121	0.0792	0.0462	0.0333	0.0269	0.0232	0.0192	0.0172	0.0161	0.0149	0.0143	0.0136	0.0134	0.013		
1000	0.173	0.0946	0.0634	0.0384	0.0284	0.0234	0.0205	0.0173	0.0157	0.0148	0.0138	0.0133	0.0128	0.0125	0.0122		
1500	0.119	0.0679	0.0473	0.0303	0.0234	0.0198	0.0177	0.0154	0.0142	0.0135	0.0127	0.0123	0.0119	0.0117	0.0114		
2000	0.0917	0.0546	0.0391	0.0262	0.0208	0.018	0.0163	0.0144	0.0134	0.0128	0.0122	0.0118	0.0114	0.0113	0.011		
2500	0.0759	0.0465	0.0342	0.0236	0.0192	0.0168	0.0154	0.0138	0.0129	0.0124	0.0118	0.0115	0.0112	0.011	0.0108		
3000	0.0655	0.0412	0.0308	0.0218	0.018	0.016	0.0147	0.0133	0.0126	0.0121	0.0116	0.0113	0.011	0.0109	0.0106		
4000	0.0526	0.0344	0.0265	0.0196	0.0165	0.0149	0.0139	0.0127	0.0121	0.0117	0.0113	0.011	0.0108	0.0106	0.0104		
5000	0.0449	0.0303	0.0239	0.0181	0.0156	0.0142	0.0134	0.0124	0.0118	0.0115	0.0111	0.0109	0.0106	0.0105	0.0103		

Friction factor, f , cont.

$\epsilon_x = 0.2$
 $\epsilon_z = 0.6$

Re_d	λ														
	.5	.75	1	1.5	2	2.5	3	4	5	6	8	10	15	20	100
10	18.1	15.9	14.9	13.9	13.5	13.2	13.	12.8	12.7	12.6	12.5	12.5	12.4	12.4	12.3
15	12.1	10.7	9.97	9.32	9.01	8.83	8.71	8.58	8.5	8.45	8.38	8.35	8.3	8.28	8.24
20	9.13	8.02	7.5	7.01	6.78	6.64	6.56	6.45	6.39	6.36	6.31	6.28	6.25	6.23	6.2
25	7.33	6.44	6.02	5.63	5.44	5.33	5.26	5.18	5.13	5.1	5.06	5.04	5.02	5.	4.98
30	6.13	5.39	5.04	4.7	4.55	4.46	4.4	4.33	4.29	4.27	4.23	4.22	4.19	4.18	4.16
40	4.62	4.07	3.8	3.55	3.43	3.37	3.32	3.27	3.24	3.22	3.2	3.18	3.17	3.16	3.14
50	3.72	3.27	3.06	2.86	2.77	2.71	2.68	2.63	2.61	2.59	2.58	2.56	2.55	2.54	2.53
75	2.52	2.22	2.07	1.94	1.87	1.84	1.81	1.79	1.77	1.76	1.75	1.74	1.73	1.72	1.71
100	1.92	1.69	1.58	1.48	1.43	1.4	1.38	1.36	1.35	1.34	1.33	1.32	1.32	1.31	1.31
150	1.32	1.16	1.09	1.02	0.983	0.964	0.952	0.937	0.928	0.922	0.916	0.912	0.907	0.904	0.899
200	1.02	0.897	0.84	0.786	0.76	0.745	0.736	0.724	0.718	0.713	0.708	0.705	0.701	0.699	0.696
250	0.836	0.738	0.692	0.647	0.626	0.614	0.606	0.597	0.591	0.588	0.584	0.581	0.578	0.576	0.573
300	0.715	0.632	0.593	0.555	0.537	0.527	0.52	0.512	0.507	0.504	0.501	0.499	0.496	0.495	0.492
400	0.564	0.5	0.469	0.44	0.426	0.417	0.412	0.406	0.402	0.4	0.397	0.395	0.393	0.392	0.39
500	0.473	0.42	0.394	0.37	0.358	0.352	0.347	0.342	0.339	0.337	0.335	0.333	0.331	0.331	0.329
750	0.352	0.313	0.295	0.277	0.269	0.264	0.261	0.257	0.255	0.253	0.251	0.25	0.249	0.248	0.247
1000	0.29	0.26	0.245	0.231	0.224	0.22	0.217	0.214	0.213	0.211	0.21	0.209	0.208	0.207	0.206
1500	0.228	0.205	0.194	0.184	0.179	0.176	0.174	0.172	0.17	0.169	0.168	0.168	0.167	0.166	0.166
2000	0.197	0.178	0.169	0.16	0.156	0.154	0.152	0.15	0.149	0.148	0.147	0.147	0.146	0.146	0.145
2500	0.177	0.161	0.154	0.146	0.142	0.14	0.139	0.137	0.136	0.136	0.135	0.134	0.134	0.134	0.133
3000	0.164	0.15	0.143	0.136	0.133	0.131	0.13	0.129	0.128	0.127	0.127	0.126	0.126	0.125	0.125
4000	0.148	0.136	0.13	0.124	0.122	0.12	0.119	0.118	0.117	0.117	0.116	0.116	0.115	0.115	0.115
5000	0.137	0.127	0.122	0.117	0.115	0.113	0.112	0.111	0.111	0.11	0.11	0.109	0.109	0.109	0.108

Friction factor, f , cont.

$$\epsilon_x = 0.4$$

$$\epsilon_z = 0.6$$

Re_d	λ														
	.5	.75	1	1.5	2	2.5	3	4	5	6	8	10	15	20	100
10	8.57	3.91	2.26	1.05	0.621	0.419	0.309	0.197	0.145	0.117	0.0877	0.0742	0.0606	0.0558	0.0496
15	5.69	2.63	1.53	0.728	0.439	0.302	0.227	0.151	0.115	0.095	0.075	0.0655	0.056	0.0526	0.0481
20	4.26	1.99	1.17	0.566	0.347	0.243	0.186	0.127	0.0996	0.0842	0.0686	0.0612	0.0537	0.051	0.0474
25	3.4	1.61	0.954	0.469	0.292	0.208	0.161	0.113	0.0904	0.0778	0.0648	0.0586	0.0523	0.05	0.047
30	2.83	1.35	0.809	0.404	0.256	0.184	0.145	0.104	0.0843	0.0734	0.0623	0.0569	0.0514	0.0494	0.0467
40	2.12	1.03	0.627	0.322	0.209	0.155	0.124	0.092	0.0766	0.068	0.059	0.0547	0.0503	0.0486	0.0463
50	1.69	0.838	0.518	0.273	0.181	0.136	0.111	0.0848	0.0719	0.0647	0.0571	0.0534	0.0496	0.0481	0.0461
75	1.13	0.582	0.371	0.206	0.143	0.112	0.0939	0.075	0.0656	0.0602	0.0545	0.0517	0.0487	0.0475	0.0458
100	0.853	0.453	0.297	0.172	0.124	0.0992	0.085	0.0699	0.0622	0.0578	0.0531	0.0508	0.0482	0.0472	0.0457
150	0.581	0.325	0.222	0.137	0.103	0.0859	0.0756	0.0645	0.0587	0.0554	0.0517	0.0498	0.0477	0.0469	0.0455
200	0.448	0.261	0.183	0.119	0.0926	0.0788	0.0706	0.0615	0.0568	0.054	0.0509	0.0493	0.0475	0.0467	0.0455
250	0.369	0.222	0.16	0.108	0.0858	0.0743	0.0674	0.0597	0.0556	0.0531	0.0504	0.049	0.0473	0.0466	0.0454
300	0.318	0.196	0.144	0.0999	0.0811	0.0712	0.0651	0.0583	0.0547	0.0525	0.05	0.0487	0.0472	0.0465	0.0454
400	0.254	0.163	0.124	0.0898	0.0749	0.0669	0.062	0.0565	0.0534	0.0516	0.0495	0.0483	0.047	0.0464	0.0454
500	0.216	0.144	0.112	0.0834	0.071	0.0642	0.06	0.0552	0.0526	0.051	0.0491	0.0481	0.0469	0.0464	0.0454
750	0.166	0.117	0.0944	0.0743	0.0652	0.0602	0.057	0.0533	0.0513	0.05	0.0485	0.0477	0.0467	0.0462	0.0453
1000	0.141	0.103	0.0854	0.0694	0.062	0.0579	0.0553	0.0522	0.0505	0.0494	0.0481	0.0474	0.0465	0.0461	0.0453
1500	0.116	0.0886	0.0758	0.064	0.0584	0.0553	0.0533	0.0509	0.0496	0.0487	0.0477	0.0471	0.0463	0.046	0.0453
2000	0.103	0.081	0.0707	0.061	0.0564	0.0538	0.0521	0.0501	0.049	0.0482	0.0474	0.0469	0.0462	0.0459	0.0453
2500	0.0949	0.0762	0.0673	0.059	0.0551	0.0528	0.0513	0.0496	0.0486	0.0479	0.0471	0.0467	0.0461	0.0459	0.0453
3000	0.0892	0.0728	0.065	0.0576	0.0541	0.0521	0.0508	0.0492	0.0483	0.0477	0.047	0.0466	0.0461	0.0458	0.0453
4000	0.0818	0.0683	0.0618	0.0557	0.0528	0.0511	0.05	0.0486	0.0479	0.0474	0.0467	0.0464	0.0459	0.0457	0.0453
5000	0.077	0.0654	0.0598	0.0544	0.0519	0.0504	0.0494	0.0483	0.0476	0.0471	0.0466	0.0463	0.0459	0.0457	0.0453

Friction factor, f , cont.

$$\epsilon_x = 0.6$$

$$\epsilon_z = 0.6$$

Re_d	λ														
	.5	.75	1	1.5	2	2.5	3	4	5	6	8	10	15	20	100
10	12.9	5.85	3.35	1.54	0.905	0.607	0.444	0.281	0.205	0.163	0.121	0.102	0.0825	0.0756	0.067
15	8.6	3.91	2.25	1.04	0.617	0.417	0.308	0.198	0.147	0.118	0.0902	0.077	0.0638	0.0591	0.0532
20	6.44	2.94	1.7	0.795	0.474	0.323	0.24	0.157	0.118	0.0962	0.0747	0.0646	0.0545	0.0509	0.0463
25	5.14	2.36	1.37	0.646	0.387	0.266	0.199	0.132	0.1	0.0828	0.0654	0.0571	0.0489	0.0459	0.0422
30	4.28	1.98	1.15	0.546	0.33	0.228	0.172	0.115	0.0886	0.0739	0.0591	0.0522	0.0451	0.0426	0.0394
40	3.2	1.49	0.874	0.421	0.258	0.18	0.138	0.0945	0.0741	0.0628	0.0514	0.0459	0.0405	0.0385	0.0359
50	2.56	1.2	0.709	0.346	0.214	0.152	0.117	0.0821	0.0654	0.0561	0.0467	0.0422	0.0377	0.036	0.0339
75	1.7	0.814	0.489	0.246	0.157	0.114	0.0899	0.0654	0.0537	0.0472	0.0405	0.0372	0.0339	0.0327	0.0311
100	1.27	0.62	0.378	0.195	0.127	0.0945	0.0761	0.057	0.0478	0.0427	0.0373	0.0348	0.0321	0.0311	0.0297
150	0.847	0.426	0.267	0.144	0.0978	0.0751	0.0621	0.0486	0.0419	0.0381	0.0342	0.0323	0.0302	0.0294	0.0284
200	0.637	0.33	0.211	0.118	0.0828	0.0651	0.0549	0.0442	0.0389	0.0358	0.0326	0.031	0.0293	0.0286	0.0277
250	0.512	0.271	0.177	0.103	0.0736	0.059	0.0506	0.0415	0.037	0.0344	0.0316	0.0302	0.0287	0.0281	0.0273
300	0.43	0.233	0.155	0.0921	0.0673	0.0548	0.0476	0.0397	0.0358	0.0335	0.031	0.0297	0.0283	0.0278	0.027
400	0.328	0.184	0.126	0.0785	0.0593	0.0495	0.0437	0.0374	0.0341	0.0322	0.0301	0.0291	0.0279	0.0274	0.0266
500	0.268	0.155	0.108	0.0701	0.0543	0.0461	0.0412	0.0359	0.0331	0.0314	0.0296	0.0286	0.0276	0.0271	0.0264
750	0.189	0.116	0.0848	0.0584	0.0472	0.0413	0.0377	0.0337	0.0316	0.0303	0.0288	0.0281	0.0272	0.0268	0.0262
1000	0.151	0.0961	0.0726	0.0522	0.0434	0.0387	0.0358	0.0325	0.0307	0.0296	0.0284	0.0277	0.027	0.0266	0.026
1500	0.113	0.0762	0.0601	0.0457	0.0393	0.0358	0.0336	0.0311	0.0298	0.0289	0.0279	0.0274	0.0267	0.0264	0.0259
2000	0.094	0.0661	0.0535	0.0421	0.037	0.0342	0.0324	0.0303	0.0292	0.0285	0.0276	0.0271	0.0266	0.0263	0.0258
2500	0.0828	0.0599	0.0494	0.0399	0.0356	0.0331	0.0316	0.0298	0.0288	0.0282	0.0274	0.027	0.0265	0.0262	0.0258
3000	0.0752	0.0556	0.0466	0.0383	0.0345	0.0324	0.031	0.0294	0.0285	0.0279	0.0273	0.0269	0.0264	0.0262	0.0258
4000	0.0656	0.0501	0.0429	0.0362	0.0331	0.0314	0.0302	0.0289	0.0281	0.0276	0.027	0.0267	0.0263	0.0261	0.0257
5000	0.0597	0.0467	0.0406	0.0349	0.0322	0.0307	0.0297	0.0285	0.0278	0.0274	0.0269	0.0266	0.0262	0.0261	0.0257

Friction factor, f , cont.

$\epsilon_x = 0.8$

$\epsilon_z = 0.6$

Re_d	λ																
	.5	.75	1	1.5	2	2.5	3	4	5	6	8	10	15	20	100		
10	17.2	7.75	4.41	2.01	1.16	0.765	0.55	0.336	0.236	0.182	0.127	0.102	0.077	0.0681	0.0571		
15	11.5	5.18	2.95	1.35	0.783	0.52	0.376	0.232	0.165	0.128	0.0917	0.0746	0.0577	0.0517	0.0442		
20	8.61	3.89	2.22	1.02	0.595	0.397	0.288	0.18	0.129	0.101	0.0738	0.0609	0.048	0.0435	0.0378		
25	6.88	3.12	1.79	0.823	0.482	0.323	0.236	0.149	0.108	0.0855	0.0631	0.0527	0.0423	0.0386	0.0339		
30	5.73	2.6	1.49	0.692	0.407	0.274	0.201	0.128	0.0935	0.0748	0.056	0.0472	0.0384	0.0353	0.0314		
40	4.29	1.96	1.13	0.528	0.313	0.212	0.157	0.102	0.0757	0.0614	0.0471	0.0403	0.0336	0.0312	0.0281		
50	3.43	1.57	0.911	0.429	0.256	0.175	0.131	0.0861	0.065	0.0534	0.0417	0.0362	0.0307	0.0287	0.0262		
75	2.28	1.06	0.619	0.297	0.181	0.126	0.0959	0.0652	0.0507	0.0427	0.0346	0.0307	0.0269	0.0255	0.0236		
100	1.7	0.801	0.473	0.231	0.143	0.101	0.0783	0.0547	0.0435	0.0373	0.031	0.028	0.0249	0.0238	0.0224		
150	1.13	0.543	0.327	0.165	0.105	0.0766	0.0606	0.0442	0.0363	0.0319	0.0274	0.0252	0.023	0.0222	0.0211		
200	0.847	0.415	0.254	0.132	0.0861	0.0641	0.0517	0.0389	0.0327	0.0292	0.0256	0.0239	0.022	0.0214	0.0204		
250	0.677	0.337	0.209	0.111	0.0745	0.0565	0.0463	0.0357	0.0305	0.0276	0.0245	0.023	0.0215	0.0209	0.02		
300	0.565	0.286	0.18	0.0979	0.0667	0.0514	0.0427	0.0335	0.029	0.0265	0.0238	0.0225	0.0211	0.0205	0.0198		
400	0.425	0.221	0.143	0.0807	0.0568	0.0449	0.038	0.0308	0.0272	0.0251	0.0229	0.0218	0.0206	0.0201	0.0195		
500	0.342	0.183	0.12	0.0703	0.0507	0.0409	0.0352	0.0291	0.026	0.0242	0.0223	0.0214	0.0203	0.0199	0.0193		
750	0.233	0.131	0.0897	0.056	0.0423	0.0353	0.0312	0.0267	0.0244	0.023	0.0215	0.0208	0.0199	0.0196	0.019		
1000	0.18	0.105	0.0743	0.0485	0.0379	0.0324	0.0291	0.0254	0.0235	0.0224	0.0211	0.0205	0.0197	0.0194	0.0189		
1500	0.128	0.0792	0.0585	0.0407	0.0332	0.0292	0.0267	0.024	0.0225	0.0216	0.0206	0.0201	0.0195	0.0192	0.0188		
2000	0.102	0.0661	0.0503	0.0366	0.0306	0.0274	0.0255	0.0232	0.022	0.0212	0.0204	0.0199	0.0194	0.0191	0.0187		
2500	0.0873	0.0581	0.0453	0.034	0.029	0.0263	0.0246	0.0227	0.0216	0.021	0.0202	0.0198	0.0193	0.0191	0.0187		
3000	0.0772	0.0528	0.0419	0.0322	0.0279	0.0255	0.024	0.0223	0.0213	0.0207	0.0201	0.0197	0.0192	0.019	0.0187		
4000	0.0648	0.046	0.0375	0.0298	0.0263	0.0244	0.0232	0.0218	0.021	0.0205	0.0199	0.0196	0.0192	0.019	0.0186		
5000	0.0573	0.0418	0.0348	0.0283	0.0253	0.0237	0.0226	0.0214	0.0207	0.0203	0.0197	0.0195	0.0191	0.0189	0.0186		

Friction factor, f_s cont.

$\epsilon_x = 0.2$
 $\epsilon_z = 0.8$

Re_d	λ														
	.5	.75	1	1.5	2	2.5	3	4	5	6	8	10	15	20	100
10	14.4	12.4	11.4	10.5	10.1	9.87	9.72	9.54	9.43	9.37	9.29	9.24	9.18	9.16	9.1
15	9.65	8.28	7.64	7.04	6.76	6.61	6.5	6.38	6.31	6.27	6.21	6.18	6.14	6.13	6.09
20	7.26	6.23	5.75	5.3	5.09	4.97	4.9	4.8	4.75	4.72	4.68	4.65	4.62	4.61	4.58
25	5.83	5.	4.62	4.26	4.09	3.99	3.93	3.86	3.81	3.79	3.75	3.74	3.71	3.7	3.68
30	4.87	4.18	3.86	3.56	3.42	3.34	3.29	3.23	3.19	3.17	3.14	3.13	3.11	3.1	3.08
40	3.68	3.16	2.92	2.69	2.58	2.52	2.48	2.44	2.41	2.39	2.37	2.36	2.35	2.34	2.32
50	2.96	2.54	2.35	2.17	2.08	2.03	2.	1.96	1.94	1.93	1.91	1.9	1.89	1.88	1.87
75	2.	1.72	1.59	1.47	1.41	1.38	1.36	1.33	1.32	1.31	1.3	1.29	1.28	1.28	1.27
100	1.53	1.31	1.22	1.12	1.08	1.05	1.04	1.02	1.01	0.998	0.99	0.985	0.979	0.976	0.97
150	1.05	0.905	0.837	0.773	0.743	0.725	0.714	0.701	0.693	0.688	0.683	0.679	0.675	0.673	0.669
200	0.81	0.7	0.648	0.598	0.575	0.562	0.553	0.543	0.537	0.533	0.529	0.526	0.523	0.521	0.518
250	0.666	0.576	0.534	0.494	0.475	0.464	0.457	0.448	0.444	0.44	0.437	0.435	0.432	0.43	0.428
300	0.571	0.494	0.458	0.424	0.408	0.398	0.392	0.385	0.381	0.378	0.375	0.373	0.371	0.37	0.368
400	0.451	0.391	0.363	0.337	0.324	0.317	0.312	0.306	0.303	0.301	0.298	0.297	0.295	0.294	0.292
500	0.378	0.329	0.306	0.284	0.274	0.268	0.264	0.259	0.256	0.254	0.252	0.251	0.249	0.249	0.247
750	0.281	0.246	0.23	0.214	0.206	0.202	0.199	0.196	0.194	0.192	0.191	0.19	0.189	0.188	0.187
1000	0.233	0.205	0.191	0.179	0.172	0.169	0.167	0.164	0.162	0.161	0.16	0.159	0.158	0.158	0.157
1500	0.183	0.162	0.153	0.143	0.138	0.136	0.134	0.132	0.131	0.13	0.129	0.128	0.128	0.127	0.127
2000	0.158	0.141	0.133	0.125	0.121	0.119	0.118	0.116	0.115	0.114	0.114	0.113	0.112	0.112	0.112
2500	0.142	0.128	0.121	0.114	0.111	0.109	0.108	0.106	0.106	0.105	0.104	0.104	0.103	0.103	0.102
3000	0.132	0.119	0.113	0.107	0.104	0.102	0.101	0.1	0.0992	0.0987	0.098	0.0977	0.0972	0.097	0.0965
4000	0.119	0.108	0.103	0.0977	0.0953	0.0939	0.093	0.0919	0.0912	0.0908	0.0903	0.0899	0.0896	0.0894	0.0889
5000	0.11	0.101	0.0964	0.0921	0.09	0.0888	0.088	0.087	0.0864	0.086	0.0856	0.0853	0.085	0.0848	0.0844

Friction factor, f , cont.

$\epsilon_x = 0.4$

$\epsilon_z = 0.8$

Re_d	λ														
	.5	.75	1	1.5	2	2.5	3	4	5	6	8	10	15	20	100
10	8.56	4.01	2.37	1.16	0.723	0.516	0.402	0.285	0.23	0.2	0.169	0.154	0.139	0.134	0.127
15	5.69	2.71	1.62	0.811	0.516	0.375	0.297	0.217	0.179	0.157	0.136	0.125	0.115	0.111	0.106
20	4.26	2.06	1.24	0.636	0.412	0.305	0.244	0.183	0.153	0.136	0.119	0.111	0.103	0.0994	0.0952
25	3.4	1.66	1.02	0.531	0.35	0.262	0.213	0.162	0.137	0.124	0.109	0.102	0.0952	0.0926	0.0889
30	2.83	1.4	0.867	0.46	0.308	0.233	0.192	0.148	0.127	0.115	0.103	0.0966	0.0904	0.088	0.0847
40	2.12	1.08	0.678	0.371	0.255	0.197	0.165	0.131	0.114	0.104	0.0944	0.0895	0.0843	0.0823	0.0795
50	1.7	0.88	0.564	0.317	0.223	0.176	0.149	0.12	0.106	0.0979	0.0894	0.0851	0.0806	0.0789	0.0764
75	1.15	0.619	0.411	0.244	0.179	0.146	0.126	0.106	0.0952	0.0891	0.0826	0.0793	0.0757	0.0743	0.0722
100	0.874	0.488	0.333	0.207	0.156	0.13	0.115	0.0981	0.0896	0.0846	0.0792	0.0764	0.0733	0.072	0.0701
150	0.606	0.357	0.254	0.168	0.132	0.114	0.103	0.0902	0.0837	0.0798	0.0756	0.0733	0.0708	0.0697	0.0668
200	0.474	0.291	0.214	0.148	0.12	0.105	0.0959	0.0859	0.0805	0.0773	0.0737	0.0717	0.0695	0.0686	0.067
250	0.397	0.252	0.189	0.135	0.112	0.0993	0.0917	0.0831	0.0785	0.0757	0.0725	0.0707	0.0687	0.0679	0.0663
300	0.346	0.225	0.172	0.126	0.106	0.0954	0.0888	0.0812	0.077	0.0745	0.0716	0.07	0.0682	0.0674	0.0659
400	0.283	0.191	0.151	0.115	0.0989	0.0902	0.0848	0.0785	0.0751	0.0729	0.0705	0.0691	0.0675	0.0667	0.0654
500	0.244	0.171	0.137	0.108	0.0943	0.0868	0.0822	0.0768	0.0738	0.0719	0.0697	0.0685	0.067	0.0664	0.0651
750	0.195	0.143	0.119	0.0974	0.0875	0.0819	0.0783	0.0741	0.0718	0.0703	0.0685	0.0676	0.0663	0.0658	0.0647
1000	0.169	0.128	0.109	0.0918	0.0837	0.079	0.0761	0.0726	0.0706	0.0694	0.0679	0.067	0.0659	0.0655	0.0644
1500	0.143	0.113	0.0988	0.0856	0.0794	0.0759	0.0736	0.0708	0.0693	0.0683	0.0671	0.0664	0.0655	0.0651	0.0642
2000	0.129	0.104	0.093	0.0821	0.077	0.074	0.0721	0.0698	0.0685	0.0676	0.0666	0.066	0.0652	0.0649	0.0641
2500	0.12	0.0991	0.0893	0.0799	0.0754	0.0728	0.0711	0.0691	0.0679	0.0672	0.0663	0.0657	0.0651	0.0647	0.064
3000	0.114	0.0954	0.0866	0.0782	0.0742	0.0719	0.0704	0.0686	0.0675	0.0669	0.066	0.0655	0.0649	0.0646	0.064
4000	0.106	0.0903	0.083	0.076	0.0727	0.0707	0.0694	0.0679	0.067	0.0664	0.0657	0.0653	0.0647	0.0645	0.0639
5000	0.1	0.087	0.0807	0.0745	0.0716	0.0699	0.0688	0.0674	0.0666	0.0661	0.0655	0.0651	0.0646	0.0644	0.0639

Friction factor, f , cont.

$\epsilon_x = 0.6$

$\epsilon_z = 0.8$

Re_d	λ														
	.5	.75	1	1.5	2	2.5	3	4	5	6	8	10	15	20	100
10	12.9	5.91	3.42	1.61	0.966	0.662	0.495	0.327	0.248	0.205	0.161	0.141	0.12	0.113	0.103
15	8.55	3.97	2.32	1.11	0.679	0.474	0.36	0.246	0.191	0.161	0.131	0.117	0.102	0.0971	0.0904
20	6.39	3.	1.77	0.865	0.536	0.379	0.293	0.205	0.163	0.14	0.116	0.105	0.0935	0.0894	0.084
25	5.11	2.42	1.44	0.715	0.449	0.322	0.252	0.18	0.146	0.127	0.107	0.0977	0.0882	0.0848	0.0802
30	4.25	2.03	1.22	0.614	0.391	0.284	0.225	0.164	0.134	0.118	0.101	0.093	0.0847	0.0817	0.0776
40	3.18	1.55	0.946	0.489	0.319	0.237	0.19	0.143	0.12	0.107	0.0935	0.087	0.0803	0.0778	0.0744
50	2.54	1.26	0.779	0.413	0.275	0.208	0.17	0.13	0.111	0.1	0.0889	0.0834	0.0776	0.0755	0.0725
75	1.7	0.873	0.556	0.31	0.215	0.168	0.142	0.113	0.0993	0.0912	0.0828	0.0786	0.0741	0.0724	0.0699
100	1.28	0.679	0.444	0.258	0.185	0.148	0.127	0.105	0.0932	0.0866	0.0797	0.0761	0.0723	0.0709	0.0686
150	0.871	0.485	0.33	0.204	0.153	0.127	0.112	0.0954	0.0869	0.0819	0.0764	0.0736	0.0706	0.0693	0.0674
200	0.67	0.388	0.272	0.176	0.137	0.116	0.104	0.0904	0.0835	0.0793	0.0747	0.0723	0.0696	0.0685	0.0667
250	0.552	0.33	0.237	0.159	0.126	0.109	0.0988	0.0873	0.0813	0.0776	0.0736	0.0715	0.0691	0.0681	0.0664
300	0.474	0.291	0.213	0.147	0.119	0.104	0.0952	0.0851	0.0797	0.0765	0.0728	0.0709	0.0687	0.0677	0.0661
400	0.378	0.241	0.183	0.132	0.109	0.0976	0.0903	0.0821	0.0776	0.0749	0.0718	0.0701	0.0682	0.0673	0.0658
500	0.321	0.212	0.164	0.122	0.103	0.0934	0.0872	0.0801	0.0762	0.0738	0.0711	0.0696	0.0678	0.067	0.0656
750	0.245	0.171	0.138	0.108	0.0947	0.0872	0.0826	0.0771	0.0741	0.0722	0.07	0.0688	0.0673	0.0666	0.0654
1000	0.208	0.151	0.125	0.101	0.0898	0.0837	0.0799	0.0754	0.0728	0.0712	0.0693	0.0683	0.067	0.0664	0.0652
1500	0.17	0.129	0.11	0.0926	0.0844	0.0798	0.0768	0.0733	0.0713	0.0701	0.0685	0.0677	0.0666	0.0661	0.0651
2000	0.15	0.118	0.102	0.0881	0.0814	0.0775	0.0751	0.0721	0.0704	0.0693	0.0681	0.0673	0.0664	0.0659	0.065
2500	0.138	0.111	0.0975	0.0852	0.0794	0.076	0.0739	0.0713	0.0698	0.0689	0.0677	0.067	0.0662	0.0658	0.065
3000	0.13	0.106	0.094	0.0831	0.0779	0.0749	0.073	0.0707	0.0694	0.0685	0.0674	0.0668	0.0661	0.0657	0.0649
4000	0.119	0.0988	0.0893	0.0803	0.0759	0.0734	0.0718	0.0698	0.0687	0.068	0.0671	0.0666	0.0659	0.0656	0.0649
5000	0.112	0.0945	0.0863	0.0784	0.0746	0.0724	0.071	0.0693	0.0683	0.0676	0.0668	0.0664	0.0658	0.0655	0.0649

Friction factor, f , cont.

$\epsilon_x = 0.8$

$\epsilon_z = 0.8$

Re_d	λ														
	.5	.75	1	1.5	2	2.5	3	4	5	6	8	10	15	20	100
10	17.3	7.98	4.66	2.25	1.39	0.986	0.764	0.541	0.436	0.378	0.32	0.293	0.266	0.256	0.244
15	11.5	5.32	3.12	1.51	0.934	0.664	0.516	0.366	0.296	0.258	0.219	0.2	0.182	0.175	0.167
20	8.62	4.	2.34	1.14	0.706	0.503	0.392	0.279	0.226	0.197	0.168	0.154	0.14	0.135	0.129
25	6.9	3.2	1.88	0.915	0.57	0.407	0.317	0.227	0.184	0.161	0.137	0.126	0.115	0.111	0.106
30	5.74	2.67	1.57	0.767	0.478	0.342	0.268	0.192	0.156	0.137	0.117	0.108	0.0982	0.0948	0.0905
40	4.3	2.01	1.19	0.581	0.364	0.262	0.205	0.148	0.121	0.107	0.0915	0.0844	0.0772	0.0746	0.0713
50	3.44	1.61	0.954	0.47	0.296	0.214	0.168	0.122	0.1	0.0884	0.0762	0.0704	0.0646	0.0625	0.0598
75	2.29	1.08	0.644	0.322	0.205	0.149	0.119	0.0873	0.0724	0.0642	0.0558	0.0519	0.0478	0.0464	0.0445
100	1.71	0.817	0.49	0.247	0.159	0.117	0.0936	0.0698	0.0584	0.0521	0.0457	0.0426	0.0395	0.0383	0.0368
150	1.14	0.551	0.335	0.173	0.113	0.0847	0.0687	0.0523	0.0444	0.04	0.0355	0.0333	0.0311	0.0303	0.0291
200	0.853	0.419	0.257	0.136	0.0904	0.0685	0.0562	0.0435	0.0374	0.0339	0.0304	0.0287	0.0269	0.0262	0.0253
250	0.682	0.339	0.211	0.113	0.0765	0.0587	0.0487	0.0382	0.0332	0.0303	0.0273	0.0259	0.0244	0.0238	0.023
300	0.568	0.286	0.18	0.0981	0.0673	0.0522	0.0436	0.0347	0.0303	0.0279	0.0253	0.024	0.0227	0.0222	0.0215
400	0.427	0.22	0.141	0.0792	0.0556	0.0439	0.0373	0.0303	0.0268	0.0248	0.0227	0.0217	0.0206	0.0202	0.0196
500	0.343	0.18	0.117	0.0677	0.0485	0.0389	0.0334	0.0276	0.0246	0.023	0.0212	0.0203	0.0193	0.019	0.0184
750	0.231	0.127	0.0855	0.0521	0.0388	0.0321	0.0281	0.0239	0.0217	0.0205	0.0191	0.0184	0.0177	0.0174	0.0169
1000	0.177	0.1	0.0695	0.0441	0.0338	0.0285	0.0254	0.022	0.0202	0.0192	0.018	0.0175	0.0168	0.0165	0.0161
1500	0.123	0.0738	0.0532	0.0359	0.0286	0.0248	0.0225	0.02	0.0187	0.0179	0.017	0.0165	0.016	0.0157	0.0154
2000	0.0969	0.0604	0.0449	0.0315	0.0259	0.0228	0.021	0.0189	0.0178	0.0172	0.0164	0.016	0.0155	0.0153	0.015
2500	0.0814	0.0523	0.0398	0.0289	0.0241	0.0216	0.02	0.0183	0.0173	0.0167	0.016	0.0157	0.0153	0.0151	0.0148
3000	0.0711	0.0469	0.0363	0.027	0.0229	0.0207	0.0193	0.0178	0.0169	0.0164	0.0158	0.0155	0.0151	0.0149	0.0146
4000	0.0584	0.0401	0.0319	0.0246	0.0213	0.0196	0.0184	0.0171	0.0164	0.016	0.0155	0.0152	0.0148	0.0147	0.0144
5000	0.0508	0.0359	0.0292	0.0231	0.0203	0.0188	0.0178	0.0167	0.0161	0.0157	0.0153	0.015	0.0147	0.0146	0.0143